MONASH University

Assembly of Colloidal Anisotropic Nanoparticles for Biomedical Applications

Shahinur Acter

A thesis submitted for the degree of *Doctor of Philosophy* at
Monash University in *2021*
School of Chemistry

Copyright notice

Abstract

In recent years, multifunctional colloidal particles have attracted growing attention in a wide range of biomedical applications including drug delivery systems. However, in the development of particle-based drug delivery systems, slow cellular uptake, inconsistent intracellular distribution of drugs, carrying sufficient quantities of drugs to targeted sites, circumventing multidrug resistance, emergence of long-term side effects, etc. have remained as huge challenges. According to recent studies on particle-based drug delivery systems, the size and shape of particles have a profound impact on regulating their properties as drug carriers, particularly in cellular internalization and intracellular distribution. In the last few years, particles with anisotropic morphologies have become a fast-moving research topic with extensive application in biomedicine, including drug delivery systems. In order to address the limitations associated with isotropic particles within biomedical applications, a number of anisotropic morphologies have been designed and prepared, such as triangles, cubes, rods, discs, stars, walnuts, bowls/cups, etc. Studies suggest that due to the morphology of certain anisotropic particles, minimal repulsive interactions with cells occur, thus accelerating their cellular uptake, enhancing circulation time, and ensuring efficient tumor penetration. Among various types of anisotropic particles, polymeric-based anisotropic particles have gained particular attention due to flexibility in engineering their desired morphology, surface chemistry, biocompatibility, and colloidal stability.

Polydopamine is a dark-brown colored biopolymer that has the capability to absorb visible light and convert it to heat, and has become a widely used polymer in various biomedical applications including drug delivery systems. In this thesis, we have synthesized various shapes and sizes of polydopamine nanoparticles including bowl-shaped mesoporous (shape anisotropic) and spherical particles with an aim to obtain efficient drug nanocarriers to overcome the current limitations of nanoparticulate drug delivery systems. An emulsion-induced anisotropic assembly method was used, and each reaction parameter was systematically tuned in order to obtain various sizes of anisotropic (bowl-shaped) mesoporous polydopamine nanoparticles. After a series of investigations, we have observed that due to their anisotropic structure, polydopamine bowl-shaped mesoporous nanoparticles show faster cellular internalization compared with their spherical counterparts. Moreover, intracellular distribution was significantly different for bowl-shaped particles as they were found to be widely distributed in the intracellular environment without any sign of aggregation, unlike spherical particles, which aggregated inside cells.

Furthermore, it has been observed that the size of bowl-shaped polydopamine nanoparticles has a crucial role, not only in their cellular internalization process but also their intracellular trafficking and endocytosis pathways. The size of the bowl-shaped polydopamine particles showed a governing role in selecting the endocytosis pathways taken to internalize them into cells. Due to the cellular uptake efficiency and wide intracellular distribution properties, polydopamine bowl-shaped mesoporous nanoparticles efficiently carried anti-cancer drugs into cells and broadly distributed them in the intracellular environment, causing significant cell death when compared to similar concentrations of free drug. Additionally, drug loaded

polydopamine bowl-shaped mesoporous nanoparticles have shown their efficiency as combined chemo- and photothermal agents for cancer treatment under near-infrared illumination. Lastly, taking advantage of the unique surface wettability of bowl-shaped polydopamine mesoporous nanoparticles, bowls were successfully used as a particulate stabilizer to obtain photothermally responsive Pickering emulsions that show potential as a near-infrared stimulated drug delivery system due to the excellent photothermal conversion efficiency of polydopamine.

Collectively, through these studies we have explored the potential of bowl-shaped polydopamine mesoporous nanoparticles not only as therapeutic agents for combined chemo- and photothermal therapy for cancer treatment but also as a potent and highly controllable near-infrared-triggered drug delivery system. This study contributes new insight into the design and development of efficient and biocompatible drug nanocarriers.

Publications during enrolment

1. **S. Acter**, M. L. P. Vidallon, S. Crawford, R. F. Tabor, B. M. Teo,* "Efficient Cellular Internalization and Transport of Bowl-Shaped Polydopamine Particles. *Particle & Particle Systems Characterization,* **2020**, 2000166".

2. **S. Acter**, M. L. P. Vidallon, S. Crawford, R. F. Tabor,* B. M. Teo* "Bowl-Shaped Mesoporous Polydopamine Nanoparticles for Size-Dependent Endocytosis into HeLa Cells", *ACS Applied Nano Nanomaterials,* **2021**, 4, 9536–9546.

3. **S. Acter**, M. L. P. Vidallon, J. P. King, B. M. Teo,* and R. F. Tabor* "Photothermally responsive Pickering emulsions stabilised by polydopamine nanobowls", (Accepted to *Journal of Materials Chemistry B*, 16-Aug-2021).

4. **S. Acter**, N. Jahan, M. L. P. Vidallon, B. M. Teo,* and R. F. Tabor* "Polydopamine Mesoporous Nanobowls for Conquer Multi Drug Resistance via Combined Chemo- and Photothermal Cancer Treatment" (Submitted for publication).

Thesis including published works declaration

I hereby declare that this thesis contains no material which has been accepted for the award of any other degree or diploma at any university or equivalent institution and that, to the best of my knowledge and belief, this thesis contains no material previously published or written by another person, except where due reference is made in the text of the thesis.

This thesis includes **three** original papers published in peer-reviewed journals and **one** submitted for publication. The core theme of the thesis is the development of anisotropic shaped nanoparticles from polydopamine for various drug delivery applications including cancer treatment. The ideas, development and writing up of all the papers in the thesis were the principal responsibility of myself, the student, working within the School of Chemistry under the supervision of A/Prof. Rico F. Tabor, Dr. Boon Mian Teo, and Prof. Bayden Wood.

The inclusion of co-authors reflects the fact that the work came from active collaboration between researchers and acknowledges input into team-based research. In the case of Chapters 2, 3, 4, and 5 my contribution to the work involved the following:

Experimental design and execution, materials development, data analysis and presentation, and manuscript drafting. Further details specific to each chapter are provided in the Table below.

Thesis Chapter	Publication Title	Status	Nature and % of Student Contribution	Co-author Name (s), Nature and % of Co-Author Contribution	Co- author (s) Monash Student (Y/N)
2	*Efficient Cellular Internalization and Transport of Bowl-Shaped Polydopamine Particles*	*Published*	*83%, experimental design and execution, data analysis, manuscript drafting*	*a) Mark Louis P. Vidallon, TEM imaging of the sample, (2%).* a) *Simon Crawford, TEM imaging of cells, (2%).* b) *Rico F. Tabor, inputs for manuscript work, (3%).* c) *Boon M. Teo, concept and inputs for manuscript work, (10%).*	*a) Y* *b) N* *c) N* *d) N*
3	*Bowl-Shaped Mesoporous Polydopamine Nanoparticles for Size-Dependent Endocytosis into HeLa Cells*	*Published*	*82%, experimental design and execution, data analysis, manuscript drafting*	*a) Mark Louis P. Vidallon, TEM imaging of the sample, (2%).* *b) Simon Crawford, TEM imaging of cells, (2%).* *c) Rico F. Tabor, inputs for manuscript work, (7%).* *d) Boon M. Teo, concept and inputs for manuscript work, (7%).*	*a) Y* *b) N* *c) N* *d) N*
4	*Polydopamine Mesoporous Nanobowls for Conquer Multi Drug Resistance via Combined Chemo- and Photothermal Cancer Treatment*	*Submitted*	*85%, experimental design and execution, data analysis, manuscript drafting*	*a) Nazneen Jahan, PI test, (1%)* *b) Mark Louis P. Vidallon, TEM imaging of the sample, (1%).* *c) Boon M. Teo, concept and inputs for manuscript work, (5%).* *d) Rico F. Tabor, concept and inputs for manuscript work, (8%).*	*a) Y* *b) Y* *c) N* *d) N*
5	*Photothermally responsive Pickering emulsions stabilised by polydopamine nanobowls*	*Published*	*83%, experimental design and execution, data analysis, manuscript drafting*	*a) Mark Louis P. Vidallon, TEM imaging of the sample, (2%).* *b) J. P. King Imaging software setup, (1%).* *c) Boon M. Teo, inputs for manuscript work, (4%).* *d) Rico F. Tabor, concept and inputs for manuscript work, (10%).*	*a) Y* *b) Y* *c) N* *d) N*

I have renumbered sections of submitted or published papers in order to generate a consistent presentation within the thesis.

Student name: Shahinur Acter

Student signature: **Date:** 01/February/ 2022

I hereby certify that the above declaration correctly reflects the nature and extent of the student's and co-authors' contributions to this work. In instances where I am not the responsible author I have consulted with the responsible author to agree on the respective contributions of the authors.

Main Supervisor name: Rico F. Tabor

Main Supervisor signature: **Date:** 01/February/ 2022

Acknowledgement

All praises to the Almighty, Allah (SWT), who gave me the strength to complete this journey of doctoral study (PhD) successfully.

I would like to convey my deepest gratitude towards my supervisors, A/Prof. Rico F. Tabor, Dr. Boon Mian Teo, and Prof. Bayden Wood, I am privileged and honored to be your PhD student. Being my main supervisor, A/Prof. Rico Tabor has been extremely supportive and motivating throughout my PhD journey. I will forever be grateful to you for accepting me as your student, your wonderful guidance in my thesis, helping me out in every single thing to become a researcher, and elevating my confidence. I am very grateful to Dr. Boon Mian Teo for giving the opportunity to do PhD at Monash University, your endless support, and encouraging me at times of high stress during this journey.

A huge thanks to all my fellow students at the Soft Materials and Colloids Laboratory (SMaC Lab) for making my PhD journey so enjoyable and memorable. Special thanks to Mark, Zhenzhen, Luke, Geos (my lovely neighbour in office), Yue for all of your support. I am so blessed to be a part of SMaC Lab. Many thanks to Dr. Ash Rozario from Bell group for teaching me cell culture.

I would like to acknowledge Monash International Tuition Scholarship (MITS) for tuition fees including Overseas Student Health Cover (OSHC) and Monash Graduate Scholarship (MGS) for stipend from Monash University. Monash Graduate Research Completion Award (GRCA) for supporting my study that was hampered during Covid-19 lockdowns, Monash Centre for Electron Microscopy (MCEM), Monash Micro Imaging, the Flow Cytometry Facility, and the Ramaciotti Centre for Cryo Electron Microscopy, Monash University.

To my parents, MD. Haider Ali and Salina Haider, you are my backbone. It is not possible to thank you enough for your unconditional love and support. Abbu (dad), I would not be able to start this PhD journey without your encouragement and support. I want to make you both proud.

I am very thankful to my husband MD. Sabbir Karim Abir for joining me in Melbourne, being with me to make this journey smooth and enjoyable, and of course, beautifully dealing with my tantrums during stressful times of my PhD journey. You are the reason I left PhD study in S. Korea in 2014 and you are the reason I started this journey in Australia in 2018, thanks for supporting every decision I made ever since we started our life together.

My heartfelt thanks to my sister Dr. Shamim-Ara Pervin, brother Dr. Mohammod Shamim Reza, and my sister in-law Dr. Esrat Jahan for encouraging me during my PhD journey and your endless support. My nephew Taheem Shayaan (8yrs) and Rushnaan Mehrab Shezaan (7 months), you both are my inspiration in doing something great in life so that, one day you

would feel proud of your aunt. Special thanks to my uncle Prof. Asm Ziaul Karim for encouraging me to do PhD and stay in touch to hear about my research progress.

To my friends, I am blessed to have such amazing people around me who have been so caring and loving, Aneesa Ansari for holding me up at bad times and I would cherish all the lovely memories we had during our PhD journey at Monash, thanks to Tomalika Rahman Ullah for being part of fun PhD group, special thanks to Maqsoora Tusnime Fouzia for all your supports at the beginning of my PhD journey.

Contents

List of Figures

List of Tables

Chapter 1

Introduction

Preface for Chapter 1

In recent years, colloidal micro- and nanoparticles with anisotropic architectures have attracted enormous research interest and attention due to their unique combination of novel morphologies and manifold potential applications in a wide range of fields including for therapeutic purposes. In this Chapter, various types of anisotropic particles with different shapes are discussed, including inorganic, metal, and polymer-based particles. By analyzing previous studies, key features, properties and applications of the different types of anisotropic particles are brought together, highlighting commonly used preparation methods. This Chapter broadly focuses on different shapes of anisotropic particles and their extensive applications in a range of biomedical fields including drug delivery, discussing their challenges as drug carriers including their long-term toxicity to biological systems, along with proposed solutions to overcome these limitations.

1.1 Anisotropic colloidal particles

Multifunctional colloidal micro- and nanoparticles with tuneable architectures have attracted increasingly significant research attention in recent years due to their promising properties and extensive applications in biotechnology, nanotechnology, electronics, and clean energy.[1-5] Anisotropy simply means that a property is direction dependent, and for particles this can refer to inhomogeneous or eccentric shape, composition, surface chemistry, etc. For example, a sphere is shape isotropic (the same in every direction), whereas a rod is elongated in one dimension, and hence shape anisotropic. Such parameters are often intersected, meaning that anisotropy can have remarkable effects on chemical, physical, and morphological characteristics of particles and their assemblies (Figure 1.1).[6-7] To maximize the utility of these effects, materials scientists have developed anisotropic colloidal particles with multiple functionalities. In the last two decades, there have been significant developments in particle design to leverage anisotropic properties, offering opportunities in fabricating particles of various sizes, shapes, chemical composition, or surface functionalities due to the presence of anisotropy.[3, 6-7]

The introduction of shape anisotropy to particles at a nanoscale level has emerged as a powerful way to access unique properties and functionality that enable the investigation of complex nanostructures across a wide range of applications.[6, 8] Shape anisotropic particles are highly desirable in fundamental studies for many applications in biomedical fields including drug delivery due to their controllable morphology, which has enormous impact on regulating their properties.[9-10]

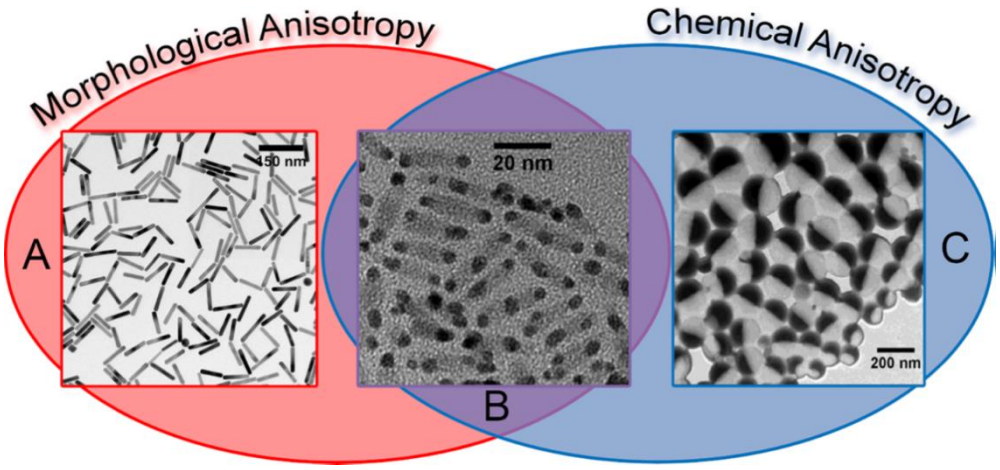

Figure 1.1. Venn diagram of morphological and chemical anisotropy of particles: (A) gold nanorods, (B) gold nanoparticles grown site selectively on cadmium selenide nanoplatelets, and (C) polymer Janus nanoparticles featuring poly(L-lactide) and poly(styrene-co-aminoethyl methacrylate) faces.[7]

According to recent studies on particle-based drug delivery systems, the size and shape of particles have a profound impact on regulating their properties as drug carriers, particularly in cellular internalization and intracellular distribution.[11-13] Studies suggest that by controlling the morphology of anisotropic particles, minimisation of repulsive interactions can be achieved, which influences interactions between cells and anisotropic particles and enables particles to more effectively cross the biological barriers of the cells, thus accelerating their cellular uptake.[11, 13] It has been demonstrated that anisotropic particles show enhanced circulation time and more efficient tumor penetration compared to their spherical counterparts.[14] Shape has been identified as one of the crucial properties of particles in a number of excellent reviews, and a wide range of investigations have been conducted on the

synthesis of various particle shapes such as cup/bowl, star, rod, disk, etc. from materials including metals, polymers, inorganics, and hybrids.[7, 9 15-16]

1.2 Anisotropic inorganic and metal particles

In recent years, there has been significant attention on design and fabrication of carbon- and silica-based anisotropic particles because of their structural stability, biocompatibility, large surface area, and flexibility in functionalization, which indicates potential in various applications including nanomedicine.[8, 17-18] To synthesize inorganic/metal based anisotropic particles, either directed growth from seeds or hard-templating are commonly used, the latter of which provides access to a wider array of morphologies, and is further classified into *in situ* and *ex situ* processes. Various shapes of anisotropic silica particles have been formed including ellipsoids, pennate structures, stomatocytes, discocytes, echinocytes, and spherocytes, etc. (Figure 1.2). Following this method, carbon based anisotropic particles have also been obtained. For instance, Shi and co-workers reported the formation of anisotropic porous carbon bowls (Figure 1.3).[19] In recent years, Tufenkji and co-workers introduced a one-pot green method for fabricating anisotropic silver nanoparticles with various shapes such as triangular, hexagonal, and dendritic (Figure 1.3).[20]

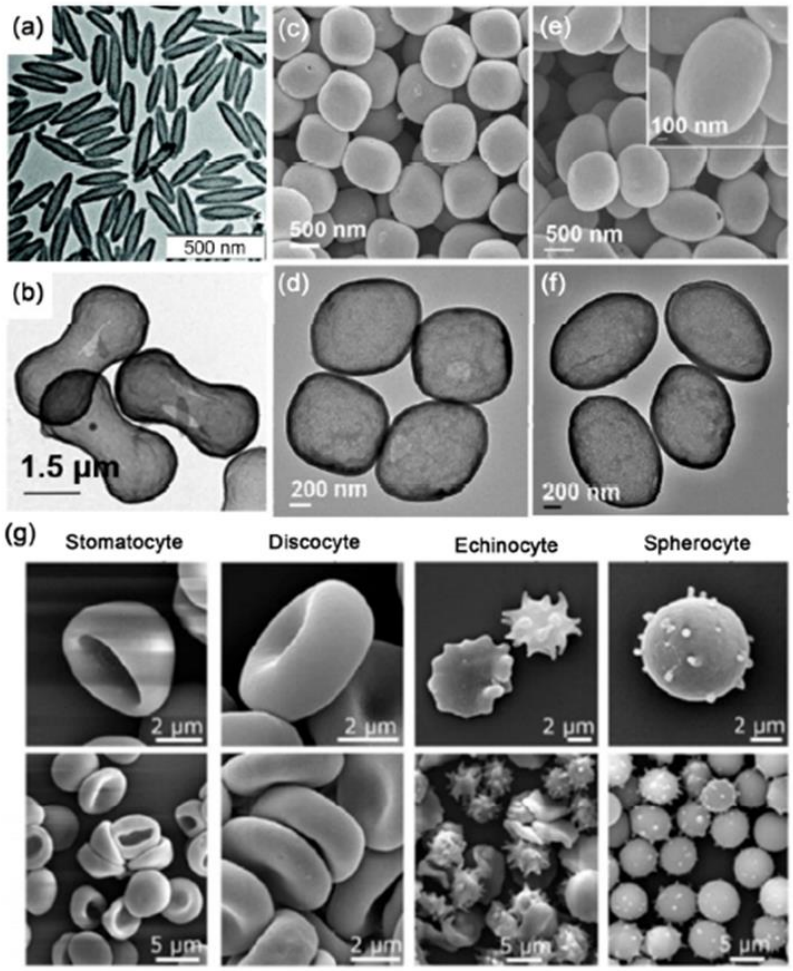

Figure 1.2. (a) and (b) Silica nanoparticles with unusual shapes using hematite cores as templates. Field emission scanning electron microscopy (FESEM) and transmission electron microscopy (TEM) images of quasi-cubic (c, d) and ellipsoidal (e, f) carbon colloidosomes using Fe_2O_3 as a template. (g) Four distinct libraries of silica composite particles templated from red blood cells.[8]

Among the various metals amenable to nanoparticle formation, anisotropic gold nanoparticles represent one of the most remarkable areas of advanced nanoscience and technology. As early as the beginning of the 20th century, materials scientists already noticed

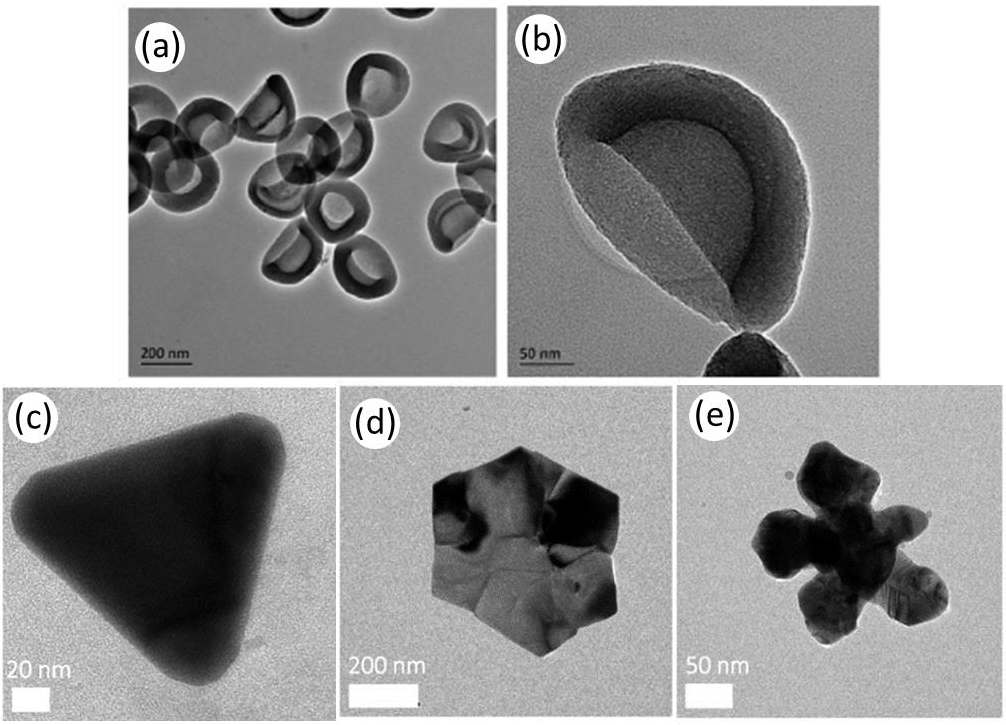

Figure 1.3. Transmission electron microscopy (TEM) images of anisotropic metallic (a, b) carbon bowls, and (c–e) anisotropic silver nanostructures, triangular, hexagonal, and dendritic shaped respectively. (a, b) Adapted from Ref 19; (c–e) adapted from Ref 20.

the existence of anisotropic structured gold particles, however, extensive research in this field has considerably accelerated since 2000.[2, 21-22] Formation of various shapes of gold nanostructures have been reported including triangles, cubes, octahedrons, plates, cones, and prisms.[23 24-30] In the last decade, a wide range of bottom-up methods and techniques involving templates or capping agents have been used to form anisotropic gold nanostructures.[2-3, 17, 31-33] Among these methods, the versatile and easily accomplished controlled seed-mediated method is widely used to achieve size and shape controlled formation of gold nanoparticles. Various shaped gold nanoparticles have been synthesized

using such seed-mediated methods including gold nanorods and gold nanotriangles (Figure 1.4.).[34-35]

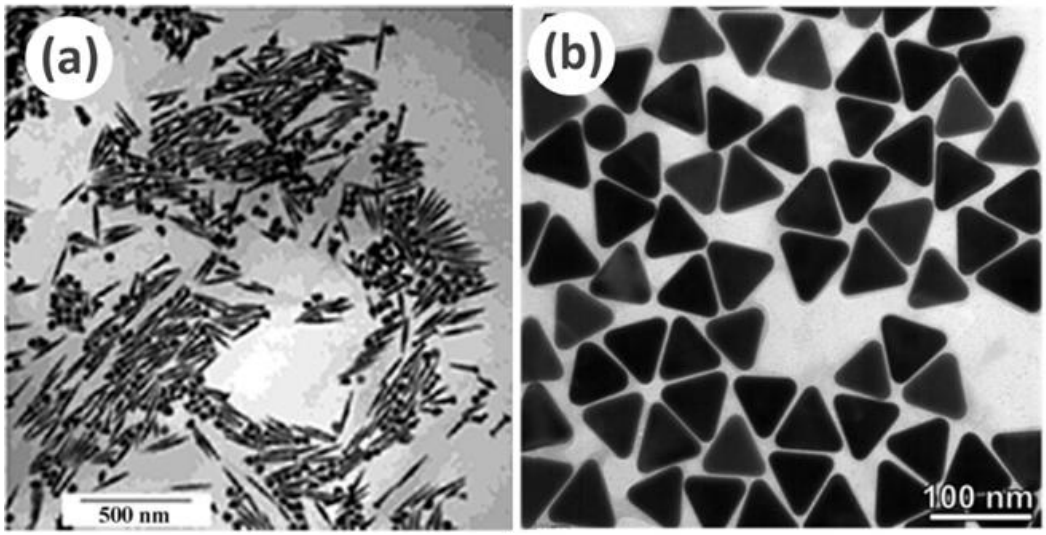

Figure 1.4. Seed-mediated synthesis of gold nanorods (AuNRs) and nanotriangles (AuNTs). (a) Adapted from Ref 21 and (b) adapted from Ref 27.

There are two steps involved in the classical seed-mediated method, and this two-step process was devised by Zsigmondy and published in his 1909 book; the process was later renamed the 'seeded-growth' method.[21] In this method, small gold nanoparticle seeds are prepared in the first step.[36] These seeds are then added to a growth solution in the second step that contains $HAuCl_4$ along with stabilizing agents and reducing agents. Freshly reduced Au (0) grows on the seed surface to form larger gold nanoparticles.[24, 36] Herein the size, shape, and surface properties of the nanoparticles can be controlled by the nature and amount of the reducing agents and stabilizer, and their ratio to the Au precursor.

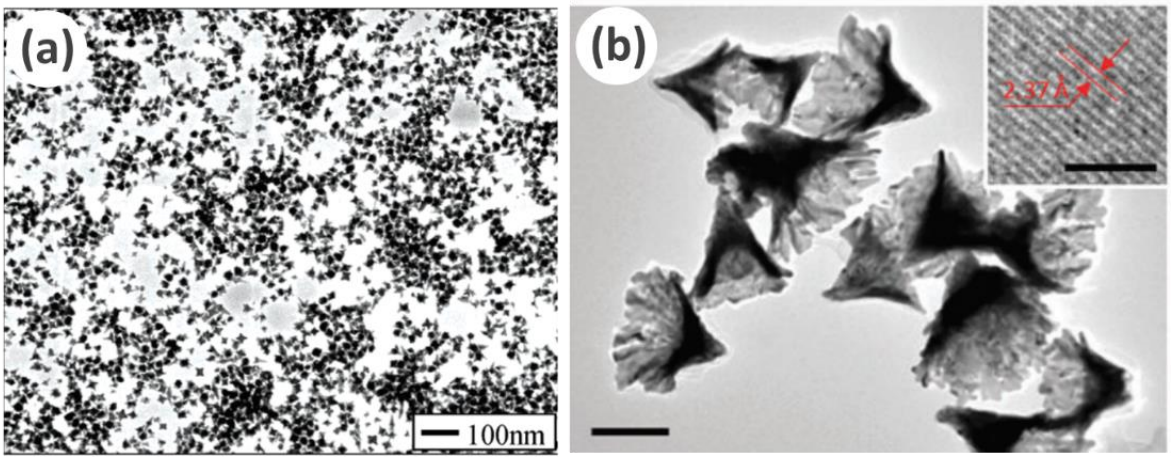

Figure 1.5. Transmission electron microscopy (TEM) images of (a) gold nanostars and (b) gold nanocones (inset of (b): high-resolution TEM image of gold nanocones). (a) Adapted from Ref 23; (b) adapted from Ref 26.

However, further developments in recent years have identified new processes for achieving unique particle geometries. For example, gold nanostars were formed by a seedless, surfactant-free, and high yielding protocol modified from a method reported by Xie and co-workers (Figure 1.5).[23] Gold cone-shaped nanoparticles/nanocones are generally formed by top-down approaches such as electron beam lithography, nanotransfer printing, and nanoimprint fabrication.[37-39] However, these methods are sophisticated processes that are costly, time-consuming, and low yielding, making them unfavourable to synthesize gold nanocones,[40] when compared to newly developed bottom-up approaches. Subsequently, Zhang and co-workers synthesized gold nanocones using an ultrasound-assisted interfacial method.[26]

Anisotropic gold nanoparticles have shape-dependent physical and chemical properties. For example, the visible colors of gold nanoparticle dispersions and their optical properties vary considerably with their shape. Of more relevance to their properties as drug carriers, it has been shown that size and shape also have significant impact on their efficiency as drug delivery systems.[41-45] For instance, Cho *et al.* demonstrated that the shape of gold nanoparticles has significant influence on their cellular uptake.[46] Another research group, Nambara *et al.* demonstrated that triangular gold nanoparticles showed higher efficiency in cellular internalization into HeLa cells relative to their spherical counterparts.[47] In a recent study, Lin and co-workers reported that among various shapes of anisotropic nanoparticles, the greatest cellular internalization occurred for nanotriangles, followed by nanorods and nanostars.[44] They also demonstrated that the shape of particles has a noticeable influence on the specific endocytosis pathways by which the particles enter cells.[44]

In biomedical applications, metal-based colloidal anisotropic nanostructures are widely used due their unique morphological and chemical composition, size-to-volume ratio, and exceptional thermal stability. However, the potential toxicity effects of these metallic anisotropic nanostructures to biological objects cannot be ignored. There are studies reporting the risk of long-term toxicity of metallic nanostructures to biological systems, including gold nanoparticles, which caused drastic damage to cells.[48-49] Therefore, further *in vitro* and *in vivo* toxicology investigations have been conducted to examine the risk of damage to cells, tissues, and organs of animals.[21, 50-51, 21, 50-51] *In vitro* studies demonstrated that the toxicity of gold nanostructures could due to the surfactant (cetyltrimethylammonium bromide, CTAB) ligands used, and not the core itself.[21] In other research, Wyatt, Murphy, and

co-workers reported that gold nanoparticles with polymer coatings such as poly(allylamine) hydrochloride were not toxic to cells.[51]

1.3 Shape anisotropic polymeric particles

Polymer-based anisotropic colloidal particles have experienced an extraordinary revolution due to their promising properties and applications in a wide range of fields including nanotechnology and biotechnology.[52-55] Because of the potential for high biocompatibility and targeting abilities, polymeric particles have attracted enormous research attention from the scientific community for biomedical applications in particular.[52, 54] Moreover, polymer-based particles can be easily tailored, with flexibility in engineering their shape anisotropy, which is increasingly gaining attention for numerous applications including as drug delivery system, biosensors, contrast agent, and imaging, etc.[16, 56-58] In the last few years, a large number of fabrication techniques have been introduced to synthesize shape anisotropic polymer particles. Fabrication methods for polymer based anisotropic particles are classified in two main categories: (a) direct formation of nonspherical particles, using techniques such as microfluidics, lithography, seed polymerization, and electrospraying, and (b) post-modification of previously prepared particles, which includes solvent based methods and film stretching.[59] Using these techniques, researchers have designed various shapes of anisotropic particles, and in last few years in particular, an extensive variety of anisotropic-shaped polymeric particles have been introduced such as rods, disks, cylinders, walnuts, needles, ellipsoids, various mesoporous structures, cups or bowls, etc. (Figure 1.6).[60-67]

1.3.1 Polymer based anisotropic particles in biomedical applications

Owing to the non-toxicity, biocompatibility, small size, flexibility in surface functionality, and unique morphological properties of many polymer particles, polymeric anisotropic particles have been recognized as suitable material for various biomedical applications including as efficient drug carriers.[16, 56, 59]

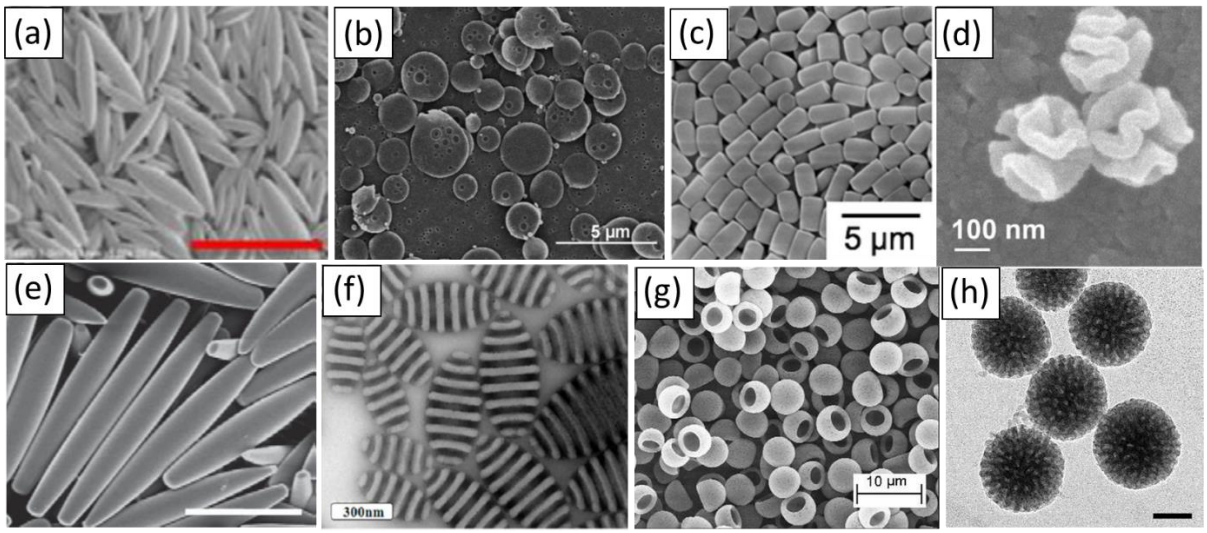

Figure 1.6. Various shapes of polymeric anisotropic particles: SEM images of (a) rod-shaped particles (scale bar 10 µm), (b) disk-like particles, (c) cylinder-shaped particles, (d) walnut-shaped particles, (e) needle-like particles (scale bar 2 µm). (f) TEM image of ellipsoid-shaped particles, (g) SEM image of cup/bowl-like particles, and (h) TEM image of mesoporous particles. (a) Adapted from Ref 60. (b) Adapted from Ref 61. (c) Adapted from Ref 62. (d) Adapted from Ref 63. (e) Adapted from Ref 64. (f) Adapted from 65. (g) Adapted from Ref 67. (h) Adapted from Ref 66.

In various studies, it has been demonstrated that anisotropic polymer particles show sustained drug release capabilities at target-specific sites.[68-69] Moreover, the shape of these nanostructures allows loading of sufficient amounts of therapeutic molecules inside.[70] Recent studies suggest that the inhibition of non-specific cellular uptake resulted in enhanced *in vivo* biodistribution, whereas a higher radius of curvature increased targeting capabilities of the anisotropic particles.[71] For instance, Smith *et al.* demonstrated that different shapes of polystyrene particles (spheres, prolate ellipsoids, and oblate ellipsoids) manipulated cellular attachment and internalization.[72] In another research, Caruso and co-workers reported that increasing the aspect ratio of rod-shaped hydrogel capsules slowed their cellular internalization.[73] Kharlampieva and co-workers found that hemispherical poly (N-vinylpyrrolidone)/tannic acid multilayer capsules were taken up at greater number in comparison to their spherical and cubic counterparts.[74] In a recent study, Gao and co-workers observed a significantly faster internalization and larger accumulation inside cells of bowl-like polystyrene colloidal particles when compared to their spherical counterparts.[71]

Among these diverse polymer-based anisotropic colloidal particles, bowl-like or cup-shaped structures have gained particular interest in the biomedical field, especially for drug delivery systems. Cup/bowl-like particles are not only efficient for loading and releasing drugs, they also show potential for targeted and controlled release drug delivery systems.[71, 74] For example, Coussios and co-workers have demonstrated that polystyrene cup-shaped particles are capable of trapping and stabilizing nanobubbles, and upon ultrasound exposure, are capable of seeding cavitation within a tumor environment, leading to enhanced delivery and penetration of drugs to the targeted region.[69] From here, we focus further on bowl/cup-

shaped nanoparticles as a specific case of shape anisotropic particles with particularly valuable properties.

1.3.2 Formation of cup/bowl-like polymeric anisotropic particles

Fabrication of polymer based anisotropic particles has become a fascinating area of research. Various fabrication methods to obtain bowl/cup-like particles have been reported, and these are summarized in the following sections.

1.3.2.1 Seed polymerization technique

To synthesize monodisperse polymer particles, seeded polymerization has been successfully used for many years. Studies show that this polymerization method has been developed to synthesize uniform polymeric particles in various sizes from 1–100 µm by using a successive monomer swelling and polymerization process.[75] Based on this well-established process, Coussios *et al.*[69] have extensively modified an interfacial seed polymerization process to synthesize monodisperse cup-shaped polymeric particles. They were able to coat polystyrene template nanoparticles with cross-linked poly (methyl methacrylate), with the goal of synthesizing nanocups (Figure 1.7). The size of synthesized nanocups varied according to the size of seed particles used in this formation process, and polydispersity of the nanocups was dependent on the degree of crosslinking within their shell (Figure 1.7). Herein, the mechanism of shape transformation from spherical to cups arises from interactions between the polystyrene core and copolymer shell. Due to these interactions, the core swells

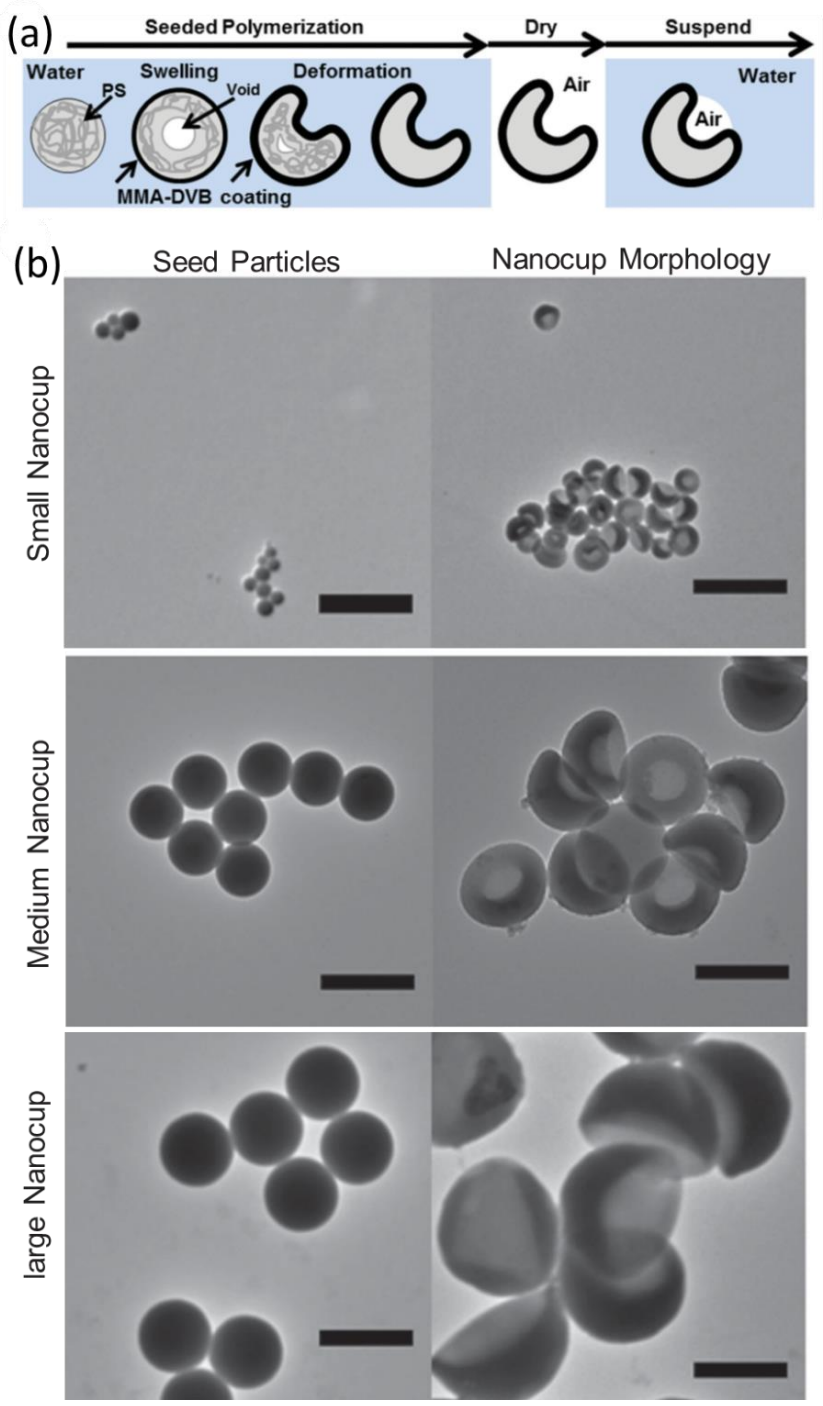

Figure 1.7. (a) Schematic of the formation of nanocups by a seeded polymerization technique, (b) TEM images of small (100 nm), medium (300 nm), and large (460 nm) seed particles and resulting nanocups. Adapted from Ref 69.

and an osmotic force bends the shell to form a depression. Changes of rigidity in the shell are significant in enabling it to be pliable enough to bend, and the shell rigidity is closely connected to the extent of crosslinking in the shell. Hence, stiffness of the shell is also important in order to prevent multiple depressions from forming. The morphology of the synthesized cup-shaped nanoparticles were confirmed by TEM imaging, where the cavity of the nanocups was found to be 230–340 nm (Figure 1.7 b).

1.3.2.2 Osmotic pressure method

The osmotic pressure method to obtain shape-anisotropic polymer nanoparticles was originally developed by Möhwald *et al.*[76] in order to measure the mechanical properties of polyelectrolyte microparticles by monitoring their collapse. More recently, the osmotic pressure controlled method has become a commonly used technique to fabricate colloidal particles. Gao *et al.* applied this method to synthesize bowl-shaped polyelectrolyte microparticles,[71] successfully achieving a shape transformation from spherical to bowl-shaped. Here, due to the effect of osmotic pressure, incubation of multilayer microcapsules in a concentrated poly (styrenesulfonate) solution yielded bowl shape particles from spherical precursors. To induce deformation, spherical capsules were coated with bovine serum albumin to increase the compactness of their shell, and then immersed in highly concentrated poly (styrenesulfonate) solution (30 wt %). The bovine serum albumin coating prevented diffusion of poly (styrenesulfonate) into the capsules, which helps invagination of the microcapsules occur under the osmotic pressure created by counterions and polyelectrolytes, as shown in Figure 1.8. No significant changes in the size of the deformed particles were observed due to their shape transformation from spherical to bowl-shaped.

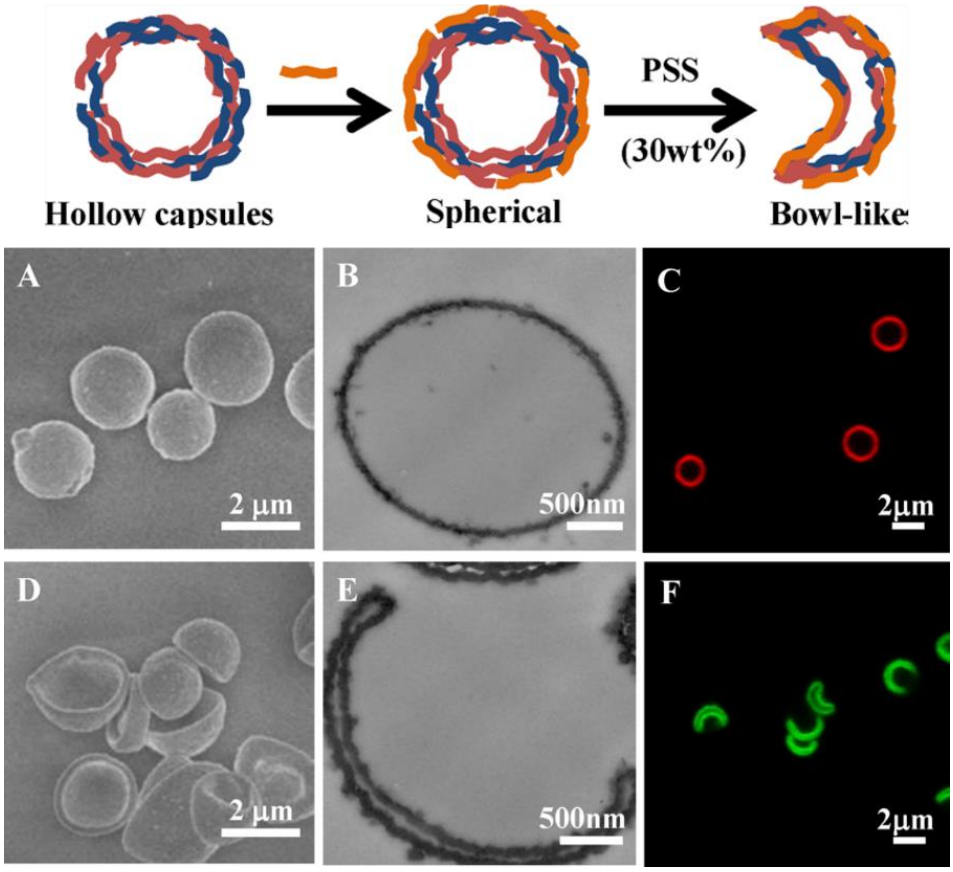

Figure 1.8. Scheme (top) showing the fabrication process of bowl-like microcapsules, (b) SEM (A, D), cross-sectional (ultramicrotomy) transmission electron microscopy (B, E), and confocal laser scanning microscopy (C, F) images of spherical (A–C) and bowl-like (D–F) (PAH/PSS)10/BSA microcapsules. The samples for SEM observation were prepared by critical point drying. The capsules for confocal laser scanning microscopy observation were incubated in a cell culture medium for 7 days, and the spherical and bowl-like microcapsules were labelled by fluorescein isothiocyanate and Rhodamine B isothiocyanate, respectively. Adapted from Ref 71.

1.3.3 Toxicity of polystyrene polymers

The majority of studies to date have been conducted on optimizing particle features such as size, morphology, drug loading, and release efficacy, while the toxicity of these particles have been broadly ignored. Despite the enormous advantages of polymer-based anisotropic particles for various biomedical applications, there are a few polymers including polystyrene where acute toxicity has been reported. It has been seen that smaller polystyrene particles (at around 460 nm) and 1 μm affected red blood cells, leading to hemolysis.[77-78] In order to enable higher therapeutic efficiency and minimum toxicity of the drug delivery system, it is crucial to select biocompatible polymers that can be easily functionalized with other molecules including therapeutic agents and targeting moieties on their surfaces. Additional requirements for effective drug delivery vectors include colloidal stability (in biological matrices) and the flexibility to provide both a high degree of control in shape and size with thermal stability. This is a challenging set of criteria, and few polymers can provide such properties while remaining biocompatible.

1.3.4 Polydopamine

In the last decade, polydopamine (PDA) has gained increasing attention in a wide range of nanotechnology applications. It is a dark brown-black coloured biopolymer formed from the polymerization of dopamine, a naturally produced neutrotransmitter. Polydopamine arises specifically as the result of oxidant-induced polymerization of dopamine (monomer) in basic pH conditions. It is assumed that in the first step of the reaction, an indole skeleton is formed by oxidative ring closure, after which monomer units are connected by dehydrogenative C–C

bond formation.[79-82] The structure of PDA offers various advantages including easy functionalization as it has carbonyl moieties, which act as electrophilic sites for amino- or mercapto-nucleophiles (Figure 1.9).[83-84]

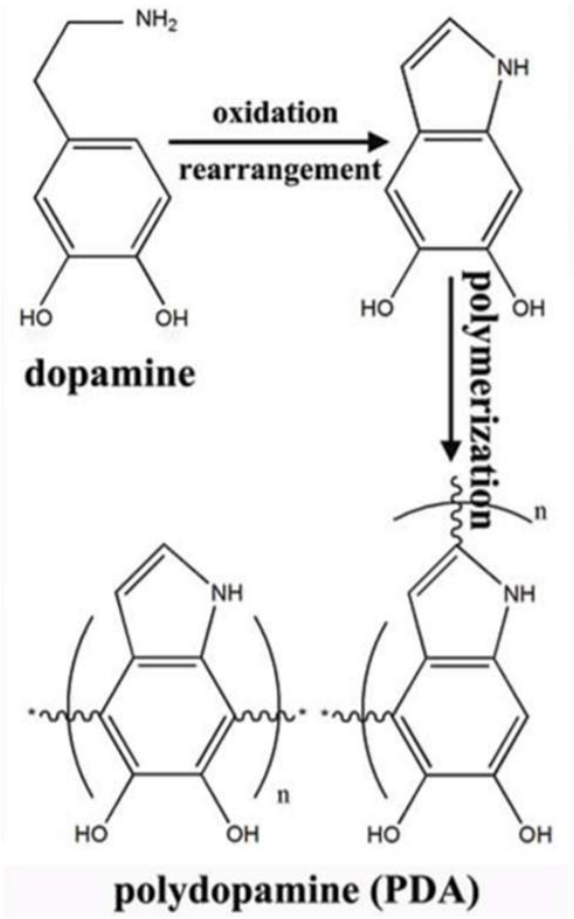

Figure 1.9. Polymerization of dopamine to polydopamine. Adapted from Ref 84.

As a result, a broad range of research has been published on melanin-like PDA nanoparticles, PDA surface functionalized magnetic nanoparticles, fluorescent PDA nanoparticles, etc. for various applications including biomedical use as a targeted drug carrier, bio-imaging or

therapeutic agent, UV-protector for skin, drug delivery vector, and even in energy storage, photonics, etc.[81, 85-89]

PDA has risen to become one of the most widely used polymeric materials in biomedical research due to a number of excellent properties it possesses, including high colloidal stability (from surface charging of catechol alcohols), mild synthesis requirements, biocompatibility, thermal stability, etc.[90] Moreover, the richness of catechol/quinone moieties in PDA offers the potential to anchor functional molecules onto produced nanoparticles by either physical bonding such as π-π stacking or hydrogen bonding or via covalent tethering. Therefore, PDA not only has higher drug loading capability and but is also convenient for drug release and targeting, which makes it an ideal material in preparing drug carriers.[86, 88] Furthermore, one of the biggest advantages of PDA is the flexibility offered by the high degree of control in the formation of various shapes and sizes of particles that can be achieved. Combined with PDA's favorable thermal stability, this offers opportunities for the synthesis of spherical and anisotropic shaped particles (bowl-shaped, and walnut-shaped) with tunable sizes.[91 63, 92] Additionally, PDA has the ability to absorb visible and infrared light and convert it into heat.[93] In recent years, PDA has been successfully applied as a photothermal agent in cancer treatment. For example, Lu and co-workers reported 40% photothermal energy conversion efficiency of PDA, indicating potential of PDA as photothermal agent for cancer treatment.[94] Another interesting property of PDA nanoparticles is that they can act as a particulate emulsifier. In a number of studies, it has been reported that PDA particles adsorb to oil–water interfaces and stabilize Pickering emulsions.[95-96]

1.3.5 Polydopamine bowl-shaped mesoporous nanoparticles

Polydopamine bowl-shaped mesoporous nanoparticles represent a unique anisotropic morphology with well-controlled radially oriented mesochannels, and mesopores. Such particles were first prepared using a novel emulsion-induced interface anisotropic assembly.[92] In this particle formation method, self-assembly of micelles provides a template for mesopores, whereas a unique dewetting phenomenon enables a bowl-shaped parent morphology to be achieved.

By combining these approaches, an efficient method to obtain anisotropic shaped particles (Figure 1.10) is obtained. Lou *et al.*[92] reported an emulsion-induced interface anisotropic assembly technique to synthesize asymmetric bowl-shaped and walnut-shaped mesoporous particles derived from dopamine. As shown in the schematic diagram in Figure 1.10, the fabrication method starts with formation of oil–water interface between 1,3,5-trimethylbenzene (TMB) and an external aqueous phase in an emulsion system. Initially, composite micelles formed by cooperative formation of surfactant Pluronic® F127, TMB, and polydopamine orient along the radial direction within the growing particles. Due to continuous cooperative assembly, the oriented growth of the mesochannels continues unidirectionally. At the TMB/water interface, composite micelles start to grow as island-shaped mesostructured polydopamine seeds.

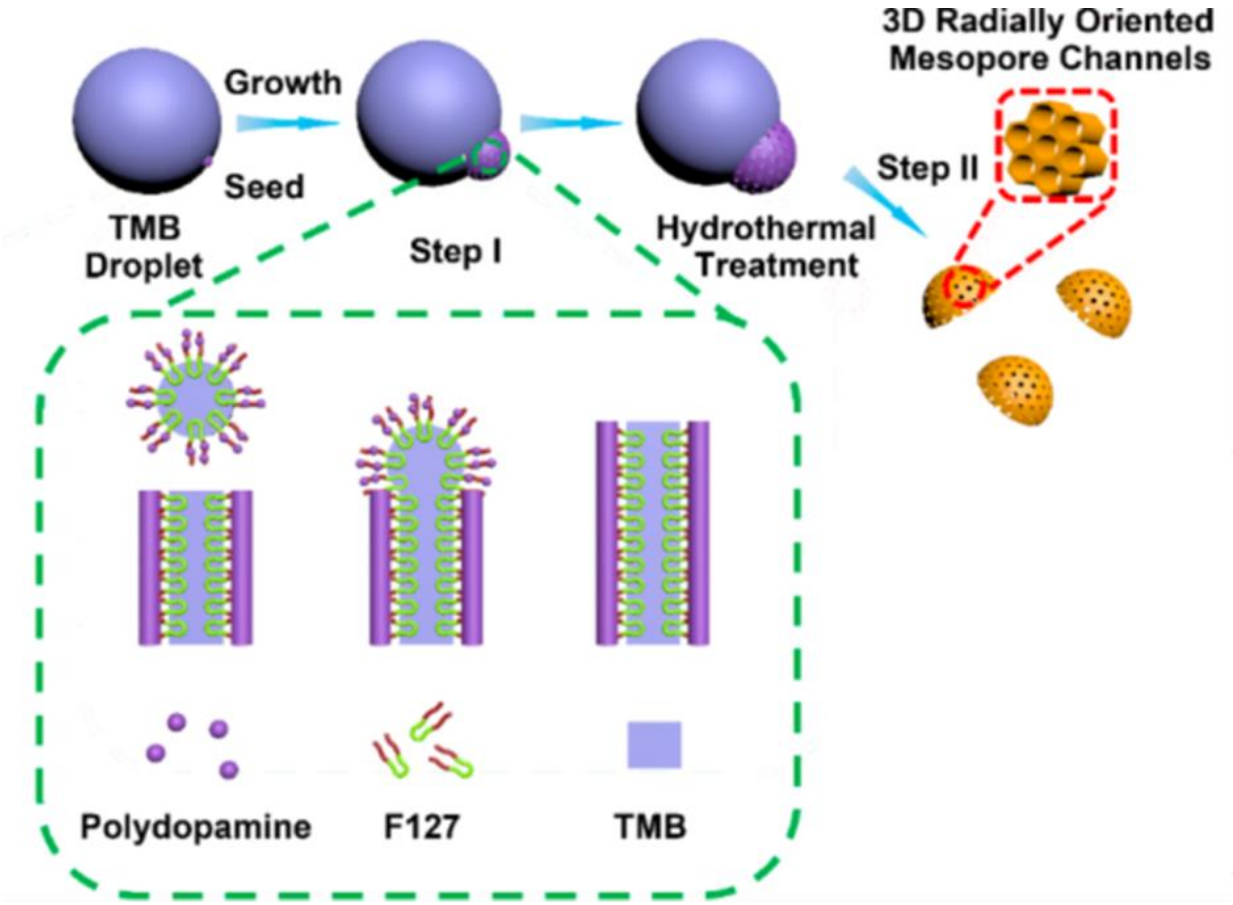

Figure 1.10. Schematic illustration of the formation process of bowl-like mesoporous particles. In step I, formation of block copolymer Pluronic® F127/ TMB/polydopamine oligomer composite micelles and emulsion induced interface anisotropic assembly of asymmetric bowl-like mesostructured polydopamine particles with radially oriented large mesochannels is seen. In step II, hydrothermal treatment of the mesostructured polydopamine nanocomposites to stabilize the structure is undertaken.[92]

This seed-mediated anisotropic growth process completes in 2 h, and is followed by a hydrothermal treatment of the synthesized bowl-shaped mesoporous polydopamine particles with radially oriented mesopores. In this process, the key steps to form the shape of the particles are creating the interface between two immiscible liquids and controlling the interactions between TMB droplet and *in situ* formed particles.

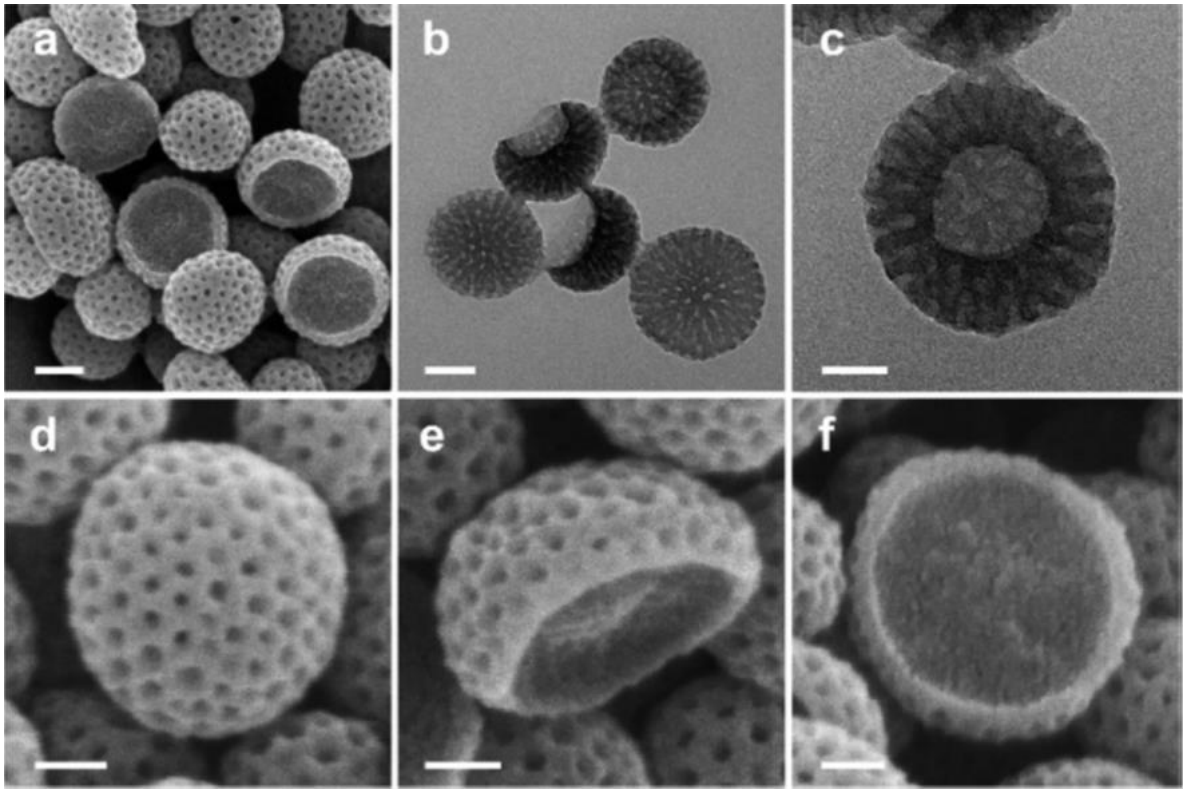

Figure 1.11 Microscopic characterization of bowl-like mesoporous polydopamine particles: (a) FESEM image; (b) TEM image; (c) magnified TEM image showing an individual bowl-like particle with radially oriented mesochannels. FESEM images showing (d) spherical face, (e) side face, and (f) sectional face. Scale bars are 100 nm (a, b) and 50 nm (c–f).[92]

The morphology of PDA bowl-shaped mesoporous nanoparticles obtained using this method was confirmed by field-emission scanning electron microscopy (FESEM) and transmission electron microscopy (TEM). As observed in Figure 1.11, the size of the bowl-shaped mesoporous nanoparticles was around 200 nm with around 70 nm curvature (Figure 1.11). Close observation of the particles in TEM imaging further reveals that the mesochannels are arranged radially from the center to the surface of the particles. The estimated total length of the mesochannels is around 21 nm, and the diameter of the mesopores is around 11 nm (Figure 1.11).

1.4 Conclusions

Over the last few decades, shape anisotropic particles have drawn enormous attention from researchers due to their enhanced physical, chemical, and biological properties in comparison with their isotropic counterparts. Therefore, various shapes of anisotropic particles of various materials including inorganics, metals, and polymers have been synthesized and applied in a wide range of biomedical fields. Herein, the potential of various types of anisotropic particles as drug carriers is discussed, emphasizing advantages of their anisotropic shape in terms of their efficiency in drug delivery systems, and summarizing their commonly used formation methods. Considering the flexibility now possible in the formation methodology and biological performance of anisotropic particles of various materials, polymeric anisotropic particles have gained additional research attention because of their exceptionally tailorable properties including shape and size, surface functionalization, simple fabrication methods, etc.

Consequently, a wide variety of anisotropically shaped biocompatible polymeric particles has been synthesized over recent years. Among the available polymer chemistries, polydopamine (PDA) offers a number of key advantages. It is a naturally inspired biopolymer with desirable properties such as excellent biodegradability, biocompatibility, and capability of loading and releasing drug molecules, making it suitable for drug delivery applications. Moreover, it has a highly efficient photothermal response under near infrared (NIR) illumination, which means it has the ability to convert radiation into thermal energy. Considering the advantages of cup/bowl-shaped particles, and the applicability of polydopamine in drug delivery systems, polydopamine bowl-shaped mesoporous nanoparticles (PDA nanobowls) in particular have the potential to overcome current limitations of drug nanocarriers for various treatments including cancer.

The following Thesis focuses on investigating the potential of PDA nanobowls as an efficient drug nanocarrier by investigating their cellular internalization behavior and intracellular fate. Another interesting property of PDA nanobowls as a Pickering stabilizer to produce a novel drug delivery modality in the form of photothermally responsive phase change Pickering emulsions is also explored.

To better understand the potential for PDA bowls to be utilized in drug delivery, various investigations were conducted. In Chapter 2, PDA nanobowls and spherical PDA nanoparticles with similar sizes were synthesized and characterized with an aim to understand the cellular internalization behavior of shape-dependent PDA nanoparticles in cervical cancer cells (HeLa cells). In Chapter 3, various sizes of monodisperse PDA nanobowls were synthesized by

systematically modifying each reaction parameter. *In vitro* studies were conducted to investigate their size-dependent cellular internalization behavior and endocytosis pathways in HeLa cells. Building on this, in Chapter 4, applicability of PDA nanobowls in cancer therapy to combat multi-drug resistance was investigated. Herein, photothermal conversion efficiency and drug loading and release efficiency of PDA nanobowls were explored, which showed potential against multi-drug resistance of cancer treatments, as the PDA bowls can be used as combined chemo- and photothermal therapeutic agents. In Chapter 5, another interesting property of PDA nanobowls was explored, showing that they have the capability to stabilize Pickering emulsion without any additional surfactant. Taking advantage of the photothermal response of PDA nanobowls, stimuli-responsive Pickering emulsions were formed for NIR-triggered drug release applications.

1.5 References

(1) Polarz, S. Shape Matters: Anisotropy of the Morphology of Inorganic Colloidal Particles – Synthesis and Function. *Advanced Functional Materials* **2011,** *21*, 3214-3230, DOI: 10.1002/adfm.201101205.
(2) Kohout, C.; Santi, C.; Polito, L. Anisotropic Gold Nanoparticles in Biomedical Applications. *Int J Mol Sci* **2018,** *19* (11), 3385, DOI: 10.3390/ijms19113385.
(3) Pearce, A. K.; Wilks, T. R.; Arno, M. C.; O'Reilly, R. K. Synthesis and applications of anisotropic nanoparticles with precisely defined dimensions. *Nature Reviews Chemistry* **2021,** *5* (1), 21-45, DOI: 10.1038/s41570-020-00232-7.
(4) Arno, M. C.; Inam, M.; Weems, A. C.; Li, Z.; Binch, A. L. A.; Platt, C. I.; Richardson, S. M.; Hoyland, J. A.; Dove, A. P.; O'Reilly, R. K. Exploiting the role of nanoparticle shape in enhancing hydrogel adhesive and mechanical properties. *Nature Communications* **2020,** *11* (1), 1420, DOI: 10.1038/s41467-020-15206-y.
(5) Potenza, M. A. C.; Albani, S.; Delmonte, B.; Villa, S.; Sanvito, T.; Paroli, B.; Pullia, A.; Baccolo, G.; Mahowald, N.; Maggi, V. Shape and size constraints on dust optical properties from the Dome C ice core, Antarctica. *Scientific Reports* **2016,** *6* (1), 28162, DOI: 10.1038/srep28162.
(6) Sajanlal, P. R.; Sreeprasad, T. S.; Samal, A. K.; Pradeep, T. Anisotropic nanomaterials: structure, growth, assembly, and functions. *Nano Rev* **2011,** *2*, 10.3402/nano.v2i0.5883, DOI: 10.3402/nano.v2i0.5883.

(7) Burrows, N. D.; Vartanian, A. M.; Abadeer, N. S.; Grzincic, E. M.; Jacob, L. M.; Lin, W.; Li, J.; Dennison, J. M.; Hinman, J. G.; Murphy, C. J. Anisotropic Nanoparticles and Anisotropic Surface Chemistry. *The Journal of Physical Chemistry Letters* **2016,** *7* (4), 632-641, DOI: 10.1021/acs.jpclett.5b02205.
(8) Chen, C.; Xie, L.; Wang, Y. Recent advances in the synthesis and applications of anisotropic carbon and silica-based nanoparticles. *Nano Research* **2019,** *12* (6), 1267-1278, DOI: 10.1007/s12274-019-2324-9.
(9) Yang, L.; Zhou, Z.; Song, J.; Chen, X. Anisotropic nanomaterials for shape-dependent physicochemical and biomedical applications. *Chemical Society Reviews* **2019,** *48* (19), 5140-5176, DOI: 10.1039/C9CS00011A.
(10) Acter, S.; Cho, J.; Kim, J. W.; Byun, A.; Park, K.-H.; Kim, J. W. Synthesis and Shape Control of Uniform Polymer Microparticles by Tailored Adsorption of Poly(ethylene oxide)-b-Poly(ε-caprolactone) Copolymer. *Bulletin of the Korean Chemical Society* **2015,** *36* (5), 1467-1473, DOI: https://doi.org/10.1002/bkcs.10288.
(11) Gratton, S. E. A.; Ropp, P. A.; Pohlhaus, P. D.; Luft, J. C.; Madden, V. J.; Napier, M. E.; DeSimone, J. M. The effect of particle design on cellular internalization pathways. *Proceedings of the National Academy of Sciences* **2008,** *105* (33), 11613, DOI: 10.1073/pnas.0801763105.
(12) Sabourian, P.; Yazdani, G.; Ashraf, S. S.; Frounchi, M.; Mashayekhan, S.; Kiani, S.; Kakkar, A. Effect of Physico-Chemical Properties of Nanoparticles on Their Intracellular Uptake. *Int J Mol Sci* **2020,** *21* (21), DOI: 10.3390/ijms21218019.
(13) Lin, J.; Miao, L.; Zhong, G.; Lin, C.-H.; Dargazangy, R.; Alexander-Katz, A. Understanding the synergistic effect of physicochemical properties of nanoparticles and their cellular entry pathways. *Communications Biology* **2020,** *3* (1), 205, DOI: 10.1038/s42003-020-0917-1.
(14) Wang, Z.; Wu, Z.; Liu, J.; Zhang, W. Particle morphology: an important factor affecting drug delivery by nanocarriers into solid tumors. *Expert opinion on drug delivery* **2018,** *15* (4), 379-395, DOI: 10.1080/17425247.2018.1420051.
(15) Paramasivam, G.; Kayambu, N.; Rabel, A. M.; Sundramoorthy, A. K.; Sundaramurthy, A. Anisotropic noble metal nanoparticles: Synthesis, surface functionalization and applications in biosensing, bioimaging, drug delivery and theranostics. *Acta Biomaterialia* **2017,** *49*, 45-65, DOI: https://doi.org/10.1016/j.actbio.2016.11.066.
(16) Meyer, R. A.; Green, J. J. Shaping the future of nanomedicine: anisotropy in polymeric nanoparticle design. *Wiley Interdiscip Rev Nanomed Nanobiotechnol* **2016,** *8* (2), 191-207, DOI: 10.1002/wnan.1348.
(17) Ortiz-Castillo, J. E.; Gallo-Villanueva, R. C.; Madou, M. J.; Perez-Gonzalez, V. H. Anisotropic gold nanoparticles: A survey of recent synthetic methodologies. *Coordination Chemistry Reviews* **2020,** *425*, 213489, DOI: https://doi.org/10.1016/j.ccr.2020.213489.
(18) Xu, M.; Song, Y.; Wang, J.; Li, N. Anisotropic transition metal–based nanomaterials for biomedical applications. *View* **2021**, DOI: 10.1002/viw.20200154.
(19) Chen, Y.; Xu, P.; Wu, M.; Meng, Q.; Chen, H.; Shu, Z.; Wang, J.; Zhang, L.; Li, Y.; Shi, J. Colloidal RBC-Shaped, Hydrophilic, and Hollow Mesoporous Carbon Nanocapsules for Highly Efficient Biomedical Engineering. *Advanced Materials* **2014,** *26* (25), 4294-4301, DOI: https://doi.org/10.1002/adma.201400303.
(20) Hosseinidoust, Z.; Basnet, M.; van de Ven, T. G. M.; Tufenkji, N. One-pot green synthesis of anisotropic silver nanoparticles. *Environmental Science: Nano* **2016,** *3* (6), 1259-1264, DOI: 10.1039/C6EN00112B.
(21) Li, N.; Zhao, P.; Astruc, D. Anisotropic Gold Nanoparticles: Synthesis, Properties, Applications, and Toxicity. *Angewandte Chemie International Edition* **2014,** *53* (7), 1756-1789, DOI: https://doi.org/10.1002/anie.201300441.
(22) Das, M.; Shim, K. H.; An, S.; Yi, D. Review on gold nanoparticles and their applications. *Toxicology and Environmental Health Sciences* **2012,** *3*, DOI: 10.1007/s13530-011-0109-y.

(23) Xie, J.; Lee, J. Y.; Wang, D. I. C. Seedless, Surfactantless, High-Yield Synthesis of Branched Gold Nanocrystals in HEPES Buffer Solution. *Chemistry of Materials* **2007,** *19* (11), 2823-2830, DOI: 10.1021/cm0700100.
(24) Sau, T. K.; Murphy, C. J. Seeded High Yield Synthesis of Short Au Nanorods in Aqueous Solution. *Langmuir* **2004,** *20* (15), 6414-6420, DOI: 10.1021/la049463z.
(25) Liao, J.; Li, W.; Peng, J.; Yang, Q.; Li, H.; Wei, Y.; Zhang, X.; Qian, Z. Combined cancer photothermal-chemotherapy based on doxorubicin/gold nanorod-loaded polymersomes. *Theranostics* **2015,** *5* (4), 345-56, DOI: 10.7150/thno.10731.
(26) Zhang, P.; He, J.; Ma, X.; Gong, J.; Nie, Z. Ultrasound assisted interfacial synthesis of gold nanocones. *Chemical Communications* **2013,** *49* (10), 987-989, DOI: 10.1039/C2CC37713F.
(27) Scarabelli, L.; Coronado-Puchau, M.; Giner-Casares, J. J.; Langer, J.; Liz-Marzán, L. M. Monodisperse Gold Nanotriangles: Size Control, Large-Scale Self-Assembly, and Performance in Surface-Enhanced Raman Scattering. *ACS Nano* **2014,** *8* (6), 5833-5842, DOI: 10.1021/nn500727w.
(28) Park, J.-E.; Lee, Y.; Nam, J.-M. Precisely Shaped, Uniformly Formed Gold Nanocubes with Ultrahigh Reproducibility in Single-Particle Scattering and Surface-Enhanced Raman Scattering. *Nano Letters* **2018,** *18* (10), 6475-6482, DOI: 10.1021/acs.nanolett.8b02973.
(29) Zhang, L.; Jang, H. J.; Yoo, S.; Cho, S.; Won, J. H.; Liu, L.; Park, S. Synthesis of octahedral gold tip-blobbed nanoparticles and their dielectric sensing properties. *Nanotechnology* **2018,** *29* (37), 375602, DOI: 10.1088/1361-6528/aace99.
(30) Ha, T. H.; Koo, H.-J.; Chung, B. H. Shape-Controlled Syntheses of Gold Nanoprisms and Nanorods Influenced by Specific Adsorption of Halide Ions. *The Journal of Physical Chemistry C* **2007,** *111* (3), 1123-1130, DOI: 10.1021/jp066454l.
(31) Pérez-Page, M.; Yu, E.; Li, J.; Rahman, M.; Dryden, D. M.; Vidu, R.; Stroeve, P. Template-based syntheses for shape controlled nanostructures. *Advances in colloid and interface science* **2016,** *234*, 51-79, DOI: 10.1016/j.cis.2016.04.001.
(32) Yang, T.-H.; Shi, Y.; Janssen, A.; Xia, Y. Surface Capping Agents and Their Roles in Shape-Controlled Synthesis of Colloidal Metal Nanocrystals. *Angewandte Chemie International Edition* **2020,** *59* (36), 15378-15401, DOI: https://doi.org/10.1002/anie.201911135.
(33) Herizchi, R.; Abbasi, E.; Milani, M.; Akbarzadeh, A. Current methods for synthesis of gold nanoparticles. *Artificial Cells, Nanomedicine, and Biotechnology* **2016,** *44* (2), 596-602, DOI: 10.3109/21691401.2014.971807.
(34) Scarabelli, L.; Sánchez-Iglesias, A.; Pérez-Juste, J.; Liz-Marzán, L. M. A "Tips and Tricks" Practical Guide to the Synthesis of Gold Nanorods. *The Journal of Physical Chemistry Letters* **2015,** *6* (21), 4270-4279, DOI: 10.1021/acs.jpclett.5b02123.
(35) Podlesnaia, E.; Csáki, A.; Fritzsche, W. Time Optimization of Seed-Mediated Gold Nanotriangle Synthesis Based on Kinetic Studies. *Nanomaterials (Basel)* **2021,** *11* (4), 1049, DOI: 10.3390/nano11041049.
(36) Wei, M.-Z.; Deng, T.-S.; Zhang, Q.; Cheng, Z.; Li, S. Seed-Mediated Synthesis of Gold Nanorods at Low Concentrations of CTAB. *ACS Omega* **2021,** *6* (13), 9188-9195, DOI: 10.1021/acsomega.1c00510.
(37) Hu, Y. S.; Jeon, J.; Seok, T. J.; Lee, S.; Hafner, J. H.; Drezek, R. A.; Choo, H. Enhanced Raman Scattering from Nanoparticle-Decorated Nanocone Substrates: A Practical Approach to Harness In-Plane Excitation. *ACS Nano* **2010,** *4* (10), 5721-5730, DOI: 10.1021/nn101352h.
(38) Kim, T.-i.; Kim, J.-h.; Son, S. J.; Seo, S.-m. Gold nanocones fabricated by nanotransfer printing and their application for field emission. *Nanotechnology* **2008,** *19* (29), 295302, DOI: 10.1088/0957-4484/19/29/295302.
(39) Kontio, J. M.; Husu, H.; Simonen, J.; Huttunen, M. J.; Tommila, J.; Pessa, M.; Kauranen, M. Nanoimprint fabrication of gold nanocones with ~10 nm tips for enhanced optical interactions. *Opt. Lett.* **2009,** *34* (13), 1979-1981, DOI: 10.1364/OL.34.001979.
(40) Mijatovic, D.; Eijkel, J. C. T.; van den Berg, A. Technologies for nanofluidic systems: top-down vs. bottom-up—a review. *Lab on a Chip* **2005,** *5* (5), 492-500, DOI: 10.1039/B416951D.

(41) Nehl, C. L.; Hafner, J. H. Shape-dependent plasmon resonances of gold nanoparticles. *Journal of Materials Chemistry* **2008,** *18* (21), 2415-2419, DOI: 10.1039/B714950F.
(42) Hua, Y.; Chandra, K.; Dam, D. H. M.; Wiederrecht, G. P.; Odom, T. W. Shape-Dependent Nonlinear Optical Properties of Anisotropic Gold Nanoparticles. *The Journal of Physical Chemistry Letters* **2015,** *6* (24), 4904-4908, DOI: 10.1021/acs.jpclett.5b02263.
(43) Huang, X.; El-Sayed, M. A. Gold nanoparticles: Optical properties and implementations in cancer diagnosis and photothermal therapy. *Journal of Advanced Research* **2010,** *1* (1), 13-28, DOI: https://doi.org/10.1016/j.jare.2010.02.002.
(44) Xie, X.; Liao, J.; Shao, X.; Li, Q.; Lin, Y. The Effect of shape on Cellular Uptake of Gold Nanoparticles in the forms of Stars, Rods, and Triangles. *Scientific Reports* **2017,** *7* (1), 3827, DOI: 10.1038/s41598-017-04229-z.
(45) Li, J.; Li, J. E. J.; Zhang, J.; Wang, X.; Kawazoe, N.; Chen, G. Gold nanoparticle size and shape influence on osteogenesis of mesenchymal stem cells. *Nanoscale* **2016,** *8* (15), 7992-8007, DOI: 10.1039/C5NR08808A.
(46) Cho, E. C.; Au, L.; Zhang, Q.; Xia, Y. The effects of size, shape, and surface functional group of gold nanostructures on their adsorption and internalization by cells. *Small* **2010,** *6* (4), 517-522, DOI: 10.1002/smll.200901622.
(47) Nambara, K.; Niikura, K.; Mitomo, H.; Ninomiya, T.; Takeuchi, C.; Wei, J.; Matsuo, Y.; Ijiro, K. Reverse Size Dependences of the Cellular Uptake of Triangular and Spherical Gold Nanoparticles. *Langmuir* **2016,** *32* (47), 12559-12567, DOI: 10.1021/acs.langmuir.6b02064.
(48) Ray, P. C.; Yu, H.; Fu, P. P. Toxicity and environmental risks of nanomaterials: challenges and future needs. *J Environ Sci Health C Environ Carcinog Ecotoxicol Rev* **2009,** *27* (1), 1-35, DOI: 10.1080/10590500802708267.
(49) Alkilany, A. M.; Murphy, C. J. Toxicity and cellular uptake of gold nanoparticles: what we have learned so far? *J Nanopart Res* **2010,** *12* (7), 2313-2333, DOI: 10.1007/s11051-010-9911-8.
(50) Boisselier, E.; Astruc, D. Gold nanoparticles in nanomedicine: preparations, imaging, diagnostics, therapies and toxicity. *Chemical Society Reviews* **2009,** *38* (6), 1759-1782, DOI: 10.1039/B806051G.
(51) Alkilany, A. M.; Nagaria, P. K.; Hexel, C. R.; Shaw, T. J.; Murphy, C. J.; Wyatt, M. D. Cellular uptake and cytotoxicity of gold nanorods: molecular origin of cytotoxicity and surface effects. *Small* **2009,** *5* (6), 701-8, DOI: 10.1002/smll.200801546.
(52) Gumargalieva, K. Z.; Horak, D.; Zaikov, G. E. Biodegradable Polymeric Microparticles in Biomedical Applications. *International Journal of Polymeric Materials and Polymeric Biomaterials* **1998,** *42* (1-2), 83-117, DOI: 10.1080/00914039808041062.
(53) Xiao, Y.; Du, J. Superparamagnetic nanoparticles for biomedical applications. *Journal of Materials Chemistry B* **2020,** *8* (3), 354-367, DOI: 10.1039/C9TB01955C.
(54) Su, S.; Kang, P. M. Systemic Review of Biodegradable Nanomaterials in Nanomedicine. *Nanomaterials* **2020,** *10* (4), DOI: 10.3390/nano10040656.
(55) Wichaita, W.; Polpanich, D.; Tangboriboonrat, P. Review on Synthesis of Colloidal Hollow Particles and Their Applications. *Industrial & Engineering Chemistry Research* **2019,** *58* (46), 20880-20901, DOI: 10.1021/acs.iecr.9b02330.
(56) Williford, J.-M.; Santos, J. L.; Shyam, R.; Mao, H.-Q. Shape control in engineering of polymeric nanoparticles for therapeutic delivery. *Biomaterials Science* **2015,** *3* (7), 894-907, DOI: 10.1039/C5BM00006H.
(57) Elsabahy, M.; Heo, G. S.; Lim, S.-M.; Sun, G.; Wooley, K. L. Polymeric Nanostructures for Imaging and Therapy. *Chem Rev* **2015,** *115* (19), 10967-11011, DOI: 10.1021/acs.chemrev.5b00135.
(58) Siddique, S.; Chow, J. C. L. Application of Nanomaterials in Biomedical Imaging and Cancer Therapy. *Nanomaterials (Basel)* **2020,** *10* (9), DOI: 10.3390/nano10091700.
(59) Mirza, I.; Saha, S. Biocompatible Anisotropic Polymeric Particles: Synthesis, Characterization, and Biomedical Applications. *ACS Applied Bio Materials* **2020,** *3* (12), 8241-8270, DOI: 10.1021/acsabm.0c01075.

(60) Cao, J.; Choi, J.-S.; Oshi, M. A.; Lee, J.; Hasan, N.; Kim, J.; Yoo, J.-W. Development of PLGA micro- and nanorods with high capacity of surface ligand conjugation for enhanced targeted delivery. *Asian Journal of Pharmaceutical Sciences* **2019,** *14* (1), 86-94, DOI: https://doi.org/10.1016/j.ajps.2018.08.008.
(61) Tuntanatewin, W.; Tani, K.; Ishikura, K.; Zhang, H.; Okamura, Y. One-pot fabrication of polymer micro/nano-discs via phase separation and a roll-to-roll coating process. *Colloids and Surfaces A: Physicochemical and Engineering Aspects* **2020,** *586*, 124274, DOI: https://doi.org/10.1016/j.colsurfa.2019.124274.
(62) Li, W.; Suzuki, T.; Minami, H. A Facile Method for Preparation of Polymer Particles Having a "Cylindrical" Shape. *Angewandte Chemie International Edition* **2018,** *57* (31), 9936-9940, DOI: https://doi.org/10.1002/anie.201805700.
(63) Guan, B. Y.; Zhang, S. L.; Lou, X. W. Realization of Walnut-Shaped Particles with Macro-/Mesoporous Open Channels through Pore Architecture Manipulation and Their Use in Electrocatalytic Oxygen Reduction. *Angewandte Chemie International Edition* **2018,** *57* (21), 6176-6180, DOI: https://doi.org/10.1002/anie.201801876.
(64) Doshi, N.; Mitragotri, S. Needle-shaped polymeric particles induce transient disruption of cell membranes. *Journal of The Royal Society Interface* **2010,** *7* (suppl_4), S403-S410, DOI: 10.1098/rsif.2010.0134.focus.
(65) Jang, S. G.; Audus, D. J.; Klinger, D.; Krogstad, D. V.; Kim, B. J.; Cameron, A.; Kim, S.-W.; Delaney, K. T.; Hur, S.-M.; Killops, K. L.; Fredrickson, G. H.; Kramer, E. J.; Hawker, C. J. Striped, Ellipsoidal Particles by Controlled Assembly of Diblock Copolymers. *Journal of the American Chemical Society* **2013,** *135* (17), 6649-6657, DOI: 10.1021/ja4019447.
(66) Zhang, L.; Yang, P.; Guo, R.; Sun, J.; Xie, R.; Yang, W. Multifunctional Mesoporous Polydopamine With Hydrophobic Paclitaxel For Photoacoustic Imaging-Guided Chemo-Photothermal Synergistic Therapy. *Int J Nanomedicine* **2019,** *14*, 8647-8663, DOI: 10.2147/IJN.S218632.
(67) Liu, J.; Rasheed, A.; Dong, H.; Carr, W. W.; Dadmun, M. D.; Kumar, S. Electrospun Micro- and Nanostructured Polymer Particles. *Macromolecular Chemistry and Physics* **2008,** *209* (23), 2390-2398, DOI: https://doi.org/10.1002/macp.200800396.
(68) Palanikumar, L.; Al-Hosani, S.; Kalmouni, M.; Nguyen, V. P.; Ali, L.; Pasricha, R.; Barrera, F. N.; Magzoub, M. pH-responsive high stability polymeric nanoparticles for targeted delivery of anticancer therapeutics. *Communications Biology* **2020,** *3* (1), 95, DOI: 10.1038/s42003-020-0817-4.
(69) Kwan, J. J.; Myers, R.; Coviello, C. M.; Graham, S. M.; Shah, A. R.; Stride, E.; Carlisle, R. C.; Coussios, C. C. Ultrasound-Propelled Nanocups for Drug Delivery. *Small* **2015,** *11* (39), 5305-14, DOI: 10.1002/smll.201501322.
(70) Castro, K. C. d.; Costa, J. M.; Campos, M. G. N. Drug-loaded polymeric nanoparticles: a review. *International Journal of Polymeric Materials and Polymeric Biomaterials* **2020**, 1-13, DOI: 10.1080/00914037.2020.1798436.
(71) Li, H.; Zhang, W.; Tong, W.; Gao, C. Enhanced Cellular Uptake of Bowl-like Microcapsules. *ACS Applied Materials & Interfaces* **2016,** *8* (18), 11210-11214, DOI: 10.1021/acsami.6b02965.
(72) Sharma, G.; Valenta, D. T.; Altman, Y.; Harvey, S.; Xie, H.; Mitragotri, S.; Smith, J. W. Polymer particle shape independently influences binding and internalization by macrophages. *J Control Release* **2010,** *147* (3), 408-412, DOI: 10.1016/j.jconrel.2010.07.116.
(73) Shimoni, O.; Yan, Y.; Wang, Y.; Caruso, F. Shape-Dependent Cellular Processing of Polyelectrolyte Capsules. *ACS Nano* **2013,** *7* (1), 522-530, DOI: 10.1021/nn3046117.
(74) Chen, J.; Kozlovskaya, V.; Goins, A.; Campos-Gomez, J.; Saeed, M.; Kharlampieva, E. Biocompatible Shaped Particles from Dried Multilayer Polymer Capsules. *Biomacromolecules* **2013,** *14* (11), 3830-3841, DOI: 10.1021/bm4008666.
(75) Kim, J.-W.; Suh, K.-D. Monodisperse polymer particles synthesized by seeded polymerization techniques. *Journal of Industrial and Engineering Chemistry* **2008,** *14* (1), 1-9, DOI: https://doi.org/10.1016/j.jiec.2007.06.001.

(76) Gao, C.; Donath, E.; Moya, S.; Dudnik, V.; Möhwald, H. Elasticity of hollow polyelectrolyte capsules prepared by the layer-by-layer technique. *The European Physical Journal E* **2001,** *5* (1), 21-27, DOI: 10.1007/s101890170083.
(77) Hwang, J.; Choi, D.; Han, S.; Jung, S. Y.; Choi, J.; Hong, J. Potential toxicity of polystyrene microplastic particles. *Scientific reports* **2020,** *10* (1), 7391-7391, DOI: 10.1038/s41598-020-64464-9.
(78) Lin, Y.-S.; Haynes, C. L. Impacts of Mesoporous Silica Nanoparticle Size, Pore Ordering, and Pore Integrity on Hemolytic Activity. *Journal of the American Chemical Society* **2010,** *132* (13), 4834-4842, DOI: 10.1021/ja910846q.
(79) Liebscher, J.; Mrówczyński, R.; Scheidt, H. A.; Filip, C.; Hădade, N. D.; Turcu, R.; Bende, A.; Beck, S. Structure of Polydopamine: A Never-Ending Story? *Langmuir : the ACS journal of surfaces and colloids* **2013,** *29* (33), 10539-10548, DOI: 10.1021/la4020288.
(80) Sedo, J.; Saiz-Poseu, J.; Busque, F.; Ruiz-Molina, D. Catechol-based biomimetic functional materials. *Advanced materials (Deerfield Beach, Fla.)* **2013,** *25* (5), 653-701, DOI: 10.1002/adma.201202343.
(81) Liu, Y.; Ai, K.; Lu, L. Polydopamine and Its Derivative Materials: Synthesis and Promising Applications in Energy, Environmental, and Biomedical Fields. *Chemical Reviews* **2014,** *114* (9), 5057-5115, DOI: 10.1021/cr400407a.
(82) Mulyati, S.; Muchtar, S.; Arahman, N.; Syamsuddin, Y.; Mat Nawi, N. I.; Yub Harun, N.; Bilad, M. R.; Firdaus, Y.; Takagi, R.; Matsuyama, H. Two-Step Dopamine-to-Polydopamine Modification of Polyethersulfone Ultrafiltration Membrane for Enhancing Anti-Fouling and Ultraviolet Resistant Properties. *Polymers (Basel)* **2020,** *12* (9), 2051, DOI: 10.3390/polym12092051.
(83) Lee, H.; Dellatore, S. M.; Miller, W. M.; Messersmith, P. B. Mussel-Inspired Surface Chemistry for Multifunctional Coatings. *Science (New York, N.Y.)* **2007,** *318* (5849), 426-430, DOI: 10.1126/science.1147241.
(84) Zhang, L.; Shi, J.; Jiang, Z.; Jiang, Y.; Qiao, S.; Li, J.; Wang, R.; Meng, R.; Zhu, Y.; Zheng, Y. Bioinspired preparation of polydopamine microcapsule for multienzyme system construction. *Green Chemistry* **2011,** *13* (2), 300-306, DOI: 10.1039/C0GC00432D.
(85) Huang, Y.; Li, Y.; Hu, Z.; Yue, X.; Proetto, M. T.; Jones, Y.; Gianneschi, N. C. Mimicking Melanosomes: Polydopamine Nanoparticles as Artificial Microparasols. *ACS Central Science* **2017,** *3* (6), 564-569, DOI: 10.1021/acscentsci.6b00230.
(86) Ding, Y. H.; Floren, M.; Tan, W. Mussel-inspired polydopamine for bio-surface functionalization. *Biosurface and biotribology* **2016,** *2* (4), 121-136, DOI: 10.1016/j.bsbt.2016.11.001.
(87) Wang, Z.; Xie, Y.; Li, Y.; Huang, Y.; Parent, L. R.; Ditri, T.; Zang, N.; Rinehart, J. D.; Gianneschi, N. C. Tunable, Metal-Loaded Polydopamine Nanoparticles Analyzed by Magnetometry. *Chemistry of Materials* **2017,** *29* (19), 8195-8201, DOI: 10.1021/acs.chemmater.7b02262.
(88) Gu, G. E.; Park, C. S.; Cho, H.-J.; Ha, T. H.; Bae, J.; Kwon, O. S.; Lee, J.-S.; Lee, C.-S. Fluorescent polydopamine nanoparticles as a probe for zebrafish sensory hair cells targeted in vivo imaging. *Scientific Reports* **2018,** *8* (1), 4393, DOI: 10.1038/s41598-018-22828-2.
(89) Lynge, M. E.; van der Westen, R.; Postma, A.; Stadler, B. Polydopamine--a nature-inspired polymer coating for biomedical science. *Nanoscale* **2011,** *3* (12), 4916-28, DOI: 10.1039/c1nr10969c.
(90) Pahuja, R.; Seth, K.; Shukla, A.; Shukla, R. K.; Bhatnagar, P.; Chauhan, L. K.; Saxena, P. N.; Arun, J.; Chaudhari, B. P.; Patel, D. K.; Singh, S. P.; Shukla, R.; Khanna, V. K.; Kumar, P.; Chaturvedi, R. K.; Gupta, K. C. Trans-blood brain barrier delivery of dopamine-loaded nanoparticles reverses functional deficits in parkinsonian rats. *ACS nano* **2015,** *9* (5), 4850-71, DOI: 10.1021/nn506408v.
(91) Luo, H.; Gu, C.; Zheng, W.; Dai, F.; Wang, X.; Zheng, Z. Facile synthesis of novel size-controlled antibacterial hybrid spheres using silver nanoparticles loaded with poly-dopamine spheres. *RSC Advances* **2015,** *5* (18), 13470-13477, DOI: 10.1039/C4RA16469E.
(92) Guan, B. Y.; Yu, L.; Lou, X. W. Formation of Asymmetric Bowl-Like Mesoporous Particles via Emulsion-Induced Interface Anisotropic Assembly. *Journal of the American Chemical Society* **2016,** *138* (35), 11306-11311, DOI: 10.1021/jacs.6b06558.

(93) Wu, X.; Jiang, Q.; Ghim, D.; Singamaneni, S.; Jun, Y.-S. Localized heating with a photothermal polydopamine coating facilitates a novel membrane distillation process. *Journal of Materials Chemistry A* **2018,** *6* (39), 18799-18807, DOI: 10.1039/C8TA05738A.
(94) Zhu, Z.; Su, M. Polydopamine Nanoparticles for Combined Chemo- and Photothermal Cancer Therapy. *Nanomaterials (Basel)* **2017,** *7* (7), DOI: 10.3390/nano7070160.
(95) Nishizawa, N.; Kawamura, A.; Kohri, M.; Nakamura, Y.; Fujii, S. Polydopamine Particle as a Particulate Emulsifier. *Polymers (Basel)* **2016,** *8* (3), DOI: 10.3390/polym8030062.
(96) Xu, J.; Ma, A.; Liu, T.; Lu, C.; Wang, D.; Xu, H. Janus-like Pickering emulsions and their controllable coalescence. *Chemical Communications* **2013,** *49* (92), 10871-10873, DOI: 10.1039/C3CC46738D.

Chapter 2

Efficient Cellular Internalization and Transport of Bowl-Shaped Polydopamine Particles

This Chapter was published as: **Shahinur Acter**, Mark Louis P. Vidallon, Simon Crawford, Rico F. Tabor, and Boon Mian Teo,* *Particle & Particle Systems Characterization* **2020**, 2000166.

Preface for Chapter 2

In this Chapter, bowl-shaped mesoporous nanoparticles were synthesized through an emulsion-induced anisotropic interfacial assembly strategy carried out at room temperature with mild stirring. Various characterization techniques were applied to characterize the synthesized nanoparticles including Fourier transform infrared spectrometry (FT-IR), dynamic light scattering (DLS), zeta potential, transmission electron microscopy (TEM), and scanning electron microscopy (SEM). Cellular internalization behavior of different shapes of polydopamine nanoparticles with similar diameter was investigated in cervical cancer (HeLa) cells. A set of characterization techniques, including flow cytometry, confocal imaging, and TEM imaging analysis were used to understand cellular uptake efficiency and intracellular trafficking of various shapes of polydopamine nanoparticle in HeLa cells, indicating the role of particle shape in endocytosis.

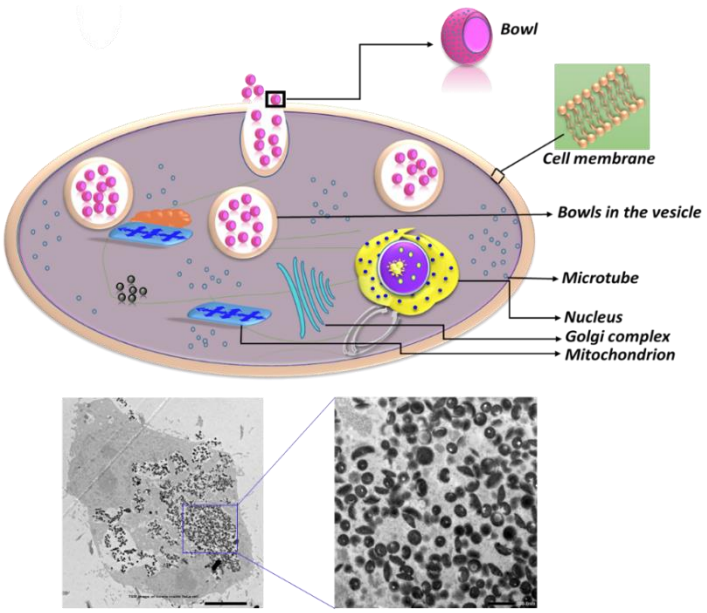

Abstract

In drug delivery applications, particle-based systems have been used widely due to their physicochemical properties such as size, shape, and surface charge to achieve desirable properties in intracellular environments. The way in which nanoparticles enter a biological cell is an important factor in determining their efficacy as drug carriers, their biodistribution, and toxicity. Most research thus far has focused on the comparison of spherical and rod-like particles on cellular internalization and transport. Here, the synthesis of bowl-shaped polydopamine (PDA) mesoporous nanoparticles with an average diameter of 200 nm and well-controlled radially oriented mesochannels are reported. By incubating bowl-shaped PDA nanoparticles and spherical nanoparticles with HeLa cells, their internalization behaviors are investigated using a suite of characterization techniques. Extensive experimental results demonstrate that bowl-shaped PDA nanoparticles adhere to the cell more efficiently and a faster rate of cellular uptake of bowl shaped nanoparticles compared to their spherical counterparts. Overall, the cellular internalization behavior of particles is shape-dependent, and such information is crucial in designing nanoparticles for biomedical applications.

2.1 Introduction

Rapid development in the field of nanotechnology has fuelled research interest in the use of nanoparticles as drug carriers due to their versatility and tunable properties.[1-4] However, one significant obstacle in the field of nanomedicine has been the inability of nanoparticulate carriers to cross the plasma membranes of cells.[5] Cell membranes provide a boundary between the interior of a cell and its surroundings to maintain crucial activities that are critical for the functioning of different cell types.[5-6] While the amphiphilic nature of biological membranes provides a highly selective barrier to permit a range of molecules to enter the cell by passive diffusion, entry is also regulated through other mechanisms such as channels, receptors or transporters.[5-8] For nanoparticulate drug carriers, their entry into cells is a crucial step in achieving high therapeutic efficacy. Understanding the intracellular fate of such systems is critical to their success, as these nanocarriers are intended for delivery of specific therapeutic molecules to the cytosol, nucleus or other specific intracellular sites.[9-11] Apart from their interactions with cell membranes, the understanding of nanoparticulates cellular uptake is crucial in designing efficient nanomedicines by tuning their physicochemical properties to optimize cellular uptake mechanisms.[12-13]

Structural features of nanoparticle based carriers that can have a pronounced effect on cellular uptake include size, shape, and surface chemistry.[14-15] While the size and surface chemistry of nanoparticulate carriers have been well investigated, shape-dependent study of particles has also gained increased attention in recent years.[16-18] The cellular internalization process of particles is known as endocytosis, and is dominated by four main mechanisms:

clathrin-mediated endocytosis (CME), caveolae-dependent endocytosis, macropinocytosis and phagocytosis (Figure 2.1).[9, 19]

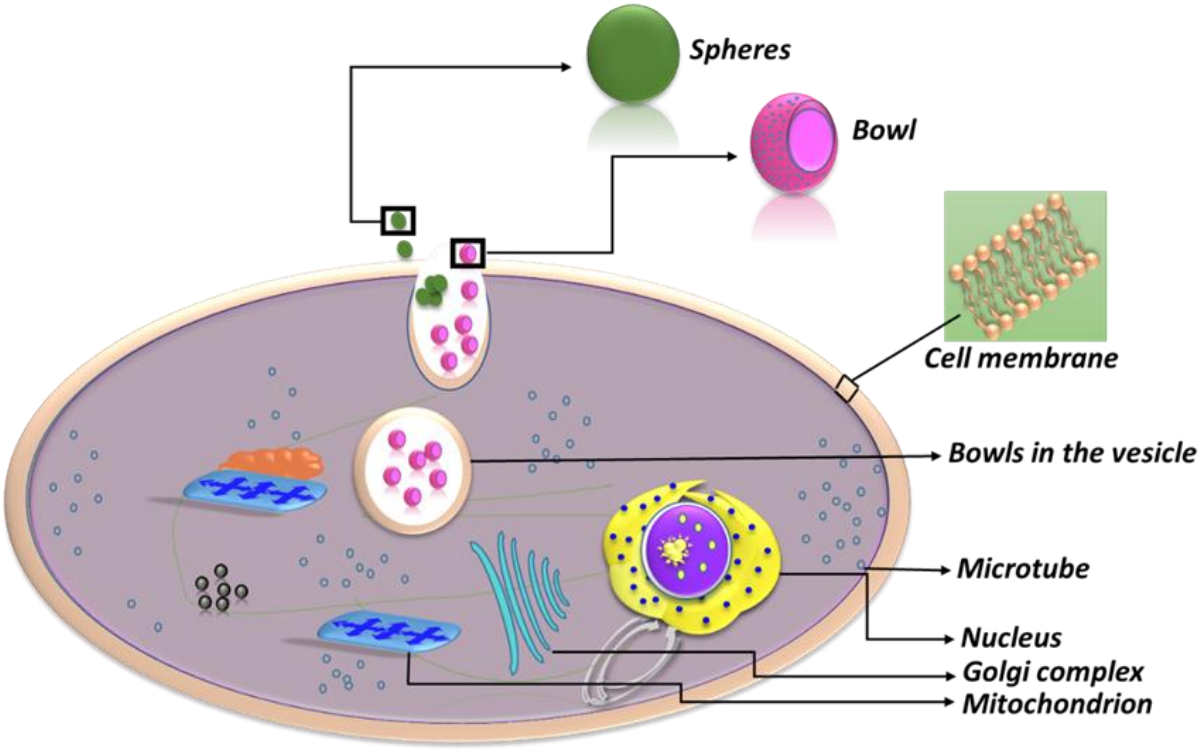

Figure 2.1. Schematic diagram showing cellular internalization of bowl-shaped and spherical nanoparticles.

Recent studies demonstrated a faster cellular uptake of anisotropic particles, such as rod-shaped, triangle-shaped, star-shaped, and bowl-shaped particles, when compared to regular spherical particles.[17, 20-21] It has been suggested that due to higher aspect ratio and sharper angular attributes, rods and tubes show a higher cellular uptake efficiency in relation to spherical particles because of their different cellular interactions.[16, 22] Most studies in this area of research have focused on the investigation of rod-shaped particles and their cellular interactions. To the best of our knowledge, there is a paucity of research on cellular interactions with bowl- or cup-shaped nanoparticles. Studying the interactions of bowl- or

cup-shaped particles is important, as several papers have highlighted the use of such particles for ultrasound-mediated drug delivery systems.[23-24]

Most studies have utilized polymeric gold nanoparticles and in particular, polymeric nanoparticulate systems in their cell research and bio-related applications.[25-26] Polymeric nanoparticles are particularly useful as they can easily entrap therapeutic agents within their core, and along with the ease of functionalization with other molecules such as targeting moieties on their surfaces.[27-28] In recent years, mussel inspired polydopamine (PDA) has gained much research interest in the field of nanomedicine.[29-33]

PDA is a naturally-inspired polymer, which is the result of the oxidant-induced polymerization of dopamine in a slightly elevated pH environment.[34] It is assumed that in the first step of the reaction, the indole skeleton is formed by oxidative ring closure, and then monomer units are connected by dehydrogenative C-C bond formation. One of the biggest advantages of PDA is the opportunity for facile functionalization, as it has carbonyl moieties, which act as electrophilic sites for amino- or mercapto-nucleophiles.[35-38] Due to its excellent biocompatibility and versatile properties, PDA has attracted considerable interest in application as a coating material for colloidal particles of diverse surface composition for various types of biomedical applications.[39-43] Recent studies have demonstrated that PDA can be used for biosensing applications by formation of PDA films on electrodes.[44-45] It has been also observed that PDA-coated gold nanoparticles show remarkable stability in vivo for a period of at least six weeks.[46] Moreover, PDA offers flexibility in terms of a high degree of control in shape and size, with favorable thermal stability, all of which offers opportunities

for the formation of different shaped particles including spherical, bowl-shaped, and walnut-shaped particles in different sizes.[47-49]

Herein, we have utilized an emulsion-induced interface anisotropic assembly method to fabricate bowl-shaped PDA mesoporous nanoparticles. The size of the cavity and internal structure (mesoporous) of the particles can be controlled by simply adjusting the concentration of trimethylbenzene (TMB), surfactant, and dopamine.[48] The cellular uptake behaviors of PDA bowl-shaped mesoporous nanoparticles and spherical nanoparticles by HeLa cells were compared. The synthesized PDA bowls and spheres showed negligible cytotoxicity in HeLa cells. We also demonstrated visualization of PDA bowls and spheres following internalization by HeLa cells using CLSM and TEM imaging techniques. Taken together, our results point to a faster cellular internalization behavior of bowl-shaped PDA nanoparticles.

2.2 Experimental Section

2.2.1 Materials

Dopamine hydrochloride,Trimethylbenzene (TMB, 98%), Pluronic® F-127, Fetal bovine serum (FBS, Gibco), Phosphate-buffered saline (PBS), Antibiotic-Antimycotic (100X), Paraformaldehyde (PFA), Cell Proliferation Kit I (MTT) and 4´, 6-diamidino-2-phenylindole (DAPI) were purchased from Sigma-Aldrich. Ammonia solution was from Ajax Finechem Pty., and ethanol 96% was from Univa. Other materials were Dulbecco's Modified Eagle's Medium

(DMEM, Life Science) and trypsin (0.25%, Merck). All reagents were used as received, without further purification.

2.2.2 Characterization of PDA nanoparticles

Fourier Transform Infrared (FTIR) spectra were obtained using a Cary 630 FTIR Spectrometer. Field-emission scanning electron microscopy (FEI Magellan 400 FEG SEM) and transmission electron microscopy (TEM, FEI Tecnai G2 T20 electron microscope under 200kv, using LaB6 emitter) were used to examine the size and morphology of the particles. Hydrodynamic diameters and zeta potential of the particles were determined using dynamic light scattering (DLS) and phase analysis light scattering (PALS) respectively, using a Brookhaven NanoBrook Omni particle sizer and zeta potential analyzer. Fluorescence absorption and emission spectra of samples were recorded using a Varian Cary Eclipse Fluorescence spectrophotometer in 1 cm quartz cuvettes.

2.2.3 Fabrication of PDA spheres

PDA nanospheres were synthesized using a typical reaction method.[50] Briefly, 30 mL of DI water was mixed with ethanol (13.33 mL) at room temperature, and aqueous ammonia (NH_4OH, 3.33 mL, 28%) was added into the abovementioned solution with mild stirring for 30 min. Thereafter, 0.166 g of dopamine hydrochloride was dissolved in 3.33 mL of DI water and then added to the reaction mixture while stirring and the reaction was allowed to proceed for 30 h. PDA nanoparticles were obtained by centrifugation and washed with water three times

followed by freeze-dried for further use. The desired size of the PDA nanospheres was achieved by adjusting the concentration of aqueous solution of ammonia.[50]

2.2.4 Synthesis of PDA bowls

Fabrication of PDA bowls was done via an emulsion-induced interface anisotropic assembly,[48] Briefly, 1.5% (w/v) of dopamine hydrochloride and 1.0% (w/v) of Pluronic® F127, were dissolved in 1:1 water and ethanol mixture with a total volume of 10 mL. Afterward, 2.0% (v/v) of TMB was added under stirring, followed by the formation of emulsion by ultra-sonication for 2 min. In the emulsion system, 3.75% (v/v) of ammonia (NH_4OH, 28%) solution was added dropwise to achieve slightly alkaline pH for the reaction to proceed. After 2 h, the synthesized nanoparticles were centrifuged for three times with water and ethanol. Subsequently, re-dispersed in 10 mL of (1:1) water ethanol mixture. To increase particle stability, the particle solution was heated in a sealed Teflon-lined autoclave (20 mL incapacity) at 100 °C for 24 h.

2.2.5 Fluorophore modification of PDA bowls and spheres

For in situ fluorophore modification, PDA bowls and spheres were coated with Rhodamine 6G (Rh 6G) following a previous method.[51] The concentration of the dye was adjusted to obtained similar fluorescence intensity in both shaped particles.

2.2.6 Cell culture

HeLa cells (human cervical cancer epithelial cells) were cultured at 37 °C under a humidified incubator with 5% CO_2 in DMEM medium supplemented with 10% FBS and 1% P/S.

2.2.7 In *vitro* cytotoxicity assay of PDA nanoparticles

Cell viability of the synthesized nanoparticles was determined using a 3-(4, 5-dimethylthiazol-2-yl)-2, 5-diphenyltetrazolium bromide (MTT) cell viability assay.[52] HeLa cells were first seeded at a density of 2×10^4 cells/mL in a 96-well plate with a volume of 50 µL in each well and left to adhere for 24 h at 37 °C and 5% CO_2. The assay was conducted in triplicates with PDA nanoparticles at varying concentrations (150, 250, and 500 µg/mL) for different time intervals (4, 24, and 48 h) at 37 °C and 5% CO_2. After the desired incubation time, the absorbance at 550 nm was recorded using a CLARIOstar microplate reader (BMG Labtech, VIC, Australia). The absorbance value of the control (untreated cells) was set at 100%, and cell proliferation was expressed as a percentage of control.

2.2.8 Flow cytometry

HeLa cells (4×10^5 cells/mL) were seeded in individual 25 mL culture flask and incubated for 24 h prior to the addition of particles. PDA bowls and spheres were added (250 µg/mL, 1000 µL) in the flask for different time intervals (4, 24, and 48 h). Subsequently, the samples were washed using three centrifugation/redispersion cycles (1200 rpm, 5 min in 1x PBS buffer solution). The supernatant was removed and 340 µL of 1x PBS was added to the aliquots for

flow cytometry analysis using flow core analysis technique (BD LSR II, LSR2a analyzer with YG585 detector).

2.2.9 Confocal imaging of HeLa cells

HeLa cells were seeded ($2x10^4$ cells/mL) on coverslip into 6-well plate and left to adhere for 24 h at 37 °C and 5% CO_2. Subsequently, PDA bowls and spheres were added (250 µg/mL, 500 µL) in each well for an incubation time of 48 h at 37 °C and 5% CO_2. After this incubation period, cells were fixed with 4% PFA for 10 min and counterstained with 0.7 µg/mL of DAPI for 10 min in dark. Fixed cells in 1X PBS were imaged using confocal laser scanning microscopy (CLSM) (Nikon C1 Upright Confocal Microscope) (60x objective, DAPI: laser 405.0 (emission: 433-468), TRITIC: laser 561.0 (for Rh 6G) (emission: 568-643). All images were acquired through Leica LSX software, then false-colored and merged using ImageJ.

2.2.10 TEM imaging of HeLa cells

Under the same experimental condition as for confocal imaging, cell samples were prepared for TEM analysis. For TEM imaging, the cell samples were centrifuged in 1.5 mL Eppendorf tubes at 10,000 rpm for 3 min. The supernatant was removed and the cells were fixed in 2.5% glutaraldehyde, 2% paraformaldehyde, and 0.075% ruthenium red in 0.1 **M** sodium cacodylate buffer for 2 h at room temperature. The fixative was removed by washing the cells three times for 15 min using 0.1 M sodium cacodylate buffer. Cells were postfixed in 1% osmium tetroxide in buffer for 1 hour at room temperature and then rinsed in milli-Q water

three times for 15 min. Cell pellets were embedded in molten 4% agarose and the agarose allowed to set at 4 ^{o}C for 60 min. The agarose plugs were removed from Eppendorf tubes, and dissected into 1 mm squares. Cells in agarose were then dehydrated by incubating in increasing concentrations of ethanol for 15 min with each step, consisting of 30%, 50%, 70%, 90%, and 100% ethanol (x2). The 100% ethanol was substituted with propylene oxide by incubating for 30 min in 100% propylene oxide. Cell pellets were incubated in a mixture of Epon resin and propylene oxide at a ratio of 1:1 for 6 h at room temperature, followed by a 2:1 Epon/propylene oxide mixture overnight. Cells were incubated in 100% freshly made Epon resin for 6 h, and a second change of 100% resin overnight. The embedded cell pellets were placed into Beem capsules with fresh resin and then the resin was polymerized for 48 h in an oven at 60 ^{o}C. Resin embedded cell pellets were sectioned with a diatom diamond knife using a Leica UCS ultramicrotome. Sections of thickness 80 to 90 nm were collected onto formvar-coated 100 mesh copper grids and stained with lead citrate for 8 min. The sections were imaged in a JEOL 1400 Plus transmission electron microscope at 80kv, and images of cells captured with a digital camera at a resolution of 2k x 2k.

2.3 Results and discussion

To compare the cellular internalization behavior of nanoparticles with different shapes, we prepared PDA spherical-shaped and bowl-shaped nanoparticles. Monodispersed PDA spherical-shaped nanoparticles or spheres were synthesized through a facile process carried out at room temperature with mild stirring.[50] Note that it is important to allow the reaction to run to completion to obtain uniformity of the final products.[50] Here, we also found that

mild stirring plays a key role in obtaining monodisperse particles. The PDA spheres are approximately 200 nm in diameter and are monodispersed as presented in the scanning electron microscope (SEM) images in Figure 2.2A and in the dynamic light scattering (DLS) data in Table 2.S1, Supporting Information. The particles possessed a zeta potential of -46.10 mV, shown by the phase analysis light scattering (PALS) data in Table 2.S1, Supporting Information. Additionally, PDI values equal and less than 0.4 are taken to be acceptable for monodispersed samples.[53]

PDA bowl-shaped nanoparticles or bowls were synthesized by following an established method.[48] Here, the formation of PDA bowls is mainly based on the simultaneous formation of block copolymer F127/TMB/polydopamine composite micelles and nucleation of polydopamine and subsequent anisotropic growth of PDA on the surface of the emulsion droplet templates.[48] The size and morphology of the PDA bowls can be controlled by simply adjusting the concentration of pore swelling agent TMB, surfactant F127, dopamine, and aqueous ammonia solution.[48] The SEM image shows that the bowls are monodisperse with a diameter of ∼200 nm and a cavity with an approximate width of 80 nm (Figure 2.2B). Higher magnification revealed that the pore size is estimated to be around 7 nm (Figure 2.2B). Furthermore, transmission electron microscopy (TEM) image of the bowls (Figure 2.S1, Supporting Information) indicated that the mesochannels are arranged radially from the center to the surface of the bowls and at a higher magnification, the center-to-center distance between adjacent mesochannels is estimated to be ∼21 nm. The size distribution and zeta potential of the PDA bowls were analyzed using DLS and PALS (Table 2.S1, Supporting Information).

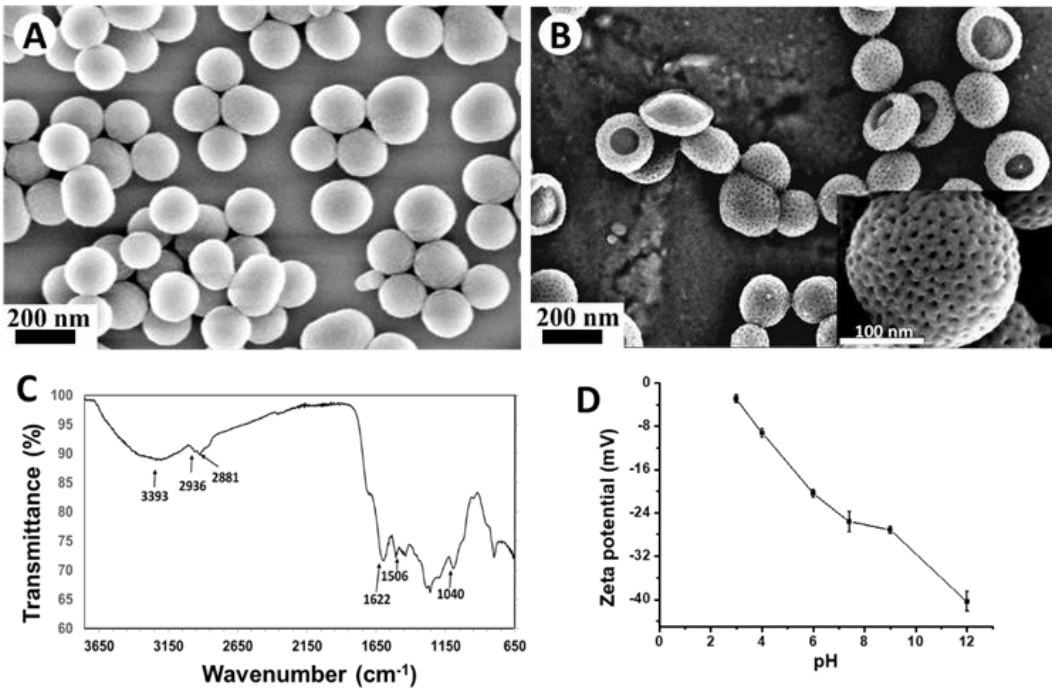

Figure 2.2. A) and B) SEM images of PDA spherical nanoparticles and bowl-shaped nanoparticles, C) FTIR analysis of PDA nanoparticles, and D) pH-dependence study of PDA nanoparticles using zeta potential measurement.

The chemical attributes of PDA particles were probed using Fourier transform infrared spectrometer (FTIR). Peaks at 1510 cm^{-1} and 1600 cm^{-1} are consistent with the indole or indoline structures while the peak at approximately 3370 cm^{-1} is in accordance with the presence of hydroxyl structures. Peaks for PDA polymer were observed in the broad-band from 3700−3300 cm^{-1}, assigned to ν (N−H) and ν (O−H) stretching modes, and peaks at 2936−2881 cm^{-1} which are due to the C−H stretching mode. Peak at 1622 cm^{-1} is assigned to stretching of aromatic C−C bonds of indole, and peak at 1506 cm^{-1} is attributed to C−N bending in indolequinone while peak at 1040 cm^{-1} is attributed to C−H in-plane deformation

(Figure 2.2C).[54] Zeta potential of the synthesized PDA bowls was measured at different solution pH values. As anticipated, the surface charge of the PDA bowls changes with increasing pH. In higher pH solutions (pH>6), negative charge increases due to deprotonation of the phenolic groups of PDA. (Figure 2.2D).[55-56]

It has been demonstrated for a range of pharmaceutical delivery systems that drug carrier toxicity is concentration dependent.[32] Ideally, the chosen drug carrier should be biocompatible and benign for use in nanomedicine. Therefore, in order to determine a suitable concentration of PDA nanoparticles that will not have toxic effects on cervical cancer cell (HeLa), the 3-(4, 5-dimethylthiazol-2-yl)-2, 5-diphenyltetrazolium bromide (MTT) cell viability assay was employed. The assay was conducted in triplicate with PDA nanoparticles for 4 , 24, and 48 h of incubation time at 37 °C and 5% CO_2 (Figure 2.3A).[52, 57] Our results show that the cell line maintained viability of over 80% upon increasing the concentration of the particles from 150 to 500 µg/mL for an incubation period of 48 h.

Fluorescently labeled PDA bowls and spheres were fabricated to incorporate Rhodamine 6G (Rh 6G) via π-π stacking.[51] Both PDA bowls and spheres showed similar fluorescence intensity (Figure 2.S2A, Supporting Information) without any morphological changes to the particles (Figure 2.S2B, 2.S2C, Supporting Information).

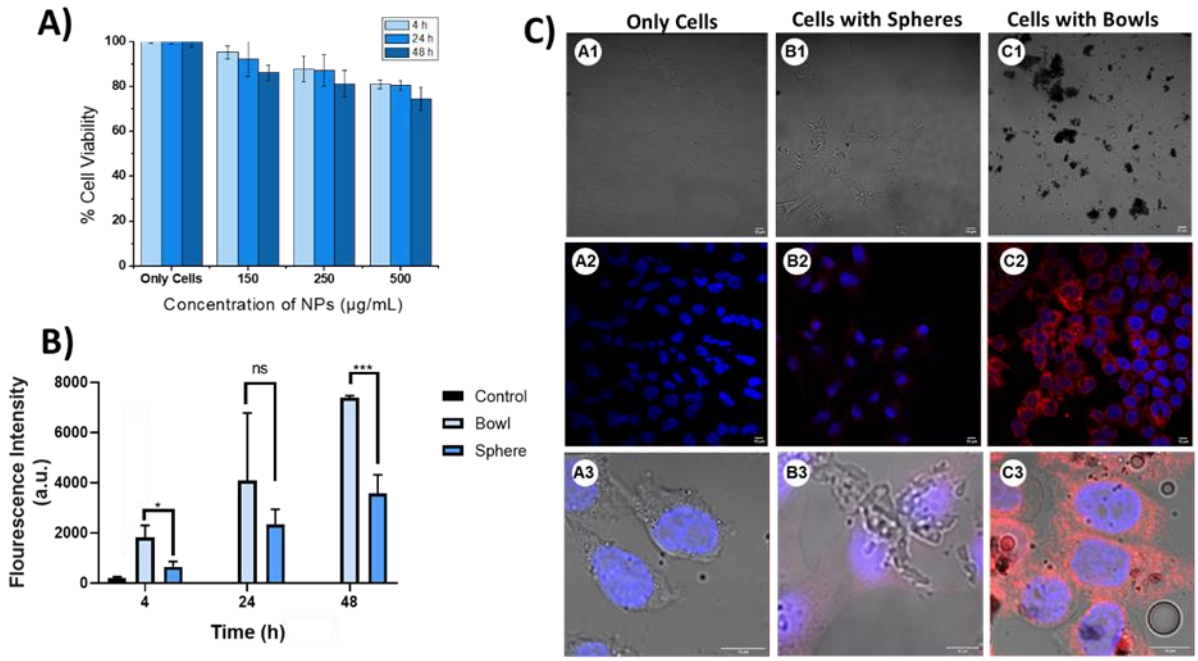

Figure 2.3. A) Cell viability of HeLa cells measured by MTT assay. B) Data from flow cytometer analysis, measured fluorescence intensity of HeLa cells (black: control) (light and deep blue: after incubation with PDA bowls and PDA spheres for 4, 24, and 48 h) (Bowls vs. Spheres- P value: $P < 0.02$ for 4 h, $P < 0.33$ for 24 h and $P < 0.001$ for 48 h). C) a) Confocal images of HeLa cells only, b) HeLa cells with PDA spheres and c) HeLa cells with PDA bowls. Here, cells were incubated with the particles for 48 h and cells were stained with DAPI (blue).

With the aim to understand the cellular uptake kinetics of the PDA bowls and spheres, the size and granularity (inner complexity) of the cells were analyzed after an incubation time of 24 h with the particles using flow cytometry analysis technique. Here, we employed three different samples: control (only cells), cells incubated with PDA spheres, and cells incubated with PDA bowls. Our results show that upon incubation with bowls, the size and granularity of the cells changed noticeably compared with the control and PDA spheres, (Figure 2.S3, Supporting Information). The possible reason for this result can be attributed to the greater

number of bowls being internalized into the cells compared with their spherical counterparts.[58-59] Subsequently, we measured the fluorescence intensity of the cells after incubation with the PDA bowls and spheres, with the aim of collecting more evidence of cellular uptake. Here, we utilized the same three samples as above and monitored the cell mean fluorescence intensity as a function of time using flow cytometer. A significant increase in cell fluorescence intensity was observed in the cell sample that had been incubated with PDA bowls compared with PDA spheres after an incubation period of 4 h. Additionally, the intensity difference between cells incubated with spheres and with bowls became more pronounced upon further incubation over a period of over 48 h (Figure 2.3B). This difference in fluorescence intensities of the two cell samples with respect to the control is an indication of a greater number of PDA bowls being internalized into the cell with respect to their spherical counterparts.[60-61]

In order to further confirm the above flow cytometry results, and visually understand the cellular uptake, fluorescence images were taken using confocal laser scanning microscopy (CLSM). Cells incubated with bowls exhibited an enhanced red fluorescence signal compared to the cells incubated with spheres (Figure 2.3C). These results suggest a faster cellular uptake and larger intracellular accumulation of PDA bowls compared with spheres. In addition, same concentrated nanoparticles has been used for all of the experiments. On average, there are 2.0×10^{11} of bowls and 1.8×10^{11} of spheres in 1 ml solution and 3.26×10^{3} and 3.65×10^{3} of fluorophore molecules on each bowl and sphere respectively.

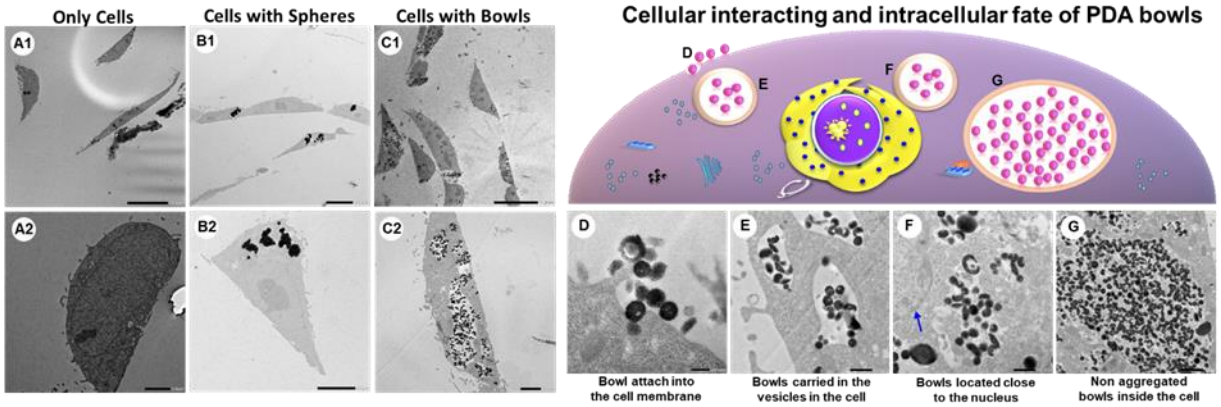

Figure 2.4. TEM images of A) HeLa cells only (control), B) cells with PDA spheres, C) cells with PDA bowls. Higher magnified TEM images of cell incubated with bowls (D to G); D) bowls interacting with the cell membrane (scale bar 200 nm), E) bowls carried inside the cell in vesicles (scale bar 500 nm), F) thus carried close to the nucleus (scale bar 500 nm), and G) assembled in intracellular environment (scale bar 1 µm). Here, cells were incubated with the nanoparticles for 48 h.

For further confirmation of the above findings and in order to visually analyze the location of the particles within the cells, TEM was adopted to scan the cells that were incubated with PDA bowls and spheres under similar experimental conditions as for CLSM analysis (Figure 2.4). The micrographs show that the PDA spheres are only located close to the cell membrane (Figure 2.4B1) and are not widely distributed within the cells (Figure 2.4B2). In contrast, bowls are widely distributed within the cell (Figure 2.4C1), and upon closer view reveal no sign of aggregation, unlike their spherical counterparts (Figure 2.4C2).[61] Note that both PDA bowls and spheres show similar surface properties in PBS and complete cell culture medium (Table 2.S1, Supporting Information).

Moreover, at higher magnification, TEM images show the location of bowls within the cells (Figure 2.4D to 2.4G).[61-62] The bowls appear to tend to enter the cell one at a time (Figure 2.4D), and are transported within the cell via vesicles (Figure 2.4E). Some of the bowls are found to be located close to the nucleus of the cell (Figure 2.4F), and subsequently, they are assembled in the intracellular environment, without any morphological change (Figure 2.4G). These results suggest that the shape of the PDA particles plays an important role in their internalization mechanism: that bowl-shaped particles are easily attached to the cell membrane from their high curvature (sharp) edge, and be engulfed by the cells, thus leading to a faster cellular uptake and higher number of bowls accumulated within the cells.[63]

2.4 Conclusions

In summary, our study demonstrates a significant difference in the cellular internalization behavior of PDA bowls compared with PDA spheres. PDA bowls exhibit a faster rate of cellular uptake in comparison to PDA spheres. PDA bowls, after entering the cells were evenly distributed without any signs of aggregation, unlike their spherical counterparts, which aggregated upon cellular internalization. Preferential attachment onto the cell membrane from their high curvature edge and easier enwrapping by the cell membranes might be possible reasons, allowing for a greater internalization of PDA bowls over their spherical counterparts. Our result is crucial to understand the role that particle shape plays in the interactions with cells, and will have important implications in the design and engineering aspects of more efficient drug carriers.

2.5 References

(1) Oroojalian, F.; Charbgoo, F.; Hashemi, M.; Amani, A.; Yazdian-Robati, R.; Mokhtarzadeh, A.; Ramezani, M.; Hamblin, M. R. Recent Advances in Nanotechnology-Based Drug Delivery Systems for the Kidney. *Journal of Controlled Release* **2020,** *321*, 442-462, DOI: 10.1016/j.jconrel.2020.02.027.
(2) Lombardo, D.; Kiselev, M.; Caccamo, M. T. Smart Nanoparticles for Drug Delivery Application: Development of Versatile Nanocarrier Platforms in Biotechnology and Nanomedicine. *Journal of Nanomaterials* **2019,** *2019*, 1-26, DOI: 10.1155/2019/3702518.
(3) Patra, J. K.; Das, G.; Fraceto, L. F.; Campos, E. V. R.; Rodriguez-Torres, M. d. P.; Acosta-Torres, L. S.; Diaz-Torres, L. A.; Grillo, R.; Swamy, M. K.; Sharma, S.; Habtemariam, S.; Shin, H.-S. Nano Based Drug Delivery Systems: Recent Developments and Future Prospects. *Journal of Nanobiotechnology* **2018,** *16* (1), 71, DOI: 10.1186/s12951-018-0392-8.
(4) Shi, J.; Votruba, A. R.; Farokhzad, O. C.; Langer, R. Nanotechnology in Drug Delivery and Tissue Engineering: From Discovery to Applications. *Nano letters* **2010,** *10* (9), 3223-3230, DOI: 10.1021/nl102184c.
(5) Zhang, R.; Qin, X.; Kong, F.; Chen, P.; Pan, G. Improving Cellular Uptake of Therapeutic Entities Through Interaction with Components of Cell Membrane. *Drug Delivery* **2019,** *26* (1), 328-342, DOI: 10.1080/10717544.2019.1582730.
(6) Barua, S.; Mitragotri, S. Challenges Associated with Penetration of Nanoparticles Across Cell and Tissue Barriers: A Review of Current Status and Future Prospects. *Nano Today* **2014,** *9* (2), 223-243, DOI: 10.1016/j.nantod.2014.04.008.
(7) Yang, N. J.; Hinner, M. J. Getting Across the Cell Membrane: An Overview for Small Molecules, Peptides, and Proteins. *Methods in Molecular Biology (Clifton, N.J.)* **2015,** *1266*, 29-53, DOI: 10.1007/978-1-4939-2272-7_3.
(8) Contini, C.; Schneemilch, M.; Gaisford, S.; Quirke, N. Nanoparticle–Membrane Interactions. *Journal of Experimental Nanoscience* **2018,** *13* (1), 62-81, DOI: 10.1080/17458080.2017.1413253.
(9) Zhao, J.; Stenzel, M. H. Entry of Nanoparticles into Cells: the Importance of Nanoparticle Properties. *Polymer Chemistry* **2018,** *9* (3), 259-272, DOI: 10.1039/C7PY01603D.
(10) Vasir, J. K.; Labhasetwar, V. Biodegradable Nanoparticles for Cytosolic Delivery of Therapeutics. *Advanced Drug Delivery Reviews* **2007,** *59* (8), 718-728, DOI: 10.1016/j.addr.2007.06.003.
(11) Parodi, A.; Corbo, C.; Cevenini, A.; Molinaro, R.; Palomba, R.; Pandolfi, L.; Agostini, M.; Salvatore, F.; Tasciotti, E. Enabling Cytoplasmic Delivery and Organelle Targeting by Surface Modification of Nanocarriers. *Nanomedicine (Lond)* **2015,** *10* (12), 1923-1940, DOI: 10.2217/nnm.15.39.
(12) Behzadi, S.; Serpooshan, V.; Tao, W.; Hamaly, M. A.; Alkawareek, M. Y.; Dreaden, E. C.; Brown, D.; Alkilany, A. M.; Farokhzad, O. C.; Mahmoudi, M. Cellular Uptake of Nanoparticles: Journey Inside the Cell. *Chemical Society Reviews* **2017,** *46* (14), 4218-4244, DOI: 10.1039/c6cs00636a.
(13) Foroozandeh, P.; Abdul Aziz, A. Insight into Cellular Uptake and Intracellular Trafficking of Nanoparticles. *Nanoscale Research Letters* **2018,** *13*, 1-12, DOI: 10.1186/s11671-018-2728-6.
(14) Albanese, A.; Tang, P.; Chan, W. The Effect of Nanoparticle Size, Shape, and Surface Chemistry on Biological Systems. *Annual Review of Biomedical Engineering* **2012,** *14*, 1-16, DOI: 10.1146/annurev-bioeng-071811-150124.
(15) Sun, X. Y.; Gan, Q. Z.; Ouyang, J. M. Size-Dependent Cellular Uptake Mechanism and Cytotoxicity Toward Calcium Oxalate on Vero Cells. *Scientific Reports* **2017,** *7*, 41949, DOI: 10.1038/srep41949.
(16) Dasgupta, S.; Auth, T.; Gompper, G. Shape and Orientation Matter for the Cellular Uptake of Nonspherical Particles. *Nano Letters* **2014,** *14* (2), 687-693, DOI: 10.1021/nl403949h.
(17) He, Y.; Park, K. Effects of the Microparticle Shape on Cellular Uptake. *Molecular Pharmaceutics* **2016,** *13* (7), 2164-2171, DOI: 10.1021/acs.molpharmaceut.5b00992.
(18) Jindal, A. The Effect of Particle Shape on Cellular Interaction and Drug Delivery Applications of Micro- and Nanoparticles. *International Journal of Pharmaceutics* **2017,** *532 (1)*, 450-465, DOI: 10.1016/j.ijpharm.2017.09.028.

(19) Kou, L.; Sun, J.; Zhai, Y.; He, Z. The Endocytosis and Intracellular Fate of Nanomedicines: Implication for Rational Design. *Asian Journal of Pharmaceutical Sciences* **2013,** *8* (1), 1-10, DOI: 10.1016/j.ajps.2013.07.001.
(20) Wang, W.; Gaus, K.; Tilley, R. D.; Gooding, J. J. The Impact of Nanoparticle Shape on Cellular Internalisation and Transport: What Do the Different Analysis Methods Tell Us? *Materials Horizons* **2019,** *6* (8), 1538-1547, DOI: 10.1039/C9MH00664H.
(21) Xie, X.; Liao, J.; Shao, X.; Li, Q.; Lin, Y. The Effect of Shape on Cellular Uptake of Gold Nanoparticles in the Forms of Stars, Rods, and Triangles. *Scientific Reports* **2017,** *7* (1), 3827, DOI: 10.1038/s41598-017-04229-z.
(22) Cong, V. T.; Gaus, K.; Tilley, R. D.; Gooding, J. J. Rod-Shaped Mesoporous Silica Nanoparticles for Nanomedicine: Recent Progress and Perspectives. *Expert Opinion on Drug Delivery* **2018,** *15* (9), 881-892, DOI: 10.1080/17425247.2018.1517748.
(23) Kwan, J. J.; Myers, R.; Coviello, C. M.; Graham, S. M.; Shah, A. R.; Stride, E.; Carlisle, R. C.; Coussios, C. C. Ultrasound-Propelled Nanocups for Drug Delivery. *Small* **2015,** *11* (39), 5305-14, DOI: 10.1002/smll.201501322.
(24) Chen, F.; Ma, M.; Wang, J.; Wang, F.; Chern, S.-X.; Zhao, E. R.; Jhunjhunwala, A.; Darmadi, S.; Chen, H.; Jokerst, J. V. Exosome-Like Silica Nanoparticles: A Novel Ultrasound Contrast Agent for Stem Cell Imaging. *Nanoscale* **2017,** *9* (1), 402-411, DOI: 10.1039/C6NR08177K.
(25) Zhang, C.; Lu, J.; Tian, F.; Li, L.; Hou, Y.; Wang, Y.; Sun, L.; Shi, X.; Lu, H. Regulation of the Cellular Uptake of Nanoparticles by the Orientation of Helical Polypeptides. *Nano Research* **2019,** *12* (4), 889-896, DOI: 10.1007/s12274-019-2319-6.
(26) Mannaris, C.; Teo, B. M.; Seth, A.; Bau, L.; Coussios, C.; Stride, E. Gas-Stabilizing Gold Nanocones for Acoustically Mediated Drug Delivery. *Advanced Healthcare Materials* **2018,** *7* (12), 1800184, DOI: 10.1002/adhm.201800184.
(27) Din, F. U.; Aman, W.; Ullah, I.; Qureshi, O. S.; Mustapha, O.; Shafique, S.; Zeb, A. Effective Use of Nanocarriers as Drug Delivery Systems for the Treatment of Selected Tumors. *International Journal of Nanomedicine* **2017,** *12*, 7291-7309, DOI: 10.2147/IJN.S146315.
(28) Chenthamara, D.; Subramaniam, S.; Ramakrishnan, S. G.; Krishnaswamy, S.; Essa, M. M.; Lin, F.-H.; Qoronfleh, M. W. Therapeutic Efficacy of Nanoparticles and Routes of Administration. *Biomaterials Research* **2019,** *23* (1), 20, DOI: 10.1186/s40824-019-0166-x.
(29) Mousavi, S. M.; Zarei, M.; Hashemi, S. A. Polydopamine for Biomedical Application and Drug Delivery System. *Medicinal Chemistry* **2018,** *8 (8)*, 218-229, DOI: 10.4172/2161-0444.1000516.
(30) Vidallon, M. L. P.; Douek, A. M.; Quek, A.; McLiesh, H.; Kaslin, J.; Tabor, R. F.; Bishop, A. I.; Teo, B. M. Gas-Generating, pH-Responsive Calcium Carbonate Hybrid Particles with Biomimetic Coating for Contrast-Enhanced Ultrasound Imaging. *Particle & Particle Systems Characterization* **2020,** *37* (2), 1900471, DOI: 10.1002/ppsc.201900471.
(31) Vidallon, M. L. P.; Yu, F.; Teo, B. M. Controlling the Size and Polymorphism of Calcium Carbonate Hybrid Particles Using Natural Biopolymers. *Crystal Growth & Design* **2020,** *20* (2), 645-652, DOI: 10.1021/acs.cgd.9b01057.
(32) Mannaris, C.; Yang, C.; Carugo, D.; Owen, J.; Lee, J. Y.; Nwokeoha, S.; Seth, A.; Teo, B. M. Acoustically Responsive Polydopamine Nanodroplets: A Novel Theranostic Agent. *Ultrasonics Sonochemistry* **2020,** *60*, 104782, DOI: 10.1016/j.ultsonch.2019.104782.
(33) Zhang, Y.; Teo, B. M.; Goldie, K. N.; Städler, B. Poly(N-isopropylacrylamide)/Poly(dopamine) Capsules. *Langmuir: the ACS Journal of Surfaces and Colloids* **2014,** *30* (19), 5592-5598, DOI: 10.1021/la5005227.
(34) Lynge, M. E.; van der Westen, R.; Postma, A.; Städler, B. Polydopamine—A Nature-Inspired Polymer Coating for Biomedical Science. *Nanoscale* **2011,** *3* (12), 4916-4928, DOI: 10.1039/C1NR10969C.
(35) Wei, Q.; Zhang, F.; Li, J.; Li, B.; Zhao, C. Oxidant-Induced Dopamine Polymerization for Multifunctional Coatings. *Polymer Chemistry* **2010,** *1* (9), 1430-1433, DOI: 10.1039/C0PY00215A.

(36) Liebscher, J.; Mrowczynski, R.; Scheidt, H. A.; Filip, C.; Hadade, N. D.; Turcu, R.; Bende, A.; Beck, S. Structure of Polydopamine: A Never-Ending Story? *Langmuir : the ACS Journal of Surfaces and Colloids* **2013,** *29* (33), 10539-48, DOI: 10.1021/la4020288.
(37) d'Ischia, M.; Napolitano, A.; Ball, V.; Chen, C. T.; Buehler, M. J. Polydopamine and Eumelanin: From Structure-Property Relationships to A Unified Tailoring Strategy. *Accounts of Chemical Research* **2014,** *47* (12), 3541-50, DOI: 10.1021/ar500273y.
(38) Park, J.; Brust, T. F.; Lee, H. J.; Lee, S. C.; Watts, V. J.; Yeo, Y. Polydopamine-Based Simple and Versatile Surface Modification of Polymeric Nano Drug Carriers. *ACS Nano* **2014,** *8* (4), 3347-56, DOI: 10.1021/nn405809c.
(39) Liu, X.; Cao, J.; Li, H.; Li, J.; Jin, Q.; Ren, K.; Ji, J. Mussel-Inspired Polydopamine: A Biocompatible and Ultrastable Coating for Nanoparticles in Vivo. *ACS Nano* **2013,** *7* (10), 9384-9395, DOI: 10.1021/nn404117j.
(40) Salazar, P.; Martín, M.; González-Mora, J. Polydopamine-Modified Surfaces in Biosensor Applications. Polymer Science: Research Advances, Practical Applications and Educational Aspects **2016**, pp 385-396.
(41) Sotoma, S.; Harada, Y. Polydopamine Coating as A Scaffold for Ring-Opening Chemistry To Functionalize Gold Nanoparticles. *Langmuir: the ACS Journal of Surfaces and Colloids* **2019,** *35* (25), 8357-8362, DOI: 10.1021/acs.langmuir.9b00762.
(42) Zhao, H.; Chao, Y.; Liu, J.; Huang, J.; Pan, J.; Guo, W.; Wu, J.; Sheng, M.; Yang, K.; Wang, J.; Liu, Z. Polydopamine Coated Single-Walled Carbon Nanotubes as A Versatile Platform with Radionuclide Labeling for Multimodal Tumor Imaging and Therapy. *Theranostics* **2016,** *6* (11), 1833-1843, DOI: 10.7150/thno.16047.
(43) Zhang, Y.; Lynge, M. E.; Teo, B. M.; Ogaki, R.; Städler, B. Mixed Poly(dopamine)/poly(l-lysine) (composite) Coatings: From Assembly to Interaction with Endothelial Cells. *Biomaterials Science* **2015,** *3* (8), 1188-1196, DOI: 10.1039/C5BM00093A.
(44) Li, C.; Liu, Z.; Yao, P. Gold Nanoparticles Coated with A Polydopamine Layer and Dextran Brush Surface for Diagnosis and Highly Efficient Photothermal Therapy of Tumors. *RSC Advances* **2016,** *6* (39), 33083-33091, DOI: 10.1039/C6RA02684B.
(45) Lin, J.; Daboss, S.; Blaimer, D.; Kranz, C. Micro-Structured Polydopamine Films Via Pulsed Electrochemical Deposition. *Nanomaterials (Basel)* **2019,** *9* (2), 242, DOI: 10.3390/nano9020242.
(46) Liu, X.; Cao, J.; Li, H.; Li, J.; Jin, Q.; Ren, K.; Ji, J. Mussel-Inspired Polydopamine: A Biocompatible and Ultrastable Coating for Nanoparticles in *Vivo*. *ACS Nano* **2013,** *7* (10), 9384-95, DOI: 10.1021/nn404117j.
(47) Yang, L.; Wang, C.; Ye, Z.; Zhang, P.; Wu, S.; Jia, S.; Li, Z.; Zhang, Z. Anisotropic Polydopamine Capsules with An Ellipsoidal Shape That Can Tolerate Harsh Conditions: Efficient Adsorbents for Organic Dyes and Precursors for Ellipsoidal Hollow Carbon Particles. *RSC Advances* **2017,** *7* (35), 21686-21696, DOI: 10.1039/C7RA02235B.
(48) Guan, B. Y.; Yu, L.; Lou, X. W. Formation of Asymmetric Bowl-Like Mesoporous Particles Via Emulsion-Induced Interface Anisotropic Assembly. *Journal of the American Chemical Society* **2016,** *138* (35), 11306-11311, DOI: 10.1021/jacs.6b06558.
(49) Guan, B. Y.; Zhang, S. L.; Lou, X. W. D. Realization of Walnut-Shaped Particles with Macro-/Mesoporous Open Channels Through Pore Architecture Manipulation and Their Use in Electrocatalytic Oxygen Reduction. *Angewandte Chemie (International Edition in English)* **2018,** *57* (21), 6176-6180, DOI: 10.1002/anie.201801876.
(50) Luo, H.; Gu, C.; Zheng, W.; Dai, F.; Wang, X.; Zheng, Z. Facile Synthesis of Novel Size-Controlled Antibacterial Hybrid Spheres Using Silver Nanoparticles Loaded with Poly-Dopamine Spheres. *RSC Advances* **2015,** *5* (18), 13470-13477, DOI: 10.1039/C4RA16469E.
(51) Amin, D. R.; Sugnaux, C.; Lau, K. H. A.; Messersmith, P. B. Size Control and Fluorescence Labeling of Polydopamine Melanin-Mimetic Nanoparticles for Intracellular Imaging. *Biomimetics (Basel, Switzerland)* **2017,** *2* (3), 17, DOI: 10.3390/biomimetics2030017.

(52) Mosmann, T. Rapid Colorimetric Assay for Cellular Growth and Survival: Application to Proliferation and Cytotoxicity Assays. *Journal of Immunological Methods* **1983,** *65* (1-2), 55-63, DOI: 10.1016/0022-1759(83)90303-4.
(53) Mozafari, M.; Danaei, M.; Dehghankhold, M.; Ataei, S.; Hasanzadeh Davarani, F.; Javanmard, R.; Dokhani, A.; Khorasany, S. Impact of Particle Size and Polydispersity Index on the Clinical Applications of Lipidic Nanocarrier Systems. *Pharmaceutics* **2018**, *10* (2), 57, DOI: 10.3390/pharmaceutics10020057.
(54) Yu, X.; Fan, H.; Liu, Y.; Shi, Z.; Jin, Z. Characterization of Carbonized Polydopamine Nanoparticles Suggests Ordered Supramolecular Structure of Polydopamine. *Langmuir : the ACS Journal of Surfaces and Colloids* **2014,** *30* (19), 5497-5505, DOI: 10.1021/la500225v.
(55) Xu, J.; Ma, A.; Liu, T.; Lu, C.; Wang, D.; Xu, H. Janus-Like Pickering Emulsions and Their Controllable Coalescence. *Chemical Communications* **2013,** *49* (92), 10871-10873, DOI: 10.1039/C3CC46738D.
(56) Ghorbani, F.; Zamanian, A.; Behnamghader, A.; Joupari, M. A Facile Method to Synthesize Mussel-Inspired Polydopamine Nanospheres as An Active Template for *In Situ* Formation of Biomimetic Hydroxyapatite. *Materials Science and Engineering C* **2019,** *94*, 729-739, DOI: 10.1016/j.msec.2018.10.010.
(57) Chen, X.; Cortez-Jugo, C.; Choi, G. H.; Björnmalm, M.; Dai, Y.; Yoo, P. J.; Caruso, F. Patterned Poly(dopamine) Films for Enhanced Cell Adhesion. *Bioconjugate Chemistry* **2017,** *28* (1), 75-80, DOI: 10.1021/acs.bioconjchem.6b00544.
(58) Ibuki, Y.; Toyooka, T. Nanoparticle Uptake Measured by Flow Cytometry. *Methods in Molecular Biology (Clifton, N.J.)* **2012,** *926*, 157-66, DOI: 10.1007/978-1-62703-002-1_11.
(59) Khetan, J.; Shahinuzzaman, M.; Barua, S.; Barua, D. Quantitative Analysis of the Correlation Between Cell Size and Cellular Uptake of Particles. *Biophysical Journal* **2019,** *116* (2), 347-359, DOI: 10.1016/j.bpj.2018.11.3134.
(60) Teo, B. M.; van der Westen, R.; Hosta-Rigau, L.; Städler, B. Cell Response to PEGylated Poly(dopamine) Coated Liposomes Considering Shear Stress. *Biochimica et Biophysica Acta (BBA) - General Subjects* **2013,** *1830* (10), 4838-4847, DOI: 10.1016/j.bbagen.2013.06.022.
(61) Yue, J.; Feliciano, T. J.; Li, W.; Lee, A.; Odom, T. W. Gold Nanoparticle Size and Shape Effects on Cellular Uptake and Intracellular Distribution of siRNA Nanoconstructs. *Bioconjugate Chemistry* **2017,** *28* (6), 1791-1800, DOI: 10.1021/acs.bioconjchem.7b00252.
(62) Gratton, S. E.; Ropp, P. A.; Pohlhaus, P. D.; Luft, J. C.; Madden, V. J.; Napier, M. E.; DeSimone, J. M. The Effect of Particle Design on Cellular Internalization Pathways. *Proceedings of the National Academy of Sciences of the United States of America* **2008,** *105* (33), 11613-8, DOI: 10.1073/pnas.0801763105.
(63) Li, H.; Zhang, W.; Tong, W.; Gao, C. Enhanced Cellular Uptake of Bowl-like Microcapsules. *ACS Applied Materials & Interfaces* **2016,** *8* (18), 11210-11214, DOI: 10.1021/acsami.6b02965.

Chapter 3

Bowl-Shaped Mesoporous Polydopamine Nanoparticles for Size-Dependent Endocytosis into HeLa Cells

This Chapter was published as: **Shahinur Acter,** Mark Louis P. Vidallon, Simon Crawford, Rico F. Tabor,* and Boon Mian Teo,* *ACS Applied Nano Materials,* **2021**, 4, 9536–9546.

Preface for Chapter 3

In this Chapter, precise experimental conditions were established in order to synthesize various sizes of polydopamine bowl-shaped mesoporous nanoparticles by tuning each reaction parameter, with an aim to investigate size-dependent cellular internalization behavior of bowl-shaped polydopamine nanoparticles and understand their endocytosis pathways in HeLa cells. Diameter and surface charge of obtained particles were characterized by dynamic light scattering analysis and zeta potential measurement, and morphological analysis of the particles was undertaken by transmission electron microscopy (TEM). Cell viability of HeLa cells was determined using an MTS (3-(4,5-carboxymethoxyphenyl)-2-(4-sulfophenyl)-2H-tetrazolium) cell viability assay. Specific biological inhibitors were used to study endocytosis pathways of bowls into HeLa cells and various analysis techniques were applied in this investigation including flow cytometry, confocal microscopy, and TEM imaging.

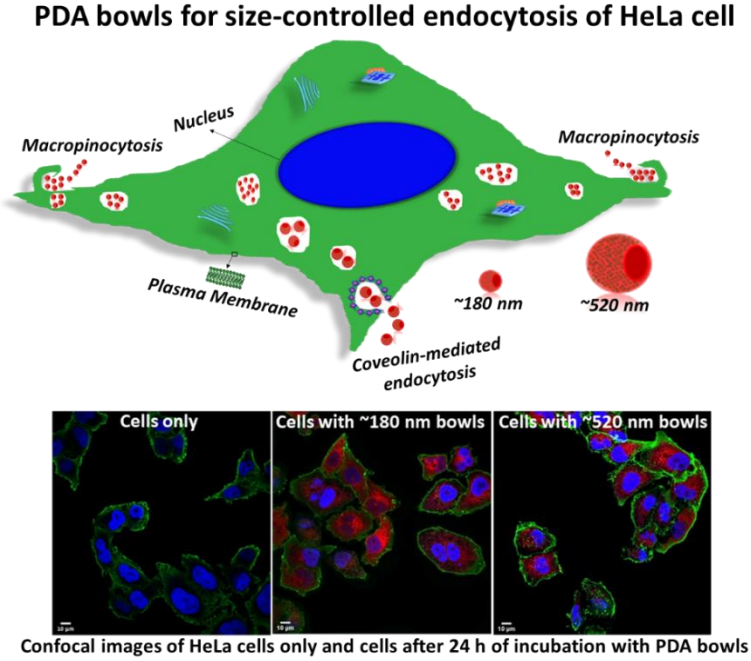

Confocal images of HeLa cells only and cells after 24 h of incubation with PDA bowls

Abstract

A comprehensive study of cellular internalization mechanisms of nanoparticles is crucial to optimize their drug delivery efficacy, as endocytosis pathways will likely determine their biological fate. Particularly for polydopamine bowl-shaped mesoporous nanoparticles (PDA bowls), their anisotropic morphology provides enhanced cellular internalization efficiency with respect to their spherical counterparts, though the mechanism of this is not yet fully understood. Herein, we report a size-controlled synthesis of PDA bowls by changing different reaction parameters and investigated their size-dependent endocytosis pathways in the HeLa cell line. The cellular internalization behavior of PDA bowls was investigated by using a suite of characterization techniques including flow cytometry, confocal microscopy, and transmission electron microscopy. Obtained results demonstrated that the uptake efficiency of PDA bowls is significantly dependent on their size. Moreover, the size of bowls also plays an important role in the endocytosis pathways followed to internalize them into cells, which was investigated by blocking certain endocytosis pathways with biological inhibitors. Taken together, this work provides fundamental understanding of the impact of reaction parameters on size controlled synthesis of PDA bowls and reveals the role of their size in regulating the cellular internalization pathways, providing key structure−function information for these unique particles, which pave the way to the optimization of engineering drug nanocarriers in cancer treatment with higher efficacy.

3.1 Introduction

In the past few decades, there has been an enormous growth of research in fabricating various types of nanoparticles such as dendrimers, liposomes, inorganic (metal and oxide) particles, and polymer particles, due to their extensive applications in biomedical fields.[1-4] Nevertheless, only a few of them have been clinically approved among this vast number of published research work on development of drug nanocarriers.[5-6] The reason can be explained as arising from the complexity in developed systems, which has resulted in several issues including long-term side effects and circumventing multi-drug resistance.[7] Although scientists devote themselves to the synthesis of nanoparticles with higher efficiency as drug carriers, combining all desired properties into a single system remains a great challenge.[8] In order to overcome these limitations, appropriate modification of such nanoparticles is required for endowing the nanoplatform with ideal biocompatibility, various functionalization, colloidal stability, and additional attributes such as photo-thermal conversion ability and faster cellular internalization.[9]

In recent years, polydopamine (PDA) has aroused great attention in developing biocompatible drug nanocarriers with colloidal stability. Therefore, the formation and functionalization of PDA nanoparticles has attracted enormous attention in various biomedical applications such as biosensors,[10-11] sensors,[12] remediation,[13] biomineralisation,[14] drug delivery,[15-16] and cancer diagnosis.[14, 17-20] Moreover, one of the most important properties of PDA is its strong adhesion to all types of surfaces due to the adhesive nature of catechols and amines, similar to those in mussel adhesive proteins.[21] On top of that, excellent biocompatibility, mild synthesis

requirements, and distinctive drug loading opportunities make PDA an appealing material for designing drug nanocarriers.[14-15, 22-25]

Studies suggest that the drug delivery efficiency of nanoparticles is significantly dependent on the way they pass through the biological barriers, their cellular uptake efficiency and biodistribution, and ultimate their intracellular fate. Generally, nanoparticles may enter the cell by a mechanism known as endocytosis; depending on their size, shape, and surface property, nanoparticles tend to follow subcategorized pathways, such as macropinocytosis, clathrin-mediated endocytosis, and caveolae-mediated endocytosis to enter into cells.[26-27] It has been demonstrated that the shape of nanoparticles is a determining factor for their cellular uptake efficiency.[27-29] For example, Gao and co-workers have found an efficient cellular uptake of bowl-like microcapsules compared to spherical ones due to the way to attach to the cell membranes.[29] We also observed shape-dependent cellular internalization behavior of PDA bowls in our previous study, where significantly higher cellular internalization of PDA bowls was found compared to their spherical counterparts.[16] The posited explanation of such internalization behavior of PDA bowls was their mode of cellular interaction, as bowls tends to attach onto cell membranes from their highly curved side, becoming enwrapped by the biological membrane, which results in a faster internalization and greater accumulation inside cells relative to their spherical counterparts.[16, 29] Considering the faster rate of cellular internalization of PDA bowls, it is highly relevant to conduct further studies of cellular uptake of PDA bowls such as their size-dependent cellular uptake and their endocytosis pathways.

Herein, we have investigated the cellular internalization behavior of various sizes of PDA bowls and the endocytosis pathways that are followed to internalize them into cells (Figure 3.1). This was conducted by blocking certain endocytosis pathways using selected biological inhibitors. To the best of our knowledge, this is the first study of its type. In order to conduct this investigation, we successfully synthesized three different sizes of PDA bowls by regulating experimental parameters, including the concentration of dopamine, polymerization time, and pH of the reaction environment, noting that size-controlled formation of PDA bowls has not been studied before. To facilitate theoretical and experimental investigations, all experiments were conducted with particles that had consistent zeta potential and surface functionality, as these are desired to elucidate the effect of only size on the efficiency, mechanism, and cytotoxicity of the internalization process. This study is crucial in designing biocompatible drug nanocarriers that are effective in cancer treatment.

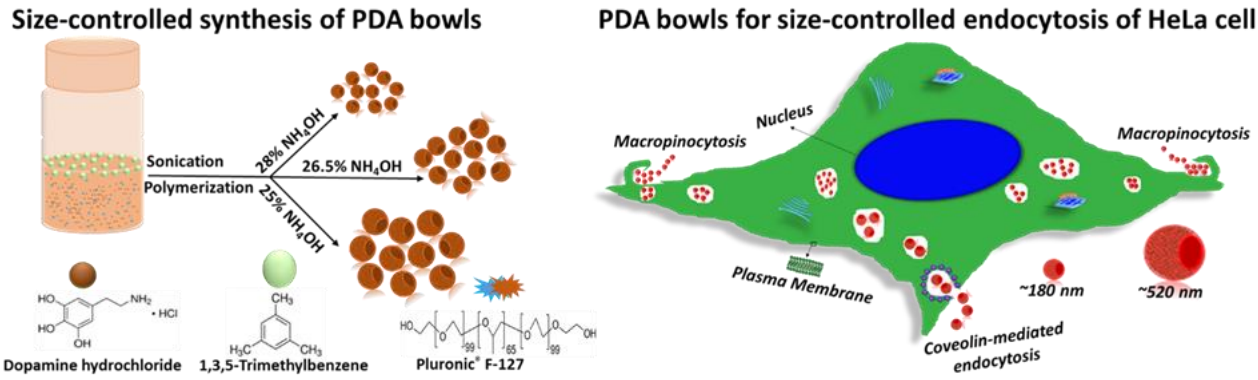

Figure 3.1. Schematic diagram showing the fabrication process parameters yielding various sizes of PDA bowls (left) and their size-dependent cellular internalization into the HeLa cells (right).

3.2 Experimental Section

3.2.1 Materials

Dopamine hydrochloride, trimethylbenzene (TMB, 98%), Pluronic® F-127, fetal bovine serum (FBS, Gibco), phosphate-buffered saline (PBS), antibiotic-antimycotic solution (100X), paraformaldehyde (PFA), MTS assay kit (Cell Proliferation) (Colorimetric), and 4´, 6-diamidino-2-phenylindole (DAPI) were purchased from Sigma-Aldrich. Ammonia solution was from Ajax Finechem Pty., and ethanol 96% was from Univa. Other materials were Dulbecco's Modified Eagle's Medium (DMEM, Life Science) and trypsin (0.25%, Merck). All reagents were used as received, without further purification.

3.2.2 Characterization of PDA Bowls

Field-emission scanning electron microscopy (FEI Magellan 400 FEG SEM) and transmission electron microscopy (TEM, FEI Tecnai G2 T20 electron microscope under 200kv, using LaB6 emitter) were used to examine the size and morphology of the particles. Hydrodynamic diameters and zeta potential of the particles were determined using dynamic light scattering (DLS) and phase analysis light scattering (PALS) respectively, using a Brookhaven NanoBrook Omni particle sizer and zeta potential analyzer. Fluorescence absorption and emission spectra of samples were recorded using a Varian Cary Eclipse Fluorescence spectrophotometer in 1 cm path-length quartz cuvettes. Chemical characterization of PDA particles was undertaken using a Cary 630 FTIR (Fourier Transform Infrared) spectrometer in our previous study.[16]

3.2.3 Formation of PDA bowls

An emulsion-induced interfacial anisotropic assembly method was used to synthesize PDA bowls. In brief, 1.5% (w/v) dopamine hydrochloride and 1.0% (w/v) Pluronic® F127 (block copolymer), were dissolved in 1:1 water and ethanol mixture with a total volume of 10 mL. Next, 2.0% (v/v) TMB [30] was added under stirring, followed by ultra- sonication for 2 min to form an emulsion. In the emulsion system, 3.75% (v/v) of ammonia (NH_4OH, 28%) solution was added dropwise to achieve an alkaline environment volume of 10 mL. Next, 2.0% (v/v) TMB [30] was added under stirring, followed by ultra-sonication for 2 min to form an emulsion. In the emulsion system, 3.75% (v/v) of ammonia (NH_4OH, 28%) solution was added dropwise to achieve an alkaline environment for the reaction to occur. After 2 h (or longer times as noted) of polymerization, the synthesized nanoparticles were centrifuged with water and ethanol for three to four times. Subsequently, particles were re-dispersed in 10 mL of (1:1) water ethanol mixture. In order to increase the stability of the particle dispersion, it was heated in a sealed Teflon-lined autoclave at 100 °C for 24 h. The size of the PDA bowls can be controlled by changing the reaction parameters such as higher concentration of dopamine, prolonged polymerization time, and tuning the pH of the reaction mixture.

3.2.4 Fluorophore modification of PDA bowls

For in situ fluorophore modification, PDA bowls were coated with Rhodamine 6G (Rh 6G) following a previously reported method.[27] Briefly, PDA particles were synthesized in Rh 6G (1:1) water: ethanol solvent. After the desired polymerization time, particles were washed three to four times (water: ethanol) by centrifugation at 9000 x g. Obtained particles were

redisperse in (1:1) water: ethanol solvent for hydrothermal treatment at 100 ^{o}C for 24 h. After that, the particles were washed several times (water: ethanol), followed by dialysis (10 kDa MWCO) for four days in ultrapure water and freeze-dried before use in cell treatment. This procedure was done to confirm the stability of the fluorescence labelling and no leaching of dye. Herein, concentration of dye was adjusted to obtain similar fluorescence intensity in both sizes of PDA bowls (Figure 3.S4).

3.2.5 In *vitro* cytotoxicity assay of PDA bowls

Cell viability of the cells incubated with the synthesized PDA bowls was determined by using the 3-(4,5-carboxymethoxyphenyl)-2-(4-sulfophenyl)-2H-tetrazolium (MTS) cell viability assay.[31] HeLa cells were seeded at a density of 2×10^4 cells/mL in a 96-well plate with a volume of 50 µL in each well and left to adhere overnight at 37 °C and 5% CO_2. The MTS assay was conducted in triplicate with PDA bowls at varying concentrations (50, 100, and 200 µg/mL) for different times (4 and 24 h) at 37 °C and 5% CO_2. After the desired incubation time, the absorbance at 490 nm was recorded using a CLARIOstar microplate reader (BMG Labtech, VIC, Australia). The absorbance values of the control (untreated cells) was set to 100%, and cell proliferation was expressed as a percentage of this control.

3.2.6 Inhibitor Treatment

To investigate the internalization mechanism of PDA bowls, cells were treated with biological inhibitors for 1 h before adding particles. Herein, the energy dependence of the interaction

between cells and PDA bowls was assessed by treatment with 20 mM sodium azide (NaN_3). Likewise, 3 µg/mL of CytD and 150 µM genistein were used to treat the cells prior to incubation with the PDA bowls for 24 h to investigate size-dependent internalization of ~180 nm and ~520 nm PDA bowls. The biological inhibitors and concentration used were selected in consideration of the size of the PDA bowls based on previous research.[31-33]

3.2.7 Flow cytometry

HeLa cells (4×10^5 cells/mL) were seeded in individual 25 mL culture flasks and incubated for 24 h prior to the addition of PDA bowls. All the experiments were carried out with 1.33258×10^{12} ~180 nm bowls and 1.30023×10^{12} ~520 nm PDA bowls. The PDA bowls of both sizes were incubated with the cells for 4 and 24 h. Subsequently, the cells were collected by trypsinization. The samples were then washed using three centrifugation/re-dispersion cycles (1200 rpm, 5 min in 1x PBS buffer solution). The supernatant was removed and 340 µL of 1x PBS was added to the aliquots for flow cytometry analysis using flow core analysis technique (BD LSR II, LSR2a analyzer with YG585 detector).

3.2.8 Confocal imaging of HeLa cells

HeLa cells were seeded (2×10^4 cells/mL) on coverslips into 6-well plates and left to adhere overnight at 37 °C and 5% CO_2. Subsequently, with the same experimental conditions as flow cytometry analysis, the cells were treated with inhibitors and incubated with PDA bowls for 24 h. After the desired incubation period, the cells were fixed with 4% PFA for 10 to 15 min

and counterstained with 0.7 µg/mL of DAPI for 10 to 15 min in the dark. Fixed cells in 1x PBS were imaged using confocal laser scanning microscopy (CLSM) (Nikon C1 Upright Confocal Microscope) (60x objective, DAPI: laser 405.0 (emission: 433-468), TRITIC: laser 561.0 (for Rh 6G) (emission: 568-643). All images were acquired through Leica LSX software, then false-colored and merged using ImageJ.

3.2.9 Transmission Electron Microscope (TEM) imaging of HeLa cells

Under the same experimental conditions as for confocal imaging, cell samples were prepared for TEM analysis. For TEM imaging, the cell samples were centrifuged in 1.5 mL Eppendorf tubes at 10,000 rpm for 3 min. The supernatant was removed and the cells were fixed in 2.5% glutaraldehyde, 2% paraformaldehyde, and 0.075% ruthenium red in 0.1 M sodium cacodylate buffer for 2 h at room temperature. The fixative was removed by washing the cells three times for 15 min using 0.1 M sodium cacodylate buffer. Cells were postfixed in 1% osmium tetroxide in buffer for 1 hour at room temperature and then rinsed in milli-Q water three times for 15 min. Cell pellets were embedded in molten 4% agarose and the agarose allowed to set at 4 ^{o}C for 60 min. The agarose plugs were removed from Eppendorf tubes, and dissected into 1 mm squares. Cells in agarose were then dehydrated by incubating in increasing concentrations of ethanol for 15 min with each step, consisting of 30%, 50%, 70%, 90%, and 100% ethanol (x2). The 100% ethanol was substituted with propylene oxide by incubating for 30 min in 100% propylene oxide. Cell pellets were incubated in a mixture of Epon resin and propylene oxide at a ratio of 1:1 for 6 h at room temperature, followed by a 2:1 Epon/propylene oxide mixture overnight. Cells were incubated in 100% freshly made Epon resin for 6 h, and a second change of 100% resin overnight. The embedded cell pellets were

placed into Beem capsules with fresh resin and then the resin was polymerized for 48 h in an oven at 60 °C. Resin embedded cell pellets were sectioned with a diatom diamond knife using a Leica UCS ultramicrotome. Sections of thickness 80 to 90 nm were collected onto formvar-coated 100 mesh copper grids and stained with lead citrate for 8 min. The sections were imaged in a JEOL 1400 Plus transmission electron microscope at 80kV, and images of cells captured with a digital camera at a resolution of 2k x 2k.

3.3 Results and discussion

3.3.1 Size-controlled synthesis of PDA bowls

An emulsion-induced interfacial anisotropic assembly strategy was used to synthesis monodisperse PDA bowls, following an established method.[34] The formation process begin with interface formation between trimethylbenzene (TMB) and water in an emulsion system stabilized by Pluronic® F 127 (F127), followed by growth of island-shaped mesostructured PDA seeds at the immiscible liquid (TMB/water) interface.[34] Herein, the island-shaped mesostructured PDA seeds assembled to form F127/TMB/PDA composite micelles, which have been identified as a key step in how this seed-mediated anisotropic growth yields the shape of the PDA bowls.[34] In our previous study, we have synthesized PDA bowls at around 180 nm in diameter.[16] We found that in 2 h of reaction time, 2.0% (v/v) of TMB, 1.5% (w/v) of dopamine, 1.0% (w/v) of F127, and 0.375 mL of 28% ammonia in 1:1 water and ethanol solvent at 25 °C are the optimum reagent ratios and conditions to synthesize this particular size of PDA bowl with uniformity in the particle population.[16] In the current work, this set of parameters (Method 1 or M1) was used as a starting point that was systematically modified,

in order to study the effects of changing each parameter to obtain various sizes of PDA bowls with a uniform size distribution. Specific components and conditions for each method are summarised in Table 3.1.

First, we explored the impact of various concentrations of TMB and F127 on the diameter of the PDA bowls, as these two features play an important role in the formation of seed particles at the interface of the TMB droplets, which turn into the final product bowls. Different sets of experiments with various concentrations of TMB (**Method 2, M2: TMB = 1 and 3% v/v**), and various concentrations of F127 (**Method 3, M3: F127 = 0.5 and 2.0% w/v**) with all other parameters similar to **M1** (See Table 3.1) were conducted. The effective diameters and zeta potentials of the obtained particles from **M1** to **M2** are shown in Table 3.2. It can be observed that the sample with 2% TMB (M1) had the smallest size with lowest polydispersity index (PDI). All the samples from M1 and M2 showed negative zeta potentials with moderate magnitudes around - 40mV, indicating colloidal stability of these particles in dispersion is due to highly negative surface charge. There is no trend in particles size and PDI with increasing TMB content; however, results of TEM imaging substantiated findings from DLS experiments, confirming the production of PDA bowls, and revealing interesting structural features of the final product (Figure 3.2). As observed in Figure 3.2 a to c, in comparison to the bowls prepared from M1 (Figure 3.2b), the morphology of the PDA bowls prepared from M2 (Figure 3.2 a and c) is variable, with polydispersity in the population.

Table 3.1. Compositions and conditions applied for the fabrication of PDA bowls.

Method	Fabrication Process Parameters						
	[TMB*] (% v/v)	**[F127*] (% w/v)**	**Ethanol (% v/v)**	**T (°C)**	**Reaction time (h)**	**[DA*] (% w/v)**	**[NH_3] (%)**
M1	2.0	1.0	50	25	2	1.5	28
M2	1.0	1.0	50	25	2	1.5	28
	3.0						
M3	2.0	0.5	50	25	2	1.5	28
		2.0					
M4	2.0	1.0	40	25	2	1.5	28
			80				
M5	2.0	1.0	50	60	2	1.5	28
				80			
M6	2.0	1.0	50	25	24	1.5	28
M7	2.0	1.0	50	25	2	2.5	28
					12		
					24		
M8	2.0	1.0	50	25	24	2.5	25
							26.5

***TMB-trimethylbenzene; F127- Pluronic F-127; DA-dopamine hydrochloride.**

DLS data shows that the sample from M3 with 0.5% F127 had similar average size to the PDA bowls from M1 (1% F127), while particles from M3 with 2% F127 had significantly larger size than the other two (Table 3.2). It can also be observed that both of the samples from M3 with

0.5% and 2% F127 had higher PDI than M1. Phase analysis light scattering (PALS) showed that **M1** and **M3** samples had negative zeta potentials with high magnitudes, indicating stability of these particles in dispersion, again arising from their negative surface charge (Table 3.2). However, there is no trend observed in particle size and PDI with increasing F127 content. The TEM images in Figure 3.2d and e show that PDA bowls were obtained and that variable particle sizes and morphologies are observed in the particles from **M3** with 0.5% and 2% F127 respectively, in comparison to the particles from **M1** with 1% F127 (Figure 3.2b). These results reflect the PDA values measured using DLS (Table 3.2). Furthermore, sample **M3** with 2% F127 showed that PDA bowls had distinct characteristics that deviate from the usual PDA bowls obtained from **M1**, specifically showing larger cavities with the central region of the cavity protruding outward, resembling the cap or pileus of a funnel cap mushroom (Figure 3.2e). The observed differences in size, morphology, and size distribution between the particles obtained from **M1**, **M2**, and **M3** verify that TMB and F127 indeed have significant impact on regulating the size of the PDA bowls. The lack of trend with increasing TMB and F127 concentrations and the morphological variability in the obtained PDA bowls from **M1**, **M2**, and **M3** suggest that a balance between TMB and F127 is required in the formation of PDA bowls with uniform size distribution.

Table 3.2. Dynamic light scattering and zeta potential analysis of the samples prepared from M1 to M8.

Method	Dynamic light scattering [35]	Polydispersity index (PDI) ± SE	Zeta Potential (mV)
M1	267.76 ± 16.40	0.20 ± 0.009	-38.56 ± 0.08
M2 (1.0% (v/v))	502.00 ± 62.17	0.52 ± 0.158	-44.27 ± 7.20
M2 (3.0% (v/v))	458.72 ± 25.59	0.26 ± 0.000	-40.37 ± 4.10
M3 (0.5% (w/v))	283.77 ± 34.36	0.87 ± 0.099	-40.37 ± 4.10
M3 (2.0% (w/v))	412.68 ± 189.64	0.73 ± 0.104	-30.49 ± 1.89
M4 (40%)	317.84 ± 3.05	0.20 ± 0.013	-32.15 ± 0.25
M4 (80%)	413.17 ± 108.85	0.20 ± 0.035	-25.63 ± 2.23
M5 (60 °C)	258.20 ± 33.12	0.24 ± 0.015	-29.71 ± 3.32
M5 (80 °C)	282.00 ± 112.50	0.45 ± 0.101	-28.89 ± 0.86
M6	404.14 ± 14.92	0.42 ± 0.015	-38.33 ± 0.09
M7 (2 h)	502.08 ± 35.90	0.52 ± 0.148	-31.95 ± 3.22
M7 (12 h)	538.74 ± 71.78	0.44 ± 0.039	-29.63 ± 0.85
M7 (24 h)	639.55 ± 121.06	0.39 ± 0.024	-35.02 ± 1.83
M8 (25.0%)	585.24 ± 6.59	0.24 ± 0.033	-38.81 ± 0.04
M8 (26.5%)	395.70 ± 9.36	0.23 ± 0.005	-40.37 ± 1.83

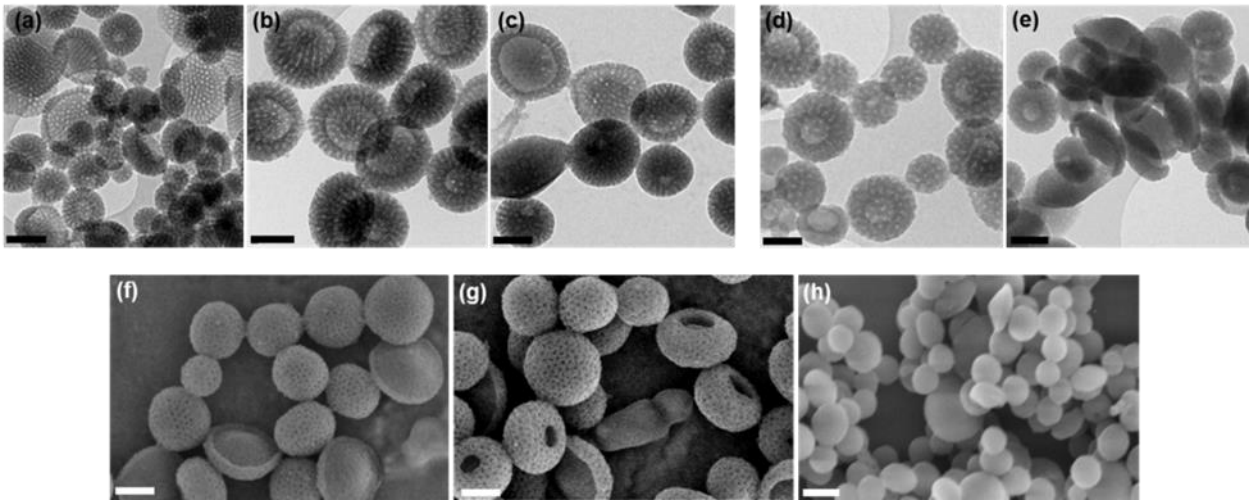

Figure 3.2. Microscopy characterization of the nanoparticles. Transmission electron microscopy (TEM) images (a to e), where a to c were synthesized with various concentrations of TMB (1.0%, 2.0%, and 3.0% (v/v)) with fixed concentration of F127 (1.0% (w/v)) (M1 and M2), particles in TEM images d and e were prepared with various concentrations of F127 (0.5% and 2.0% (w/v)) with fixed concentration of TMB (2.0% (v/v)) (M3). Scanning electron microscopy (SEM) images (f to h); samples were prepared with different volume fractions of ethanol, 40%, 50%, and 80% respectively, with 1.0% (w/v) of F127 and 2.0% (v/v) of TMB (M4). Scale bar: 100 nm.

Since TMB is the dispersed phase, the droplets of TMB act as nucleation sites for PDA, and it is expected that increasing the TMB concentration with fixed F127 content would increase the TMB droplet sizes and, in effect, the PDA bowl sizes. Meanwhile, F127 acts as the stabilizer of the emulsion droplets.[34] Increasing the F127 concentration is expected to cause a decrease in the TMB droplet size (by providing the ability to stabilize more oil/water interface) and therefore in the diameters of resulting PDA bowls; however, since the sonication time was

fixed at 2 min for all of the fabrication methods, the TMB droplets are probably not comminuted enough to realize this outcome. Thus, even with increased F127 concentration, smaller droplets with consistent sizes are not guaranteed without an appropriate or optimized dispersing method.

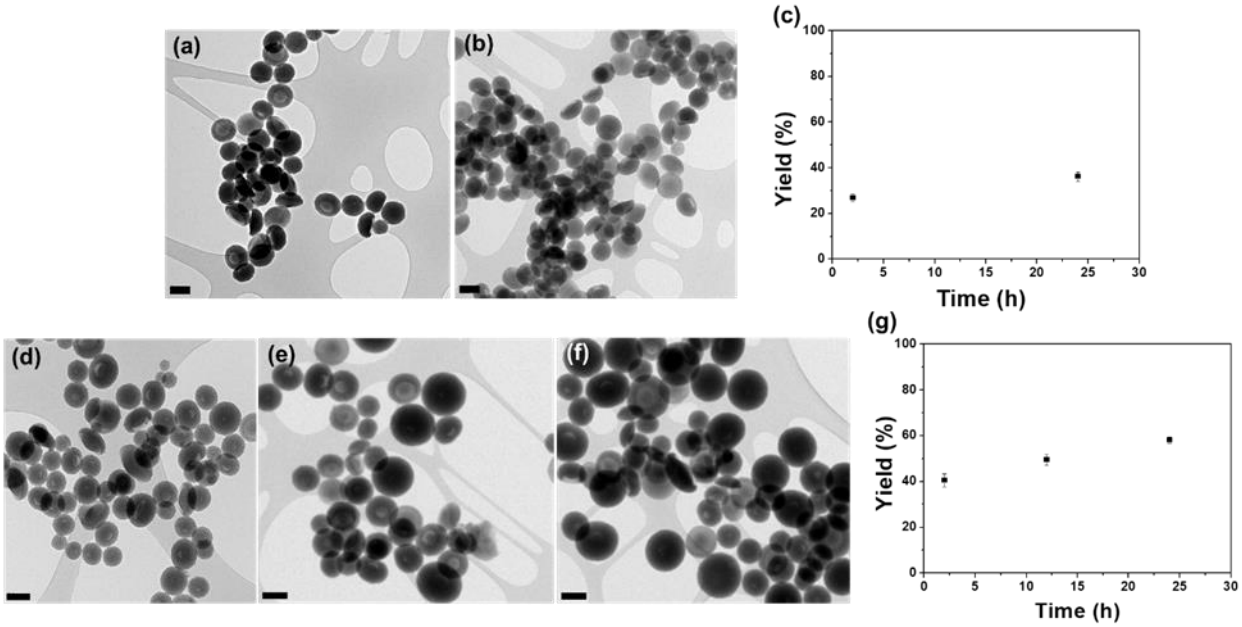

Figure 3.3. TEM images (a and b) of PDA bowls prepared from M1 (a) and M6 (b) and figure c is showing the yield of the final product prepared in 2 h (M1)and 24 h (M6) of polymerization time. TEM images d, e, and f showing PDA bowls prepared from M7 (2, 12, and 24 h of reaction time respectively) and figure g is showing the yield of the final product from M7. Scale bar: 200 nm.

Previous work suggests that formation of well-dispersed PDA nanoparticles is strongly dependent on the volume fraction of ethanol in water[36], as more controllable oxidative

polymerization of dopamine proceeds in a water–ethanol solvent system.[37-38] Thus, the influence of ethanol content on the size of PDA bowls was verified by conducting the polymerization in solvents comprising various water–ethanol ratios (**Method 4, M4 = 40% and 80%**), while retaining the other parameters of **M1** (which used an ethanol concentration of 50%). Synthesized products from **M4** show that particles were obtained with variable size and morphology relative to the particles obtained from **M1,** as clearly observed from DLS data (Table 3.2) and scanning electron microscopy (SEM) images in Figure 3.2f, g, and h. SEM images clearly reveal that irregular shaped hemispherical nanoparticles to mushroom-shaped bowls with protruding central regions of their cavities were obtained from **M4** with 80% ethanol (Figure 3.2h), while other samples from **M4** with 40% ethanol (Figure 3.2f) and **M1** with 50% ethanol content (Figure 3.2g) were found to have well-dispersed PDA bowls with a consistent diameter of ~180 nm. The structure and size variance in the product of reaction **M4** with 80% ethanol can be described as the result of slowing the polymerization rate of dopamine at high ethanol concentration, which is unfavourable for the formation of bowl-structured particles.[34, 37]

We also explored the effect of the reaction temperature by polymerizing the samples at elevated temperatures (**Method 5**, **M5= 60 °C and 80 °C**), while retaining the other parameters of **M1** (where reaction temperature was 25 °C). The most notable observation in both **M5** samples is the absence of cavities in the particles (Figure 3.S1 a and b). At 60 °C, mesoporous nanospheres of around 250 nm in size were obtained (Figure 3.S1a) and at 80 °C smooth PDA nanospheres of around 200 nm diameter were observed (Figure 3.S1b). These are significantly different structures compared to the well-dispersed, ~180 nm PDA bowls

with ~80 nm cavity and ~6 nm size mesopores from **M1** (Figure 3.2g). Obtained results demonstrate that elevated temperatures disrupt the stability of F127/TMB/polydopamine composite micelles, which are crucial for the formation of both mesopores and the internal cavity.[34]

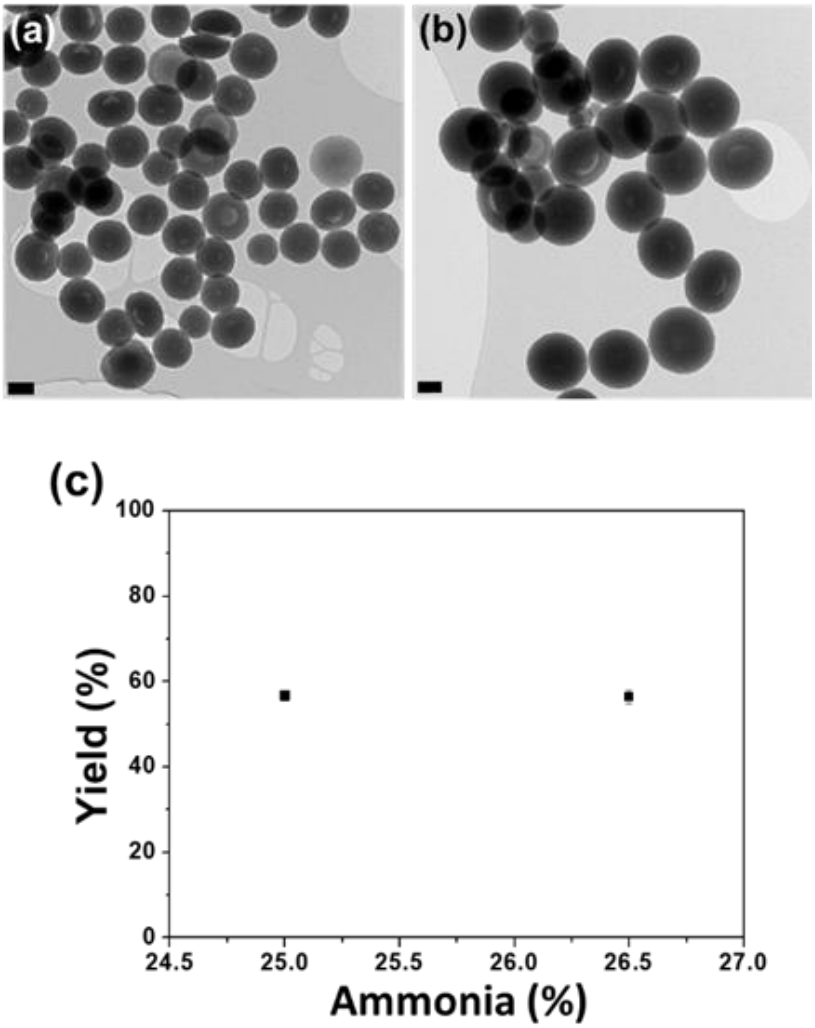

Figure 3.4. TEM images of PDA bowls from M8, where a and b prepared in 26.5% and 25% of ammonia respectively, figure c showing the yield of the final product of M8. Scale bar: 200 nm.

The fast self-polymerization of dopamine can be initiated after adding ammonia, due to the high sensitivity of dopamine to basic pH and oxygen. A rapid color change in the reaction mixture from white to pale brown confirms that dopamine polymerization has initiated (Figure 3.S2). While in the current work, a two-hour polymerization time was used in the first five methods including **M1**, which produces PDA bowls at around 180 nm size, some reports in the literature suggest that longer polymerization times (at least 12 h) are required in order to obtain PDA nanoparticles with maximum yield.[15, 22, 39] Considering this, we prolonged the reaction time (**Method 6, M6 = 24 h of polymerization time**), while maintaining the other parameters of **M1** (where polymerization time was 2 h). TEM images of the samples from **M6** confirm the morphology of the particles (Figure 3.3b); it is seen that there is no increase in particle size in compared to the samples of **M1** (Figure 3.3a and 2.2b), however, a larger proportion of particles had larger cavities with the central region of the cavity protruding outward (Figure 3.3b). DLS data shows that the sample of **M6** with longer polymerization time yielded particles with larger diameter than the samples prepared in 2 h (**M1**) with similar surface charge (Table 3.2). Additionally, it has been observed that the yield of the particles from **M6** increased by 10% compared with sample **M1** (Figure 3.3c), indicating polymerization of unreacted dopamine in the reaction mixture.[40]

Previous studies suggest that the diameter of PDA nanoparticles increase with increasing dopamine concentration after prolonged reaction time.[22, 40] Therefore, the influence of dopamine concentration in reactions undertaken for various times on the size of PDA bowls was investigated by conducting polymerization for 2, 12, and 24 h (**Method 7, M6 = 2.5% w/v dopamine, polymerization time= 2, 12, and 24 h**), noting that other parameters were

identical to **M1**. DLS data show that the effective diameter of the particles increasing with increasing reaction time, and negative zeta potential values indicated colloidal stability of these particles in dispersion due to their highly negative surface charge (Table 3.2). TEM images show that resulting PDA bowls from all the samples obtained from **M7** were variable in particles size, with evident polydispersity (Figure 3.3 d, e, and f) and the number of larger sized bowls increased in the particle population with increasing reaction time. To be more specific, the number of bowls >350 nm within the population increased in 24 h of reaction time compared to 12 h. Additionally, the yield of resulting nanoparticles increased with reaction time (Figure 3.3g). This result may be interpreted as a higher concentration of dopamine and prolonged polymerization time favouring a high degree of self-polymerization, which leads to a rise in the diameter of the PDA bowls and yield of the final products.[41] Herein, polydispersity in the particle population (Figure 3.3 d to f) can be explained as an outcome of higher agglomeration due to uncontrolled self-polymerization of dopamine.[41] It has been suggested that agglomeration can be controlled by tuning the pH of the reaction mixture, which assists in retaining a mild and controllable self-polymerization of dopamine.[42-43]

Considering this, we conducted the formation process at various ammonia concentrations (**Method 8, M8 = 26.5% and 25% ammonia**), while the other parameters were identical to those used in **M7** and the duration of the polymerization kept fixed at 24 h. DLS data in Table 3.2 show a significant increase in particle diameter with decreasing ammonia concentration from 26.5% to 25% (**M8**), and both samples of **M8** had negative zeta potentials with high magnitudes, indicating colloidal stability of these particles in dispersion. TEM images in Figure 3.4 a and b support size analysis data from DLS, and reveal the morphology of the particles,

where two different sized uniform populations of PDA bowls were observed at around 350 and 520 nm, resulting from 26.5% and 25% ammonia respectively. Obtained results can be interpreted by assuming that the kinetic rate constant of dopamine polymerization increases with an increased solution pH, triggering the nucleation process of PDA, and in turn resulting particle with smaller diameter.[40, 44] Additionally, no significant changes were observed in the yield of the final product prepared from **M8** (Figure 3.4c). High-magnified TEM images in Figure 3.S3 clearly show that the diameter of the PDA bowls noticeably increases by tuning the concentration of dopamine and ammonia at prolonged reaction times. Taken together, it is worth mentioning that the concentration of ammonia, an appropriate concentration of dopamine, and an adequate polymerization time are all significant factors in size-controlled synthesis of PDA bowls. We have now systematically mapped out the phase space for this reaction, allowing highly tuned synthesis of specific sizes, morphologies, and dispersity of PDA bowls.

3.3.2 In vitro cytotoxicity assay of PDA bowls

It has been demonstrated that the viability reduction of cells correlates with the size of internalized particles.[45] However, considering the biocompatible properties of PDA, PDA bowls were expected to show low cytotoxicity. Nevertheless, cytotoxicity of ~180 and ~520nm PDA bowls was evaluated in HeLa cells, where a standard 3-(4,5-dimethylthiazole-2-yl)-5-(3-carboxymethoxyphenyl)-2-(4-sulfophenyl)-2H-tetrazoliumin (MTS) was employed to assess cell viability.[31] The assay was conducted in triplicate with ~180 nm (M1) and ~520 nm (M8 with 25% NH_4OH) PDA bowls for 4 and 24 h of incubation time. In Figure 3.5A, obtained

results show that the cell line maintained viability of over 90% upon increasing the concentration of both sizes of PDA bowls from 50 to 200 µg/mL for an incubation period of 24 h.

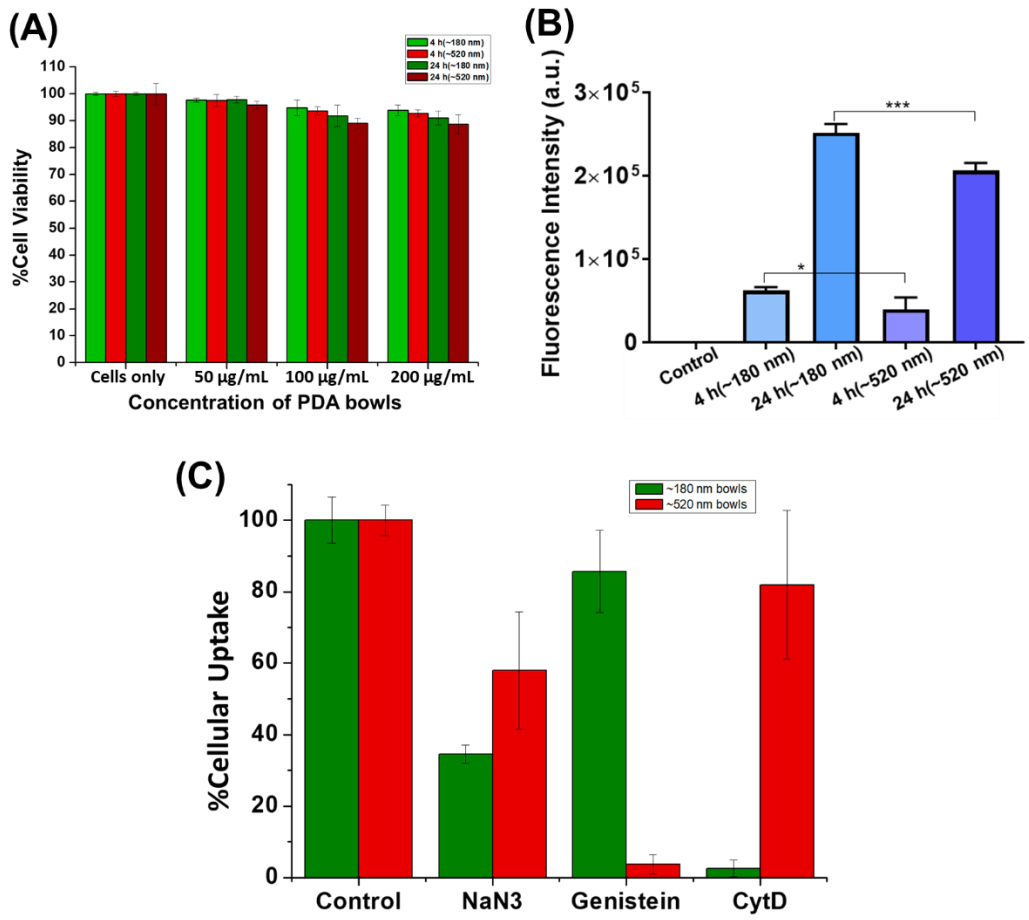

Figure 3.5. (A) Cell viability of HeLa cells measured by MTS assay. (B) Data from flow cytometry analysis showing measured fluorescence intensity of HeLa cells after 4 h (~180 nm vs. ~520 nm-P value: $P < 0.0247$) and 24 h (~180 nm vs. ~520 nm-P value: $P < 0.0002$) of incubation with various sizes of PDA bowls (light and deep blue: ~180 nm PDA bowls) (light and deep purple: ~520 nm PDA bowls). (C) Control (cells without inhibitor treatment) and impact of inhibitor treatment on cellular uptake of PDA bowls at around 180 nm (green) and 520 nm.

3.3.3. Efficiency of cellular uptake of PDA bowls based on their size

Considering the significant size difference between ~180 and ~520 nm PDA bowls, these two sets of particles were selected to utilise for obtaining a clear understanding of bowls size-dependent endocytosis. This investigation was conducted by incubating PDA bowls with human cervical carcinoma epithelial (HeLa) cells for 4 and 24 h. The quantity of PDA bowls that had been internalized into the HeLa cells was analyzed using flow cytometry. The obtained results indicated that these two sizes of bowls internalization into the HeLa cells relatively rapidly. After 4 h of incubation, a high concentration of bowls had been internalized, and this increased significantly after 24 h (Figure 3.5B). Additionally, a considerably higher fluorescence intensity was recorded in cells incubated with bowls (~180 nm) compared to the larger ones (~520 nm) (Figure 3.5B). These results suggest a faster cellular uptake of smaller PDA bowls (~180 nm), which might be the result of stronger adhesion of the smaller sized bowls to the cell surface.[46]

3.3.4 Possible uptake pathways for different-sized PDA bowls

To understand the effect of size of PDA bowls on their internalization pathways into cells, HeLa cells were treated with selected inhibitors of energy-dependent processes, macropinocytosis, and caveolae-mediated endocytosis. The role of the inhibitors is to block certain pathways and inhibit particle uptake through that particular pathway into the cell. First, to investigate energy dependence, cells were treated with sodium azide (NaN_3/2-deoxyglucose (NaN_3/DOG)) prior incubation with PDA bowls (~180 nm and ~520 nm). Herein, sodium azide blocks cellular ATP synthesis of the cells,[47] and we observed a significant

decrease in the cellular internalization of both sizes of PDA bowls compared with the control (which was not treated with any inhibitors), indicating that cellular internalization of PDA bowls is an energy dependent process (Figure 3.5C). To be more specific, Figure 3.5C shows that compared with the control (non treated cells incubated with ~180 nm bowls), only 35% of the PDA ~180 nm PDA bowls were internalized into the cells, whereas, 57% of ~520 nm PDA were found to be internalized relative to the control (non treated cells incubated with ~520 nm bowls). Obtained results suggest a higher tendency for energy dependence behavior when internalizing smaller sized PDA bowls into the HeLa cells. Additionally, it is notable that complete inhibition was not observed, which is most likely due to exogenous ATP and glucose present in the cell culture media.[31] The predominant role of sodium azide in endocytosis and the impact of particle size in this process have been demonstrated in earlier studies, and this is congruent with our findings here for PDA bowls.[31, 48]

Next, cells were treated with cytochalasin D (CytD), an inhibitor of macropinocytosis, which disrupts particle internalization by disrupting F-actin polymerization.[31, 49] Our results show that internalization of ~180 nm bowls into HeLa cells was significantly blocked by CytD (Figure 3.5C). Precisely, in comparison to the control, around 93% of the bowls were inhibited from internalization by CytD relative to the control, as shown in Figure 3.5C. This strongly suggests that PDA bowls at around 180 nm are internalized by macropinocytosis, and these result is consistent with previous studies on other particles types.[31] In contrast, the changes in the level of internalization of ~520 nm PDA bowls into the CytD treated cells was insignificant when compared to the nontreated cells, and this internalization behavior of particles at around 500 nm has also been demonstrated previously for latex particles (Figure 3.5C).[32]

For further investigation, cells were treated with genistein before incubation with PDA bowls of both sizes (~180 nm and ~520 nm) for 24 h. Earlier studies have demonstrated that genistein blocks caveolae-mediated endocytosis by local disruption of the actin network.[33, 50] Flow cytometry data in Figure 3.5C shows that PDA bowls at ~520 nm were significantly inhibited from cellular uptake by genistein. In contrast, inhibition of bowls at around 180 nm was not noted. To be more specific, when compared to non-treated cells, the quantity of ~520 nm bowls uptaken by cells was inhibited by >90%, suggesting larger sized bowls (~520 nm) were taken up by caveolae-mediated endocytosis. However, uptake of ~180 nm bowls was diminished by only around 8% with genistein.

Taken together, flow cytometry analysis results (Figure 3.5C) demonstrate that uptake of PDA bowls by HeLa cells is an energy-dependent process, and macropinocytosis is prominently involved in the internalization of smaller size PDA bowls (~180 nm), whereas a caveolae-mediated process is the preferred endocytosis pathway for larger bowls at around 520 nm to internalize into cells. These results are entirely consistent with previous studies on different particles with very different surface chemistry around these sizes, where the same trends for internalization by these pathways are seen.[31-32] This results further hint that particles surface chemistry may be secondary to particles size/shape in modulating cell internalization pathways.

The internalization mechanism of two sets of PDA bowls was also investigated by confocal microscopy analysis. Images in Figure 3.6 demonstrate that relative to a control (only cells), a

high degree of bowls of both sizes were internalized into HeLa cells during the incubation time course of 24 h. In comparison to non-treated cells, a tendency of reduction of internalization upon treatment with NaN_3 was observed for both sizes of bowls, which further confirms that the internalization of PDA bowls into HeLa cells is an energy-dependent process.

Confocal images in Figure 3.6B and C clearly show the morphological changes of inhibitor treated cells relative to non-treated ones, which occurs due to inhibitor treatment, and this behavior of cells has been demonstrated in previous studies.[51, 52-53] Genistein an inhibitor of caveolae-mediated internalization by local disruption of the actin network and CytD binds to the fast-growing ends of actin nuclei and filaments, preventing addition of monomeric actin to these sites, thus blocking macropinocytosis.[50, 54]

As observe, internalization of ~180 nm bowls was entirely stopped by CytD, and complete inhibition of ~520 nm bowls was observed on addition of genistein (Figure 3.6 B and C), suggesting the predominant role of macropinocytosis and caveolae mediated endocytosis in the internalization of ~180 and ~520 nm bowls respectively. These confocal results are fully consistent with the flow cytometry data presented above (Figure 3.5C).

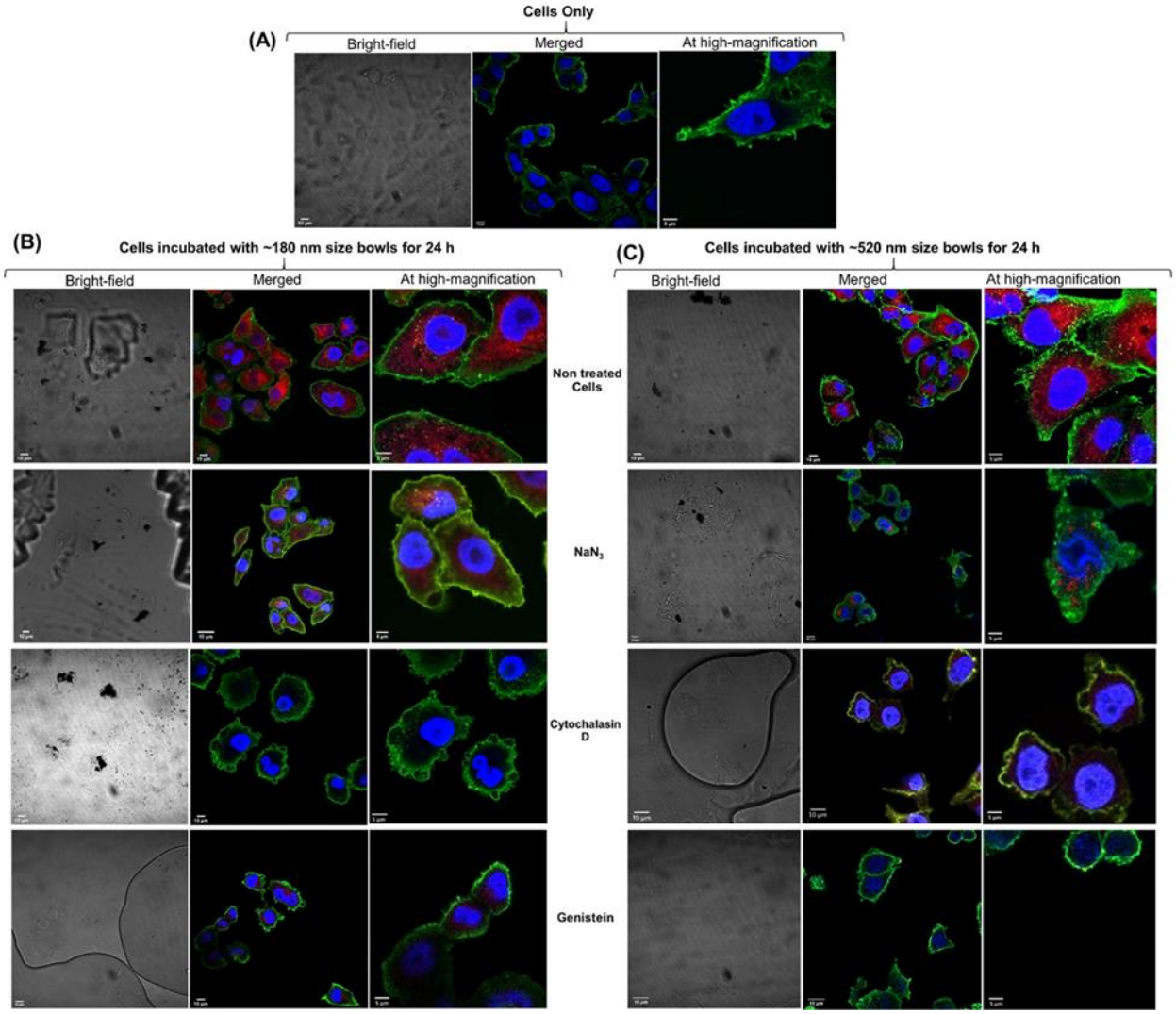

Figure 3.6. Confocal images of HeLa cells, (A) Control. (B) and (C) non-treated and inhibitor treated cells, where, (B) ~180 nm sizes of bowls and C) ~520 nm sizes of bowls. (24 h of incubation time). Here, blue represent nucleus of the cell, green is the cell membrane, and red fluorescence signal represents internalized particles.

Transmission electron microscopy (TEM) was adopted to further confirm the above findings and visually analyze the location of particles within the cells. In our previous study, we observed that PDA bowls tend to be widely distributed within cells;[16] here, indistinguishable

internalization behavior of both sets of PDA bowls were observed in the non-treated cells shown in Figure 3.7. The micrographs show a noticeable reduction in the number of bowls present in the imaged cells after treatment with NaN_3 in both sets of PDA bowls. High magnification view reveals that only three ~180 nm bowls were located within the cell, and one was found close to the cell membrane, while seven ~520 nm bowls were located around the cell membrane area in the cell, and one was located outside of the cells, strongly supporting the results obtained by flow cytometry analysis (Figure 3.5C). As observed in TEM image of CytD treated cells, internalization of smaller sized PDA bowls (~180 nm) was entirely inhibited, and few of them were located outside of the cells.

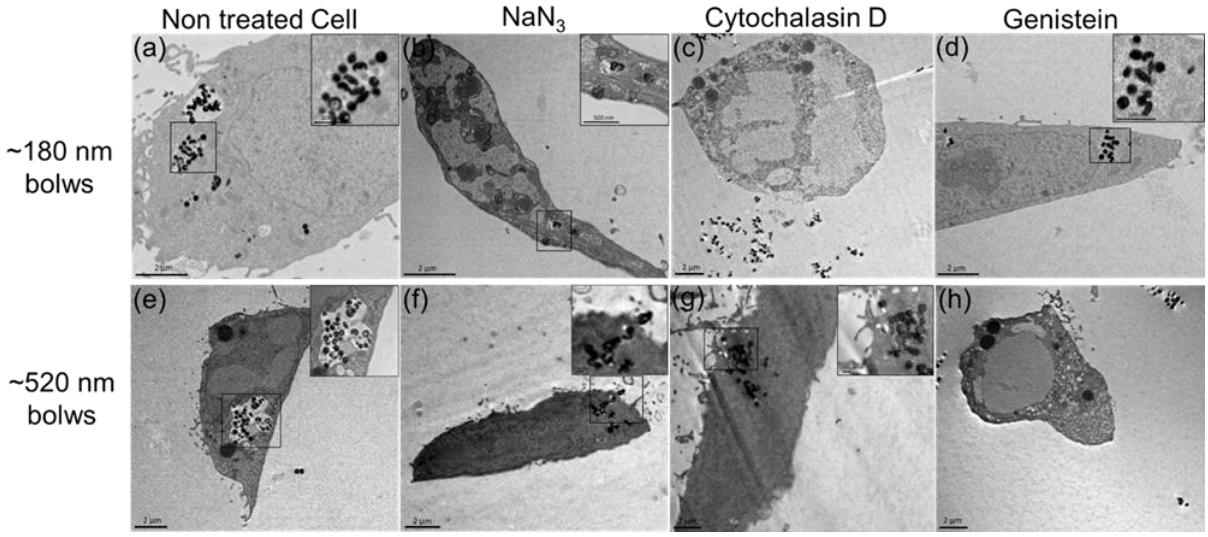

Figure 3.7. TEM images of HeLa cell. Non-treated and inhibitor treated cells incubated with ~180 nm sizes of PDA bowls (a) to (d) and ~520 nm sizes of PDA bowls (e) to (h) for 24 h. Scale bar: 2µm (low magnified view) and 500 nm (high magnified view).

In contrast, a large number of larger sized PDA bowls (~520 nm) were internalized in CytD treated cells, confirming the predominant role of macropinocytosis in uptake of smaller sized bowls (~180 nm), also observed in confocal imaging and flow cytometry analysis. TEM imaging further confirms that inhibition of ~520 nm bowls was caused by treatment of the cells with genistein, while this particular inhibitor did not show any significant disruption to the uptake of ~180 nm bowls. These results further confirm that the cellular internalization of PDA bowls is an energy-dependent process, and size of the PDA bowls has a significant role in selecting endocytosis pathways to internalize them into HeLa cells.

3.4 Conclusions

In summary, we established precise experimental conditions to synthesize various sizes of PDA bowls with well-defined and reproducible physicochemical properties. Obtained results demonstrate that both the size and morphology of PDA bowls plays an exceptionally important role in cellular internalization processes. The size of PDA bowls has been identified as a dominant factor in their uptake efficiency and intracellular trafficking, and these are strongly connected with the ultimate efficacy of drug nanocarriers. Herein, we observed that PDA bowl size specifically governs the endocytosis pathway for such particles in HeLa cells. Taken together, our study contributes to establishing standardized experimental conditions for size-controlled fabrication of biocompatible anisotropic nanoparticles like PDA bowls. Moreoever, these findings advance the field because it is found that the size of PDA bowls, in the absence of surface modification of the particles, can regulate endocytosis mechanism. We anticipate that the effects seen here would equally correspond to other nanoparticles

with similar surface chemistries especially from biologically inspired or natural materials. Therefore, this study contributes significant knowledge towards the development of efficient drug nanocarriers to the desired sites of the therapeutic action for a range of cancer therapies.

3.5 References

(1) Zhu, Y.; Liu, C.; Pang, Z. Dendrimer-Based Drug Delivery Systems for Brain Targeting. *Biomolecules* **2019,** *9* (12), 790, DOI: 10.3390/biom9120790.
(2) Zylberberg, C.; Matosevic, S. Pharmaceutical Liposomal Drug Delivery: A Review of New Delivery systems and A Look at the Regulatory Landscape. *Drug Delivery* **2016,** *23* (9), 3319-3329, DOI: 10.1080/10717544.2016.1177136.
(3) Chen, S.; Hao, X.; Liang, X.; Zhang, Q.; Zhang, C.; Zhou, G.; Shen, S.; Jia, G.; Zhang, J. Inorganic Nanomaterials as Carriers for Drug Delivery. *Journal of Biomedical Nanotechnology* **2016,** *12* (1), 1-27, DOI: 10.1166/jbn.2016.2122.
(4) Sung, Y. K.; Kim, S. W. Recent Advances in Polymeric Drug Delivery Systems. *Biomaterials Research* **2020,** *24* (1), 12, DOI: 10.1186/s40824-020-00190-7.
(5) Bobo, D.; Robinson, K. J.; Islam, J.; Thurecht, K. J.; Corrie, S. R. Nanoparticle-Based Medicines: A Review of FDA-Approved Materials and Clinical Trials to Date. *Pharmaceutical Research* **2016,** *33* (10), 2373-87, DOI: 10.1007/s11095-016-1958-5.
(6) Wilhelm, S.; Tavares, A.; Dai, Q.; Ohta, S.; Audet, J.; Dvorak, H.; Chan, W. Analysis of Nanoparticle Delivery to Tumours. *Nature Reviews Materials* **2016,** *1*, 16014, DOI: 10.1038/natrevmats.2016.14.
(7) Pasut, G. Grand Challenges in Nano-Based Drug Delivery. *Frontiers in Medical Technology* **2019,** *1*, 1-4, DOI: 10.3389/fmedt.2019.00001.
(8) De Jong, W. H.; Borm, P. J. A. Drug Delivery and Nanoparticles: Applications and Hazards. *International Journal of Nanomedicine* **2008,** *3* (2), 133-149, DOI: 10.2147/ijn.s596.
(9) Vega-Vásquez, P.; Mosier, N. S.; Irudayaraj, J. Nanoscale Drug Delivery Systems: From Medicine to Agriculture. *Frontiers in Bioengineering and Biotechnology* **2020,** *8* (79), 1-16, DOI: 10.3389/fbioe.2020.00079.
(10) Li, S.; Liu, Y.; Ma, Q. A Novel Polydopamine Electrochemiluminescence Organic Nanoparticle-Based Biosensor for Parathyroid Hormone Detection. *Talanta* **2019,** *202*, 540-545, DOI: 10.1016/j.talanta.2019.05.022.
(11) Salazar, P.; Martín, M.; González-Mora, J. Polydopamine-Modified Surfaces in Biosensor Applications. *Polymer Science: Research Advances, Practical Applications and Educational Aspects* **2016**; pp 385-396.
(12) Zhang, J.; Mou, L.; Jiang, X. Hydrogels Incorporating Au@Polydopamine Nanoparticles: Robust Performance for Optical Sensing. *Analytical Chemistry* **2018,** *90* (19), 11423-11430, DOI: 10.1021/acs.analchem.8b02459.
(13) Posati, T.; Nocchetti, M.; Kovtun, A.; Donnadio, A.; Zambianchi, M.; Aluigi, A.; Capobianco, M. L.; Corticelli, F.; Palermo, V.; Ruani, G.; Zamboni, R.; Navacchia, M. L.; Melucci, M. Polydopamine Nanoparticle-Coated Polysulfone Porous Granules as Adsorbents for Water Remediation. *ACS Omega* **2019,** *4* (3), 4839-4847, DOI: 10.1021/acsomega.8b02900.

(14) Liu, Y.; Ai, K.; Lu, L. Polydopamine and Its Derivative Materials: Synthesis and Promising Applications in Energy, Environmental, and Biomedical Fields. *Chemical Reviews* **2014,** *114* (9), 5057-5115, DOI: 10.1021/cr400407a.
(15) Zhang, L.; Yang, P.; Guo, R.; Sun, J.; Xie, R.; Yang, W. Multifunctional Mesoporous Polydopamine with Hydrophobic Paclitaxel For Photoacoustic Imaging-Guided Chemo-Photothermal Synergistic Therapy. *International Journal of Nanomedicine* **2019,** *14*, 8647-8663, DOI: 10.2147/IJN.S218632.
(16) Acter, S.; Vidallon, M. L. P.; Crawford, S.; Tabor, R. F.; Teo, B. M. Efficient Cellular Internalization and Transport of Bowl-Shaped Polydopamine Particles. *Particle & Particle Systems Characterization* **2020,** *37*, 2000166, DOI: 10.1002/ppsc.202000166.
(17) Li, T.-D.; Zhang, R.; Chen, H.; Huang, Z.-P.; Ye, X.; Wang, H.; Deng, A.-M.; Kong, J.-L. An Ultrasensitive Polydopamine Bi-Functionalized SERS Immunoassay for Exosome-Based Diagnosis and Classification of Pancreatic Cancer. *Chemical Science* **2018,** *9* (24), 5372-5382, DOI: 10.1039/C8SC01611A.
(18) Mrówczyński, R. Polydopamine-Based Multifunctional (Nano) Materials for Cancer Therapy. *ACS Applied Materials & Interfaces* **2018,** *10* (9), 7541-7561, DOI: 10.1021/acsami.7b08392.
(19) Poinard, B.; Neo, S. Z. Y.; Yeo, E. L. L.; Heng, H. P. S.; Neoh, K. G.; Kah, J. C. Y. Polydopamine Nanoparticles Enhance Drug Release for Combined Photodynamic and Photothermal Therapy. *ACS Applied Materials & Interfaces* **2018,** *10* (25), 21125-21136, DOI: 10.1021/acsami.8b04799.
(20) Ball, V. Polydopamine Nanomaterials: Recent Advances in Synthesis Methods and Applications. *Frontiers in Bioengineering Biotechnology* **2018,** *6*, 109-109, DOI: 10.3389/fbioe.2018.00109.
(21) Ryu, J. H.; Messersmith, P. B.; Lee, H. Polydopamine Surface Chemistry: A Decade of Discovery. *ACS Applied Materials & Interfaces* **2018,** *10* (9), 7523-7540, DOI: 10.1021/acsami.7b19865.
(22) Zmerli, I.; Michel, J.-P.; Makky, A. Bioinspired Polydopamine Nanoparticles: Synthesis, Nanomechanical Properties, and Efficient PEGylation Strategy. *Journal of Materials Chemistry B* **2020,** *8* (20), 4489-4504, DOI: 10.1039/C9TB02769F.
(23) Deng, Y.; Yang, W.-Z.; Shi, D.; Wu, M.; Xiong, X.-L.; Chen, Z.-G.; Wei, S.-C. Bioinspired and Osteopromotive Polydopamine Nanoparticle-Incorporated Fibrous Membranes for Robust Bone Regeneration. *NPG Asia Materials* **2019,** *11* (1), 39, DOI: 10.1038/s41427-019-0139-5.
(24) Jin, A.; Wang, Y.; Lin, K.; Jiang, L. Nanoparticles Modified by Polydopamine: Working as “Drug” Carriers. *Bioactive Materials* **2020,** *5* (3), 522-541, DOI: 10.1016/j.bioactmat.2020.04.003.
(25) Sun, Y.; Davis, E. Bowl-Shaped Polydopamine Nanocapsules: Control of Morphology via Template-Free Synthesis. *Langmuir : the ACS Journal of Surfaces and Colloids* **2020,** *36* (32), 9333-9342, DOI: 10.1021/acs.langmuir.0c00790.
(26) Liu, X.; Wu, F.; Tian, Y.; Wu, M.; Zhou, Q.; Jiang, S.; Niu, Z. Size Dependent Cellular Uptake of Rod-like Bionanoparticles with Different Aspect Ratios. *Scientific Reports* **2016,** *6* (1), 24567, DOI: 10.1038/srep24567.
(27) Toy, R.; Peiris, P. M.; Ghaghada, K. B.; Karathanasis, E. Shaping Cancer Nanomedicine: the Effect of Particle Shape on the in *Vivo* Journey of Nanoparticles. *Nanomedicine (Lond)* **2014,** *9* (1), 121-134, DOI: 10.2217/nnm.13.191.
(28) Truong Phuoc, N.; Whittaker, M.; Mak, C.; Davis, T. The Importance of Nanoparticle Shape in Cancer Drug Delivery. *Expert Opinion on Drug Delivery* **2015,** *12*, 129-142, DOI: 10.1517/17425247.2014.950564.
(29) Li, H.; Zhang, W.; Tong, W.; Gao, C. Enhanced Cellular Uptake of Bowl-like Microcapsules. *ACS Applied Materials & Interfaces* **2016,** *8* (18), 11210-11214, DOI: 10.1021/acsami.6b02965.
(30) Mulyati, S.; Muchtar, S.; Arahman, N.; Syamsuddin, Y.; Mat Nawi, N. I.; Yub Harun, N.; Bilad, M. R.; Firdaus, Y.; Takagi, R.; Matsuyama, H. Two-Step Dopamine-to-Polydopamine Modification of Polyethersulfone Ultrafiltration Membrane for Enhancing Anti-Fouling and Ultraviolet Resistant Properties. *Polymers (Basel)* **2020,** *12* (9), 2051, DOI: 10.3390/polym12092051.
(31) Gratton, S. E. A.; Ropp, P. A.; Pohlhaus, P. D.; Luft, J. C.; Madden, V. J.; Napier, M. E.; DeSimone, J. M. The Effect of Particle Design on Cellular Internalization Pathways. *Proceedings of the National Academy of Sciences* **2008,** *105* (33), 11613, DOI: 10.1073/pnas.0801763105.

(32) Rejman, J.; Oberle, V.; Zuhorn, I. S.; Hoekstra, D. Size-Dependent Internalization of Particles Via the Pathways of Clathrin- and Caveolae-Mediated Endocytosis. *The Biochemical Journal* **2004,** *377* (Pt 1), 159-69, DOI: 10.1042/bj20031253.
(33) Rejman, J.; Bragonzi, A.; Conese, M. Role of Clathrin- and Caveolae-Mediated Endocytosis in Gene Transfer Mediated by Lipo- and Polyplexes. *Molecular Therapy : the Journal of the American Society of Gene Therapy* **2005,** *12* (3), 468-74, DOI: 10.1016/j.ymthe.2005.03.038.
(34) Guan, B. Y.; Yu, L.; Lou, X. W. Formation of Asymmetric Bowl-Like Mesoporous Particles *Via* Emulsion-Induced Interface Anisotropic Assembly. *Journal of the American Chemical Society* **2016,** *138* (35), 11306-11311, DOI: 10.1021/jacs.6b06558.
(35) Burrows, N. D.; Vartanian, A. M.; Abadeer, N. S.; Grzincic, E. M.; Jacob, L. M.; Lin, W.; Li, J.; Dennison, J. M.; Hinman, J. G.; Murphy, C. J. Anisotropic Nanoparticles and Anisotropic Surface Chemistry. *The Journal of Physical Chemistry Letters* **2016,** *7* (4), 632-641, DOI: 10.1021/acs.jpclett.5b02205.
(36) Jiang, X.; Wang, Y.; Li, M. Corrigendum: Selecting Water-Alcohol Mixed Solvent for Synthesis of Polydopamine Nano-Spheres Using Solubility Parameter. *Scientific Reports* **2014,** *4*, 6070, DOI: 10.1038/srep06070.
(37) Yue, Q.; Wang, M.; Sun, Z.; Wang, C.; Wang, C.; Deng, Y.; Zhao, D. A Versatile Ethanol-Mediated Polymerization of Dopamine for Efficient Surface Modification and the Construction of Functional Core–Shell Nanostructures. *Journal of Materials Chemistry B* **2013,** *1* (44), 6085-6093, DOI: 10.1039/C3TB21028F.
(38) You, I.; Jeon, H. J.; Lee, K.; Do, M.; Seo, Y. C.; Lee, H. A.; Lee, H. Polydopamine Coating in Organic Solvent for Material-Independent Immobilization of Water-Insoluble Molecules and Avoidance of Substrate Hydrolysis. *Journal of Industrial and Engineering Chemistry* **2017,** *46*, 379-385, DOI: 10.1016/j.jiec.2016.11.007.
(39) Luo, H.; Gu, C.; Zheng, W.; Dai, F.; Wang, X.; Zheng, Z. Facile Synthesis of Novel Size-Controlled Antibacterial Hybrid Spheres Using Silver Nanoparticles Loaded with Poly-Dopamine Spheres. *RSC Advances* **2015,** *5* (18), 13470-13477, DOI: 10.1039/C4RA16469E.
(40) Ho, C. C.; Ding, S. J. The pH-Controlled Nanoparticles Size of Polydopamine for Anti-Cancer Drug Delivery. *Journal of Materials Science. Materials in Medicine* **2013,** *24* (10), 2381-90, DOI: 10.1007/s10856-013-4994-2.
(41) Wang, Y.; Fang, Z.; Zhao, S.; Ng, D.; Zhang, J.; Xie, Z. Dopamine Incorporating Forward Osmosis Membranes with Enhanced Selectivity and Antifouling Properties. *RSC Advances* **2018,** *8* (40), 22469-22481, DOI: 10.1039/C8RA03166E.
(42) Xi, Z.; Xu, Y.; Zhu, L.; Wang, Y.; Zhu, B.-k. A Facile Method of Surface Modification for Hydrophobic Polymer Membranes Based on the Adhesive Behavior of Poly(DOPA) and Poly(dopamine). *Journal of Membrane Science* **2009,** *327*, 244-253, DOI: 10.1016/JMEMSCI.2008.11.037.
(43) Zhao, J.; Su, Y.; He, X.; Zhao, X.; Li, Y.; Zhang, R.; Jiang, Z. Dopamine Composite Nanofiltration Membranes Prepared by Self-Polymerization and Interfacial Polymerization. *Journal of Membrane Science* **2014,** *465*, 41–48, DOI: 10.1016/j.memsci.2014.04.018.
(44) Bisaglia, M.; Mammi, S.; Bubacco, L. Kinetic and Structural Analysis of the Early Oxidation Products of Dopamine: Analysis of the Interactions with Alpha-Synuclein. *The Journal of Biological Chemistry* **2007,** *282* (21), 15597-605, DOI: 10.1074/jbc.M610893200.
(45) Kim, T.-H.; Kim, M.; Park, H.-S.; Shin, U. S.; Gong, M.-S.; Kim, H.-W. Size-Dependent Cellular Toxicity of Silver Nanoparticles. *Journal of Biomedical Materials Research Part A* **2012,** *100A* (4), 1033-1043, DOI: 10.1002/jbm.a.34053.
(46) Hoshyar, N.; Gray, S.; Han, H.; Bao, G. The Effect of Nanoparticle Size on in *Vivo* Pharmacokinetics and Cellular Interaction. *Nanomedicine (Lond)* **2016,** *11* (6), 673-692, DOI: 10.2217/nnm.16.5.
(47) Schwoebel, E. D.; Ho, T. H.; Moore, M. S. The Mechanism of Inhibition of Ran-Dependent Nuclear Transport by Cellular ATP Depletion. *Journal of Cell Biology* **2002,** *157* (6), 963-974, DOI: 10.1083/jcb.200111077.

(48) Kim, J.-S.; Yoon, T.-J.; Yu, K.-N.; Noh, M.-S.; Woo, M.; Kim, B.-G.; Lee, K.-H.; Sohn, B.-H.; Park, S.-B.; Lee, J.-K.; Cho, M.-H. Cellular Uptake of Magnetic Nanoparticle is Mediated Through Energy-Dependent Endocytosis in A549 Cells. *Journal of Veterinary Science* **2006,** *7* (4), 321-326, DOI: 10.4142/jvs.2006.7.4.321.
(49) Xie, X.; Liao, J.; Shao, X.; Li, Q.; Lin, Y. The Effect of Shape on Cellular Uptake of Gold Nanoparticles in the Forms of Stars, Rods, and Triangles. *Scientific Reports* **2017,** *7* (1), 3827, DOI: 10.1038/s41598-017-04229-z.
(50) Singh, J.; Michel, D.; Chitanda, J. M.; Verrall, R. E.; Badea, I. Evaluation of Cellular Uptake and Intracellular Trafficking as Determining Factors of Gene Expression for Amino Acid-Substituted Gemini Surfactant-Based DNA Nanoparticles. *Journal of Nanobiotechnology* **2012,** *10* (7), 1-14, DOI: 10.1186/1477-3155-10-7.
(51) Cui, S.; Wienhoefer, N.; Bilitewski, U. Genistein Induces Morphology Change and G2/M Cell Cycle Arrest by Inducing p38 MAPK Activation in Macrophages. *International Immunopharmacology* **2014,** *18* (1), 142-150, DOI: 10.1016/j.intimp.2013.11.016.
(52) Francia, V.; Reker-Smit, C.; Boel, G.; Salvati, A. Limits and Challenges in Using Transport Inhibitors to Characterize How Nano-Sized Drug Carriers Enter Cells. *Nanomedicine (Lond)* **2019,** *14* (12), 1533-1549, DOI: 10.2217/nnm-2018-0446.
(53) dos Santos, T.; Varela, J.; Lynch, I.; Salvati, A.; Dawson, K. A. Effects of Transport Inhibitors on the Cellular Uptake of Carboxylated Polystyrene Nanoparticles in Different Cell Lines. *PLOS ONE* **2011,** *6* (9), e24438, DOI: 10.1371/journal.pone.0024438.
(54) He, L.; Sayers, E. J.; Watson, P.; Jones, A. T. Contrasting Roles for Actin in the Cellular Uptake of Cell Penetrating Peptide Conjugates. *Scientific Reports* **2018,** *8* (1), 7318, DOI: 10.1038/s41598-018-25600-8.

Chapter 4

Polydopamine Mesoporous Nanobowls to Conquer Multi Drug Resistance *via* Combined Chemo- and Photothermal Cancer Treatment

This Chapter has been submitted for publication: **Shahinur Acter,** Nazneen Jahan, Mark Louis P. Vidallon, Boon Mian Teo,* and Rico F. Tabor*

Preface for Chapter 4

In this Chapter, polydopamine bowl-shaped mesoporous nanobowls (PDA nanobowls) at around 180 nm diameter were synthesized. These particles were characterized with dynamic light scattering, zeta potential measurement, SEM, and TEM. The anti-cancer drug doxorubicin (DOX) was loaded into the PDA nanobowls via π-π stacking interactions, and drug release kinetics were evaluated in an acidic environment typical of tumor sites, at pH 5.5. Fluorescence spectrophotometry was used to quantify the amount of released DOX at different time intervals. This was followed by an *in vitro* study, where HeLa cells underwent incubation with various treatments, including DOX loaded PDA bowls, only PDA bowls, and free DOX without and with near-infrared illumination for 5 mins; untreated cells were used as control. After these various treatments, cytotoxicity and viability of the cells were evaluated via biochemical assay testing. Morphological analysis of the cell samples was undertaken by confocal imaging analysis, indicating the effectiveness of drug delivery via PDA nanobowls.

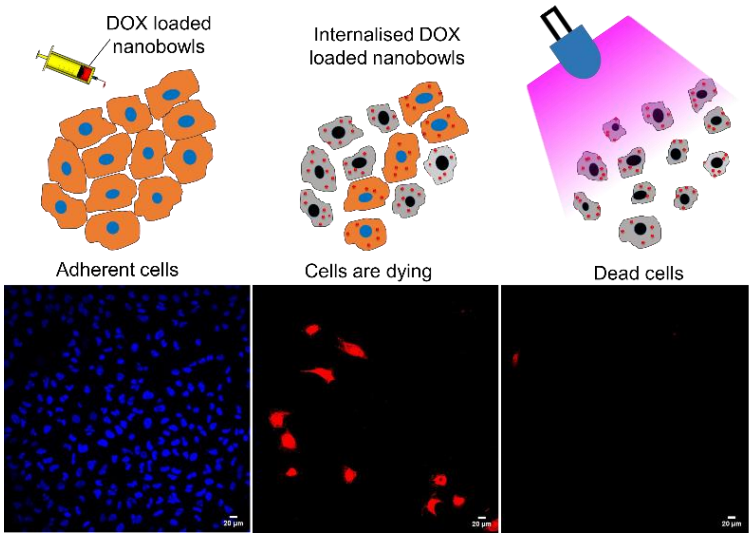

Abstract

Multidrug resistance is a complex defending mechanism in cancer to the chemotherapy drugs, which is a major obstacles in achieving high therapeutic efficacy in cancer therapy. Consequently, combined chemo- and photothermal therapy has rapidly developed that has been demonstrated significantly higher therapeutic efficacy, however long term cytotoxicity, in particular poor biodegradability of the nanoparticles remains a big challenge. We demonstrate a new approach toward cancer treatment that combines chemo- and photothermal therapy to kill cancer cells using bio-derived polydopamine (PDA) bowl-shaped mesoporous nanoparticles (PDA mesoporous nanobowls). Herein, the suitability and potential of PDA mesoporous nanobowls as a new chemo- and photothermal agent was explored to conquer multi drug resistance by loading anti-cancer drug doxorubicin (DOX) into the nanobowls and investigating their photothermal performance upon near-infrared illumination (NIR). Strikingly, DOX loaded nanobowls show significantly higher pharmaceutical cytotoxicity to HeLa cells in comparison with free DOX, and following this by photothermal treatment resulted in nearly 100% cell death from combined treatment of DOX loaded nanobowls and NIR illumination. This proposed approach highlights the great potential of PDA mesoporous nanobowls as a universal scaffold for combined chemo- and photothermal therapy for cancer treatment that sheds new light on the challenges of chemo- and photothermal therapy against advanced cancer.

4.1 Introduction

Nanoparticles have been extensively used to transport chemotherapeutic drugs to malignant tissues/cells for cancer treatment, as they can be tailored to cross biological barriers, enable selective targeting of malignant cells, and offer strategies for sustained release of drugs to the targeted site.[1-3] A wide range of nanoparticles have been fabricated to use as drug delivery systems to target cancer cells including carbon, silica, gold, and various polymers, yet the long-term toxicity of these nanocarriers remain a significant challenge.[4-6] Besides, cellular uptake efficiency of the nanocarriers and delivering an effective dose of drug to targeted tumor sites before particles are cleared remain big barriers to their ultimate success as drug nanocarriers for cancer treatment.[7-8] Moreover, traditional cancer treatment is insufficient to completely kill cancer cells due to multiple drug resistance of malignant tissue/cells increasing their tolerance to toxic drugs.[8-10]

Recently, extensive research has been carried out on developing combined treatment of near infrared (NIR) induced photothermal therapy and chemotherapy to augment the cytotoxicity of chemotherapeutic agents.[11] Researchers have devoted efforts to the development of photothermal therapy agents that include carbon-based nanomaterials, noble metal nano-structures, semiconductors, black phosphorus, and their composites, comprehensively utilizing their intense absorption characterized by a large molar extinction coefficient and relatively high photothermal conversion efficiency.[12-15] Nevertheless, not only the fabrication process of these particular nanomaterials is elaborate and challenging, but also the majority of these substances show long-term toxicity, which remains problematic.[11, 14, 16-18]

There is an urgent demand for effective cancer therapies that possess a unique combination of photothermal and chemotherapeutic benefits, and which can eliminate large solid tumors as well as disseminated, metastatic nodules, while simultaneously preventing tumor recurrence without any residual toxicity. By selecting drug nanocarriers with long-term biocompatibility, free-radical-scavenging activity, cellular internalization efficiency, and by loading sufficient dosage of drug in combination with photothermal response, it may be possible to treat local tumors with improved therapeutic outcomes in malignant cancers.

In recent years, the melanin-like, naturally inspired biopolymer, polydopamine (PDA), has been widely used in various biomedical applications including drug delivery due to its excellent biocompatibility, colloidal stability, and distinctive drug loading facility.[19-23] Moreover, due to the adhesive nature of catechols and amines, similar to those in mussel adhesive proteins, PDA tends to show strong adhesion to all types of surfaces.[24-25] Finally, PDA has high photothermal conversion efficiency, making it ideal for photothermal transduction in the IR region of the spectrum. For instance, Lu and co-workers have demonstrated 40% photothermal energy conversion efficiency of PDA, indicating promising applications in photothermal-based cancer therapeutics, which is emerging as a powerful technique in cancer therapy due to the potential for localised treatment and minimal invasiveness.[20, 26-30] Additionally, due to its excellent flexibility through a high degree of control in shape and size of nanostructures that can be formed, and with high thermal stability (when compared to many nanostructured soft matter delivery systems), PDA offers opportunities for synthesis of various shapes and sizes of nanoparticles including spherical, cup-/bowl-shaped, and walnut-

shaped.[31-33] For Instance, in a previous study we successfully synthesized various sizes of PDA mesoporous nanobowls by tuning reaction parameters.[34]

In order to select a drug nanocarrier, shape and size are important factors to consider, as these features determine their efficiency at passing through biological barriers, their cellular uptake efficiency and biodistribution, and ultimately their intracellular fate.[35-38] For example, Gao and co-workers have demonstrated a faster cellular uptake of bowl-like particles relative to spherical ones.[39] More recently, in our previous work, we found faster cellular internalization of PDA bowls compared to their spherical counterpart, as bowls tends to use their curved side to attach onto the cell membrane and thus are enwrapped faster by the cell membrane leading to faster uptake.[35] Considering this, PDA bowl-shaped mesoporous nanoparticles (PDA mesoporous nanobowls) can be an ideal candidate as they show significantly faster cellular uptake relative to spherical nanoparticles with the same chemistry[35] and can load a sufficient quantity of drugs in their cavity and mesopores.

With an aim to meet the current challenges of combined chemo- and photothermal therapy for cancer treatment herein, we developed a simple and versatile strategy to efficiently kill cancer cells with a combined treatment of doxorubicin (DOX) loaded PDA mesoporous nanobowls with NIR phothothermal transduction (Figure 4.1). Considering the size-dependent endocytosis pathways of PDA mesoporous nanobowls in HeLa cells (human cervical carcinoma epithelial cells) and their photothermal responsive properties in our previous studies,[30, 34] we selected nanobowls of around 180 nm diameter in this work. We demonstrate a significant decrease in cell viability upon incubation with DOX loaded

nanobowls followed by NIR illumination on HeLa cells. To our knowledge, this is the first demonstration indicating combined chemo- and phothothermal therapeutic potential for cancer treatment *in vitro* using particles of this type, indicating them as a promising cancer treatment modality.

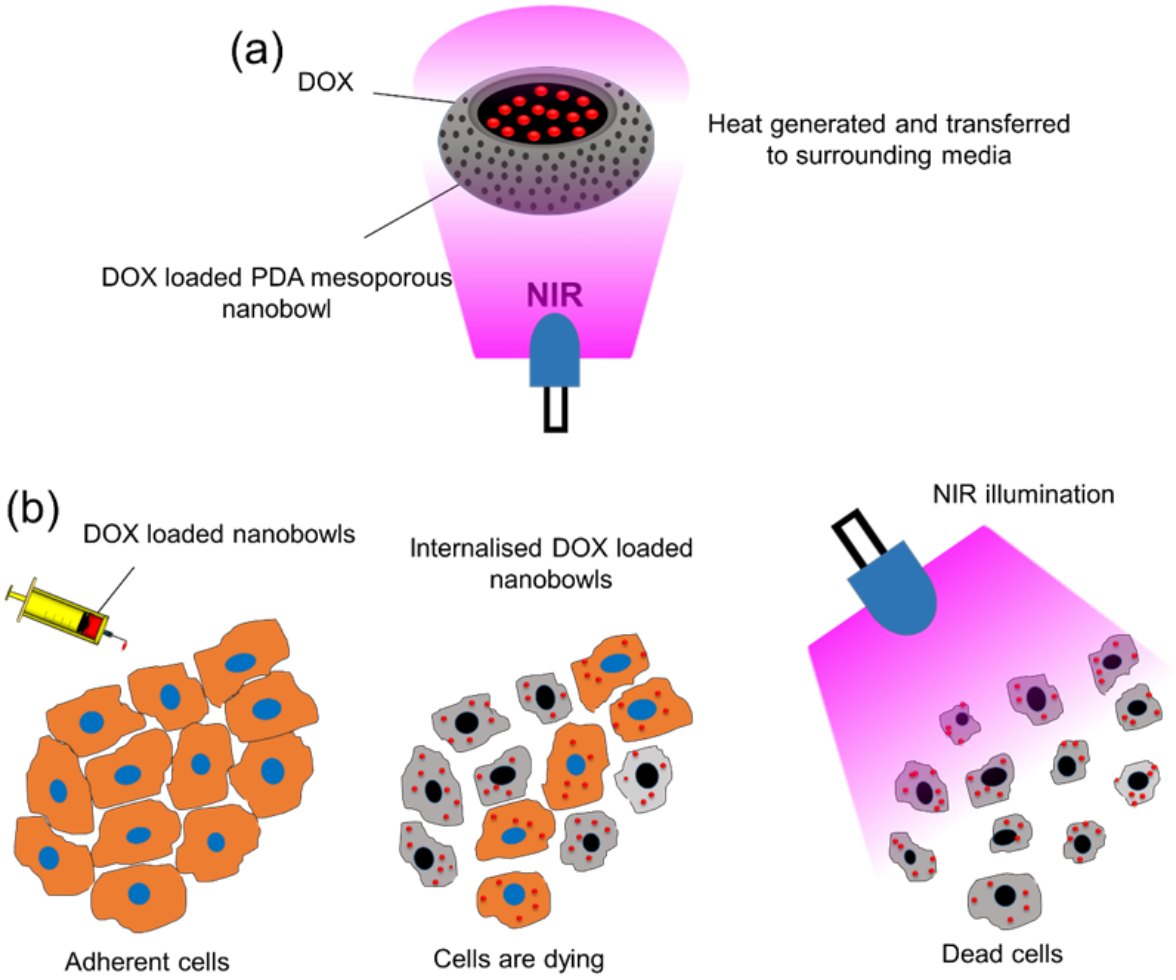

Figure 4.1. Schematic diagram showing chemo- and photothermal properties of PDA mesoporous nanobowls (a), and (b) Heathy adherent HeLa cells, after incubating with DOX loaded PDA mesoporous nanobowls showing morphological changes and a few of them are dying, followed by near-infrared illumination, almost all the cells are dead, causing their detachment from the surface.

4.2 Experimental Section

4.2.1 Materials

Trimethylbenzene (TMB, 98%), dopamine hydrochloride, Pluronic®F-127, phosphate-buffered saline (PBS), fetal bovine serum (FBS, Gibco), paraformaldehyde (PFA), MTS colorimetric cell proliferation assay kit (where MTS is 3-(4,5-carboxymethoxyphenyl)-2-(4-sulfophenyl)-2H-tetrazolium), antibiotic-antimycotic solution (100X), and 4′,6-diamidino-2-phenylindole (DAPI) were purchased from Sigma-Aldrich. Ammonia solution was from Ajax Finechem Pty., and ethanol 96% was from Univa. Propidium Iodide (PI) was purchased from Merck. Other materials were Dulbecco's Modified Eagle's Medium (DMEM, Life Science) and trypsin (0.25%, Merck). All reagents were used as received, without further purification.

4.2.2 Characterization of PDA mesoporous nanobowls

Hydrodynamic diameters and zeta potential of particles were determined using dynamic light scattering (DLS) and phase analysis light scattering (PALS) respectively, using a Brookhaven NanoBrook Omni particle sizer and zeta potential analyzer. To examine the size and morphology of the particles, transmission electron microscopy (TEM, FEI Tecnai G2 T20 electron microscope under 200kv, using LaB6 emitter) and field-emission scanning electron microscopy (FEI Magellan 400 FEG SEM) analysis techniques were undertaken. Fluorescence absorption and emission spectra of samples were recorded using a Varian Cary Eclipse Fluorescence spectrophotometer in 1 cm path-length quartz cuvettes. Chemical

characterization of PDA particles was undertaken using a Cary 630 FTIR (Fourier Transform Infrared) spectrometer in our previous study.[35]

4.2.3 Synthesis of PDA mesoporous nanobowls

PDA mesoporous nanobowls were synthesized following an established method known as an emulsion-induced interfacial anisotropic assembly.[32] Briefly, 1.5% (w/v) dopamine hydrochloride (DA) and 1.0% (w/v) Pluronic® F127 (block copolymer), were dissolved in 1:1 water: ethanol mixture (total volume 10 mL) followed by addition of 2.0% (v/v) TMB under stirring. An emulsion was formed by ultra-sonication (2 min). In order to achieve an alkaline environment (pH 12.1), ammonia solution (3.75% (v/v), 28%) was added dropwise into the emulsion system. Synthesized nanoparticles were centrifuged with water and ethanol three to four times after 2 h of polymerization time. Eventually, particles were re-dispersed in 10 mL of (1:1) water ethanol mixture for hydrothermal treatment in a sealed Teflon-lined autoclave at 100 °C for 24 h. The final product was washed with water and freeze dried for characterization and future use.

4.2.4 Loading doxorubicin (DOX) to PDA mesoporous nanobowls

To evaluate the drug delivery properties of PDA mesoporous nanobowls, anti-cancer drug doxorubicin (DOX) was loaded into the particles. A 1 mg/mL nanobowls (total volume 5 mL) suspension was prepared for loading DOX. Various quantities of of DOX (0.5, 1.5, and 3 mg) were dispersed in the above nanobowls suspension and this mixture was stirred for 24 h at room temperature to allow binding to the nanobowls. Afterwards, DOX loaded nanobowls

were washed by centrifugation with ultrapure water three to four times to remove free DOX, followed by freeze-drying for future use. All supernatants were collected to estimate the drug loading capacity. Loading efficiency of DOX in nanobowls was determined by fluorescence spectrophotometry at an excitation wavelength of 480 nm and an emission wavelength of 590 nm by comparison to a standard curve (Figure 4S2). Herein, DOX loading efficiency into the nanobowls was calculated by subtracting the mass of the DOX in the supernatant from the total mass of the DOX in the initial solution divided by total amount of DOX and expressing as a percentage.[40]

4.2.5 Release profile of PDA mesoporous nanobowls/DOX

To evaluate drug release kinetics, 1 mL PDA mesoporous nanobowls/DOX particle dispersion was loaded into a dialysis bag (molecular weight cutoff 3.5 kDa) with 25 mL 1x PBS buffer solution (pH 5.5). At different time intervals, 1 mL of PBS solution was collected to quantify the amount of released DOX by fluorescence spectrophotometry at wavelength at 590 nm. Note that 1 mL of fresh PBS (pH 5.5) was added into the solution at each sampling time to keep the total volume constant.[41]

4.2.6 Photothermal performance of PDA mesoporous nanobowls

Measurement of photothermal performance of the nanobowls was done by monitoring temperature under NIR illumination (from an OSLON® 9 PowerCluster IR, an array of nine OSRAM IR OSLON Black Series LEDs, wavelength = 850 nm, mounted on a heatsink and

connected to a power source, providing 1 W/cm^2 radiant power at the sample). A thermocouple probe was used to record the temperature of the dispersions every 30 s. In this experiment, 300 µL of dispersions containing nanobowls of various concentrations including 25, 50, 100, and 200 µg/mL were deposited into wells of a 96 well plate.

Herein, all measurements were done in triplicate and NIR illumination duration was 500 s.

4.2.7 Cell culture

Human cervical cancer cells (HeLa cells) were cultured at 37 °C in a humidified incubator with 5% CO_2 in complete medium (DMEM medium supplemented with 10% FBS and 1% P/S).

4.2.8 Cell cytotoxicity analysis with flow cytometry

HeLa cells were seeded at a density of 4×10^5 cells/mL in individual 25 mL culture flasks and left to adhere overnight at 37 °C and 5% CO_2. Before any treatments, the original medium was replaced with fresh medium to remove any dead cells. Afterwards, cells were treated with DOX loaded mesoporous PDA nanobowls, or free DOX at equivalent drug concentration of 6.8 µg/mL, or unloaded PDA mesoporous nanobowls, for different time periods (4 and 24 h). Herein, particle concentration was kept fixed at 100 µg/mL. After the desired incubation time, cells were treated with NIR operating at 1 W/cm^2 for 5 min followed by trypsinisation and washing steps (centrifugation/re-dispersion cycles 3 times, 1200×g, for 5 min with 1x PBS buffer solution). Finally, the supernatant was removed and 340 µL of 1x PBS solution was added to aliquots for flow cytometry analysis using flow core analysis technique (Fortessa

X20c Flow Cytometry analyzer with B710 detector). Herein, propidium iodide (PI) was used as a red fluorescent nuclear and chromosome counterstain, which penetrates cells with damaged membrane and is excited at 488 nm. Cell samples were stained with PI dye (0.5 µg/mL) and kept in the dark for 15 min before flow cytometry analysis. Note that before the washing steps, supernatants of the cell samples were collected and stained with PI for flow cytometry analysis to determine the total number of dead cells in the cell population. To calculate cell percentages, 20,000 events per samples were read.

4.2.9 In *vitro* cytotoxicity assay of HeLa cells

The MTS (3-(4,5-carboxymethoxyphenyl)-2-(4-sulfophenyl)-2H-tetrazolium) cell viability assay was conducted to investigate in *vitro* cytotoxicity of HeLa cells after various treatments.[29] For this experiment, cells were seeded at a density of 2×10^4 cells/mL in a 96-well plate with a volume of 50 µL in each well and allowed to adhere overnight at 37 °C and 5% CO_2 before being exposed to any treatments. After the desired treatments, absorbance at 490 nm was recorded using a CLARIOstar microplate reader (BMG Labtech, VIC, Australia). Data was analyzed by setting the absorbance value of the control (untreated cells) to 100%, and cell proliferation was expressed as a percentage of this control. The MTS assay was conducted in triplicate.

4.2.10 Confocal imaging of HeLa cells after various treatments

For imaging analysis, HeLa cells were seeded (2×10^4 cells/mL) on coverslips into 6-well plates and allowed to adhere overnight at 37 °C and 5% CO_2 prior to undergoing treatments. Under the same experimental conditions as flow cytometry analysis, the cells were treated with PDA mesoporous nanobowls, free DOX, DOX loaded PDA mesoporous nanobowls, and/or NIR illumination. Eventually, samples were washed with 1x PBS solution 3 to 4 times by gentle pipetting to remove unbound or loosely attached particles or drugs. Afterwards the cells were fixed with 4% PFA for 10 to 15 min and washed 3 to 4 times with 1x PBS to remove excess PFA, followed by counterstaining with 0.7 μg/mL DAPI for 10 to 15 min in the dark, after which the same washing steps were undertaken to remove excess DAPI from the cell samples. Fixed cells in 1x PBS were imaged using confocal laser scanning microscopy (CLSM, Nikon C1 Upright Confocal Microscope) (20× objective, DAPI: laser 405 nm (emission: 433–468 nm), TRITIC: laser 561 nm (for DOX) (emission: 568–643 nm). All images were acquired using the Leica LSX software, then false-coloured and merged using ImageJ.

4.3 Results and discussion

4.3.1 Synthesis of PDA nanobowls

PDA mesoporous nanobowls were synthesized following an established emulsion-induced interface anisotropic assembly method.[32] Briefly, formation of the nanobowl is based on the simultaneous formation of F127/TMB/polydopamine composite micelles and nucleation of

polydopamine and subsequent anisotropic growth of PDA on the surface of emulsion droplet templates. Morphology of the final product was confirmed by SEM imaging (Figure 4.2a), which revealed mesoporous nanobowls of ~180 nm diameter with ~80 nm cavity and ~7 nm mesopores. The TEM image in Figure 4.2b further confirms the morphology of the nanoparticles and reveals that the mesopores form connecting channels known as mesochannels that are arranged radially from the centre to the surface of the nanobowls.[32]

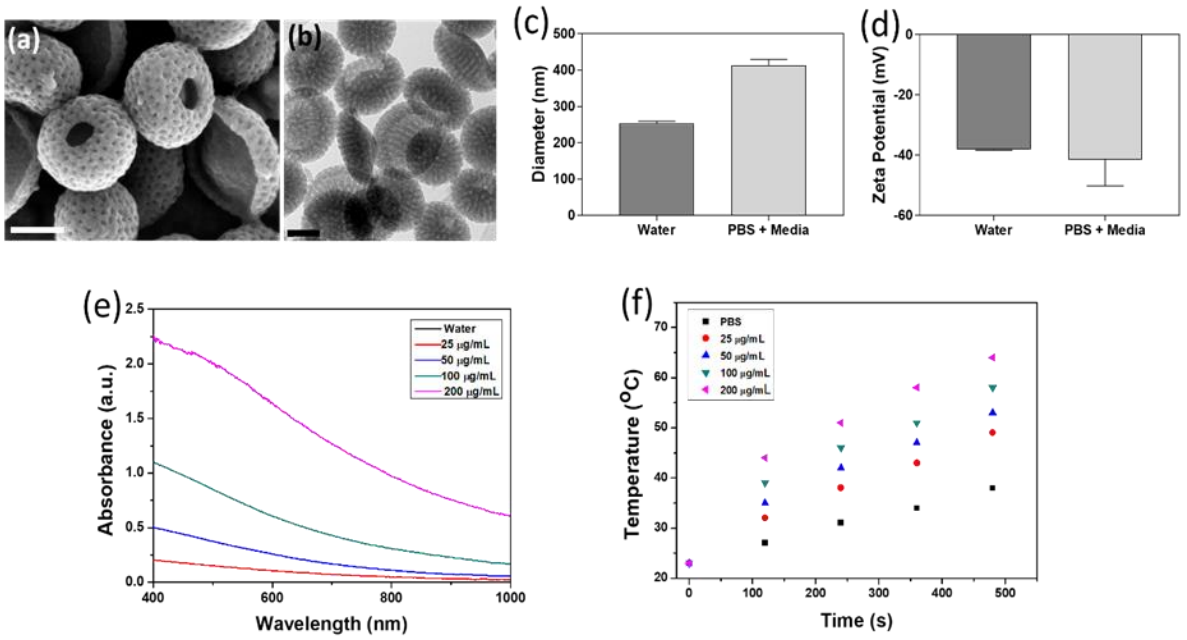

Figure 4.2. (a) Scanning electron microscope (SEM) and (b) transmission electron microscope (TEM) image of PDA mesoporous nanobowls, (b) Hydrodynamic diameter and (c) Zeta potential values of PDA mesoporous nanobowls in water (25 °C) and PBS+Media (37 °C). Figures (e) shows the UV-Vis absorbance spectrum of various concentration of PDA mesoporous nanobowls and (f) shows temperature changes of phosphate buffered saline (PBS) and various concentrations of PDA mesoporous nanobowls suspension in PBS upon NIR illumination (850 nm laser irradiation, 1 W/cm^2).

The size distribution and zeta potential of the nanobowls were analyzed using dynamic light scattering (DLS) and phase analysis light scattering (PALS) respectively (Figure 4. 2c and d).

These nanobowls have appropriate sizes for cell internalization and a remarkably narrow size distribution, as has been noted previously. Figure 4.2d shows negative zeta potentials of the nanobowls with moderate magnitudes in both water and cell culture medium, suggesting colloidal stability of the nanobowls in dispersion due to their negative surface charge. Chemical characterization of the nanobowls was accomplished using Fourier transform infrared spectrometer (FTIR) in our previous study.[35]

4.3.2 Photothermal effect of PDA mesoporous nanobowls

Photothermal conversion efficiency of PDA mesoporous nanobowls was investigated. Experimental results in Figure 4.2 e and f demonstrate that PDA mesoporous nanobowls suspended in PBS absorb light under NIR illumination, which is converted into thermal energy, thus increasing the temperature of the surrounding medium. After 500 s of NIR illumination, temperature of the surrounding medium increased significantly with increasing concentration of nanobowls (0, 25, 50, 100, and 200 μg/mL particle loadings gave final temperatures of 37, 49, 53, 58, and 64 ºC respectively). Duration of NIR exposure was also an important factor in photothermal transduction, suggesting photothermal conversion efficiency is strongly dependent on NIR exposure time and concentration of the PDA mesoporous nanobowls.

4.3.3 Loading DOX into PDA mesoporous nanobowls and their drug release profile *in vitro*

PDA mesoporous nanobowls are functionalized with aromatic rings, which provide favorable π-π stacking interactions when loading the anti-cancer drug doxorubicin (DOX, Figure 4.3a).[27, 42] Obtained results in Figure 4.3b show a remarkably higher loading efficiency of drugs with increasing concentration. The distinctive DOX peak at around 590 nm confirms adsorption of DOX into the nanobowls (Figure 4.S1).[27] A standard curve of DOX was used to calculate loading efficiency of drugs into the nanobowls (Figure 4.S2). Previously it has been demonstrated that in comparison to nonporous PDA nanoparticles, mesoporous PDA nanoparticles have higher capacity for loading DOX.[27, 43] In addition to π-π stacking, electrostatic attractions also contribute to loading DOX into the mesopores and cavity of PDA mesoporous nanobowls due to their negative surface charge.[27, 35, 44] It is assumed that their mesoporous structure also facilities greater drug adsorption due to increased surface area to mass ratio.

DOX release kinetics were investigated after adsorbing DOX into the nanobowls. It has been previously reported that acidic environments are generally ideal to mimic tumour cell extracellular spaces, and considering this, drug release profiles were characterized here in acidic environments (pH = 5.5).[45-46] Obtained results in Figure 4.3c demonstrate that cumulative release of DOX reached over 90% in 24 h at pH 5.5. Previous studies have suggested that this type of acidic environment is favorable for the disruption of π-π stacking between PDA mesoporous nanobowls and DOX due to protonation of the amine group of PDA.[41, 47]

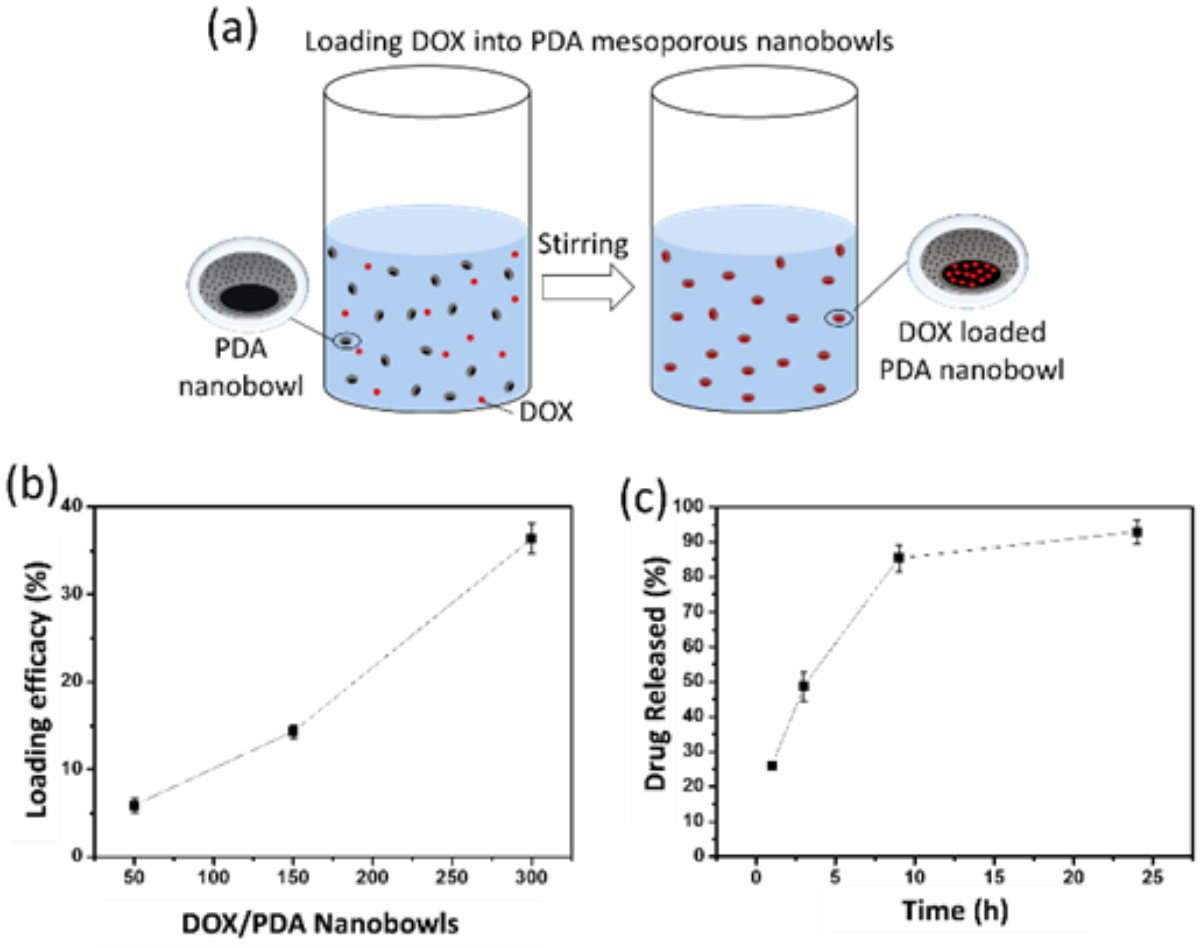

Figure 4.3. (a) Schematic diagram showing drug loading into PDA mesoporous nanobowls and release in PBS. (b) Drug loading efficacy at various DOX/PDA bowl mass ratios. (c) Drug release kinetics *in vitro* (pH 5.5).

4.3.4 Cytotoxicity test of HeLa cells in response to various treatments

With the aim of investigating the efficiency of PDA mesoporous nanobowls as nanocarriers, and the impact of combined treatments of DOX loaded PDA mesoporous nanobowls and NIR on HeLa cells (Figure 4.4a), propidium iodide (PI) testing was conducted using flow cytometry

analysis. To undertake this investigation, first HeLa cells were incubated with PDA mesoporous nanobowls, free DOX, or DOX loaded PDA mesoporous nanobowls for 4 and 24 h, and untreated HeLa cells were used as a control. Obtained results in Figure 4.4b demonstrate a large number of dead HeLa cells in the population that was incubated with DOX loaded PDA mesoporous nanobowls (~75 and ~86% at 4 and 24 h respectively). In contrast, negligible cytotoxicity was recorded for cells incubated with free DOX (DOX alone, ~10 and ~20% at 4 and 24 h respectively, Figure 4.4b). These findings not only indicate a faster internalization of DOX loaded PDA mesoporous nanobowls when compared to free DOX, but also suggest the wide distribution of DOX within the cells when carried by nanobowls, causing a greater incidence of cell death.

These results suggest that PDA mesoporous nanobowls have successfully played a role as an efficient nanocarrier by carrying DOX inside the cells and evenly distributing it within the cells, while free DOX was not internalized as quickly or efficiently as PDA mesoporous nanobowls. This result can only be indicative of the cellular internalization mechanism of PDA mesoporous nanobowls. In our previous study, we have observed that PDA nanobowls use their curved edge to attach to the cell membrane, which is favorable for easier enwrapping by the cell membrane leading to faster internalization into HeLa cells.[35] We also demonstrated the location of the nanobowls within the cells, where they were found assembled and widely distributed in the intracellular environment.[35, 48] However, chemotherapeutic drug resistance was observed as ~ 14% viable cells were found in the cell population after 24 h of incubation with DOX loaded nanobowls, indicating that the combined energy of chemo- and photothermal therapy is needed to completely destroy the cancer cells.

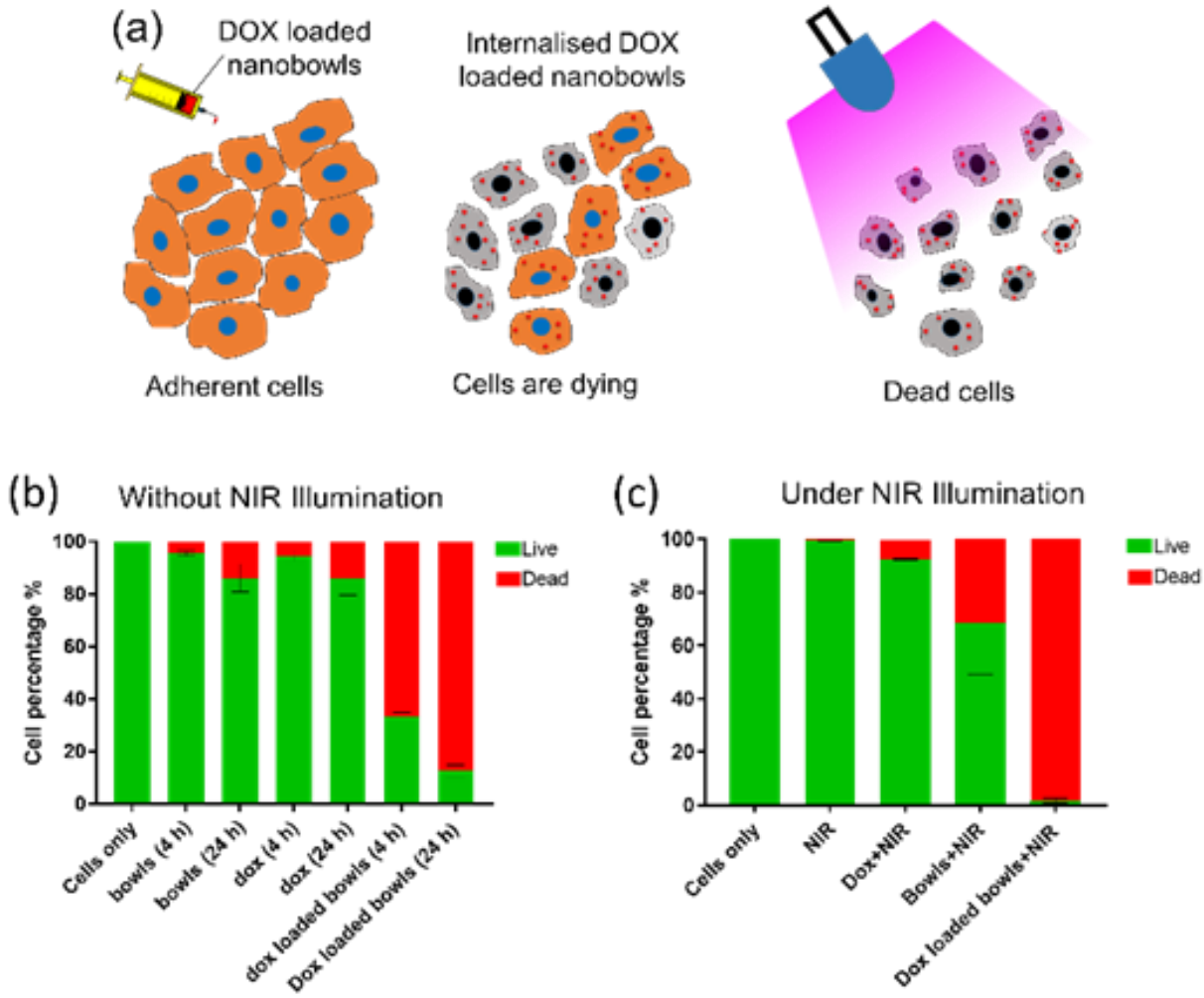

Figure 4.4. (a) Schematic diagram showing cellular fate when exposed to combined treatments of DOX loaded PDA mesoporous nanobowls and NIR illumination. (b) and (c) show the impact of various treatments on HeLa cells without and with NIR illumination (1 W/cm^2, 5 min) respectively and 24 h of incubation time with the Dox loaded Bowls, only Bowls, and free DOX. Green and red bars represent live and dead cells, respectively.

Considering the above findings, the cell samples (untreated cells, cells treated with PDA mesoporous nanobowls, free DOX, and DOX loaded PDA mesoporous nanobowls) were exposed to NIR irradiation (as shown schematically in Figure 4.4a). As observed in Figure 4.4c, NIR alone was insufficient to cause noticeable changes in cell viability. In contrast, combined treatment of DOX loaded nanobowls and NIR radiation resulted in significant cytotoxicity to the cells, where ~ 98.2% dead cells were observed in the cell population. On the other hand, in comparison to the free DOX sample, nanobowl-incubated cells indicated greater cell death due to the presence of PDA, which efficiently absorbs light and converts it to thermal energy.[26]

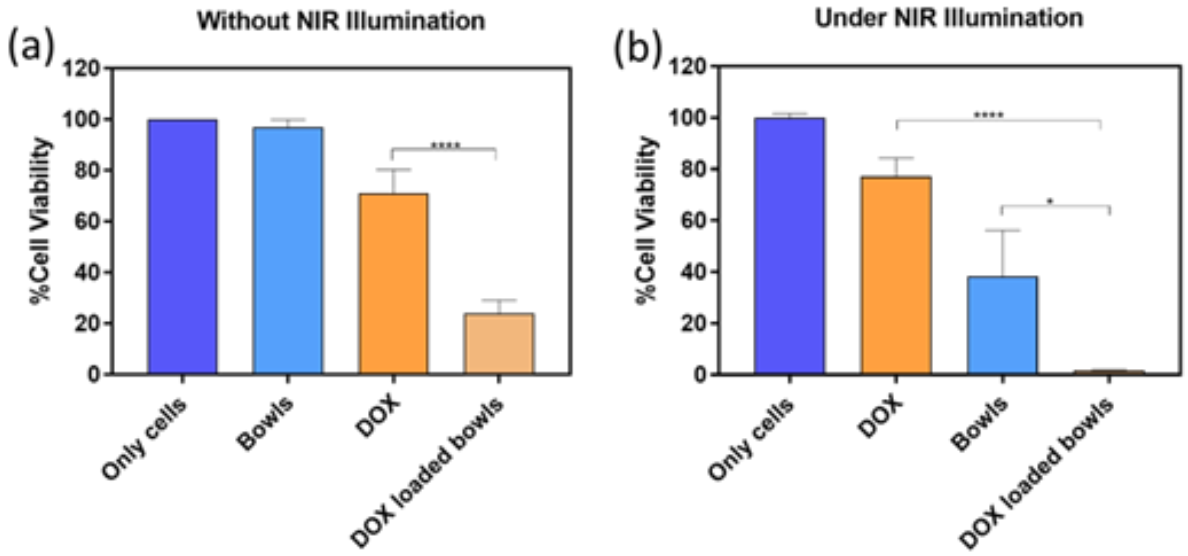

Figure 4.5. Viability of HeLa cells as indicated by MTS assay after various treatments and (a) without or (b) with NIR illumination. (24 h incubation time, NIR power 1 W/cm^2 for 5 min).

Taken together, the above results suggest a greater therapeutic efficacy of PDA mesoporous nanobowls for combined chemo- and photothermal treatments on HeLa cells, when compared to any component on therapy on its own.

4.3.5 MTS cell proliferation assay of HeLa cells upon various treatments

To further confirm the above flow cytometry analysis results, MTS assay testing was conducted with the same experimental design at 24 h of incubation time. Figure 4.5a shows that cell viability was ~ 95%, ~ 72%, and ~20% after treatment with PDA mesoporous nanobowls, free DOX, and DOX loaded PDA mesoporous nanobowls respectively. These results demonstrate that significantly higher reduction of cell viability was caused by DOX loaded PDA mesoporous nanobowls as they were internalized faster and broadly distributed the drugs inside cells, which supports the data obtained by PI testing (Figure 4.5a and 4.4b). After 24 h of incubation with DOX loaded PDA mesoporous nanobowls followed by NIR irradiation, cell viability decreased by 98%, in contrast to negligible changes in cell viability observed with free DOX and NIR treatment (Figure 4.5b). Additionally, around 70% cell viability was found upon treatment of PDA mesoporous nanobowls and NIR, which indicates the impact of photothermal conversion of PDA on cells (Figure 4.5b). These findings further confirm that only DOX (free DOX) is incapable of rapid, efficient internalization into cells compared to when loaded into PDA mesoporous nanobowls, revealing the nanobowl's tremendous potential as a combined chemo- and photothermal therapeutic agent to kill HeLa cells.

4.3.6 Confocal imaging of HeLa cells upon combined chemo- and photothermal treatments

Confocal laser scanning microscopy (CLSM) analysis was undertaken to further confirm the above findings, and visually understand the impact of combined treatments of DOX loaded PDA mesoporous nanobowls and NIR irradiation on HeLa cells. Herein, cell samples were prepared using the same experimental design as flow cytometry analysis and MTS assay testing above. In Figure 4.6, we first focus on confocal images showing a red channel fluorescence signal indicating the presence of DOX. Note that DOX molecules that were loosely attached to the cell membrane were removed during multiple washing steps, whereas cells that were treated with DOX loaded PDA mesoporous nanobowls showed a significant red fluorescence signal relative to similarly concentrated free DOX, indicating significantly higher intracellular DOX accumulation when carried by PDA mesoporous nanobowls. In our previous study, we demonstrated the intracellular location of PDA mesoporous nanobowls by TEM and CLSM imaging analysis, where they were found broadly distributed inside the cells without any aggregation.[35]

Consequently, these data provide further evidence that DOX loaded PDA mesoporous nanobowls were internalized quickly and evenly distributed the drugs inside the cells, which resulted in significant cell death within 4 h of incubation (Figure 4.6, d_1 to d_4), and could kill around 80% of the cells in 24 h of incubation (Figures 4.6, e_1 to e_4). In contrast, negligible cytotoxicity was observed in the cells after 24 h of incubation with free DOX (Figure 4.6, c_1 to c_4).

Moreover, cells were exposed to photothermal treatment (NIR illumination for 5 min) after 24 h of incubation with DOX loaded PDA mesoporous nanobowls. This process destroyed up to 98% cells (Figure 4.6, f_1 to f_4). Additionally, cells incubated with PDA mesoporous nanobowls did not show any obvious toxicity (Figure 4.6, b_1 to b_4). This outcome aligns with the findings of flow cytometry analysis and MTS assay testing.

The above results suggest a significantly greater therapeutic efficacy of DOX loaded PDA mesoporous nanobowls in comparison with only DOX, which also indicates a synergistic effect of combined chemo- and photothermal treatment for cancer treatment.

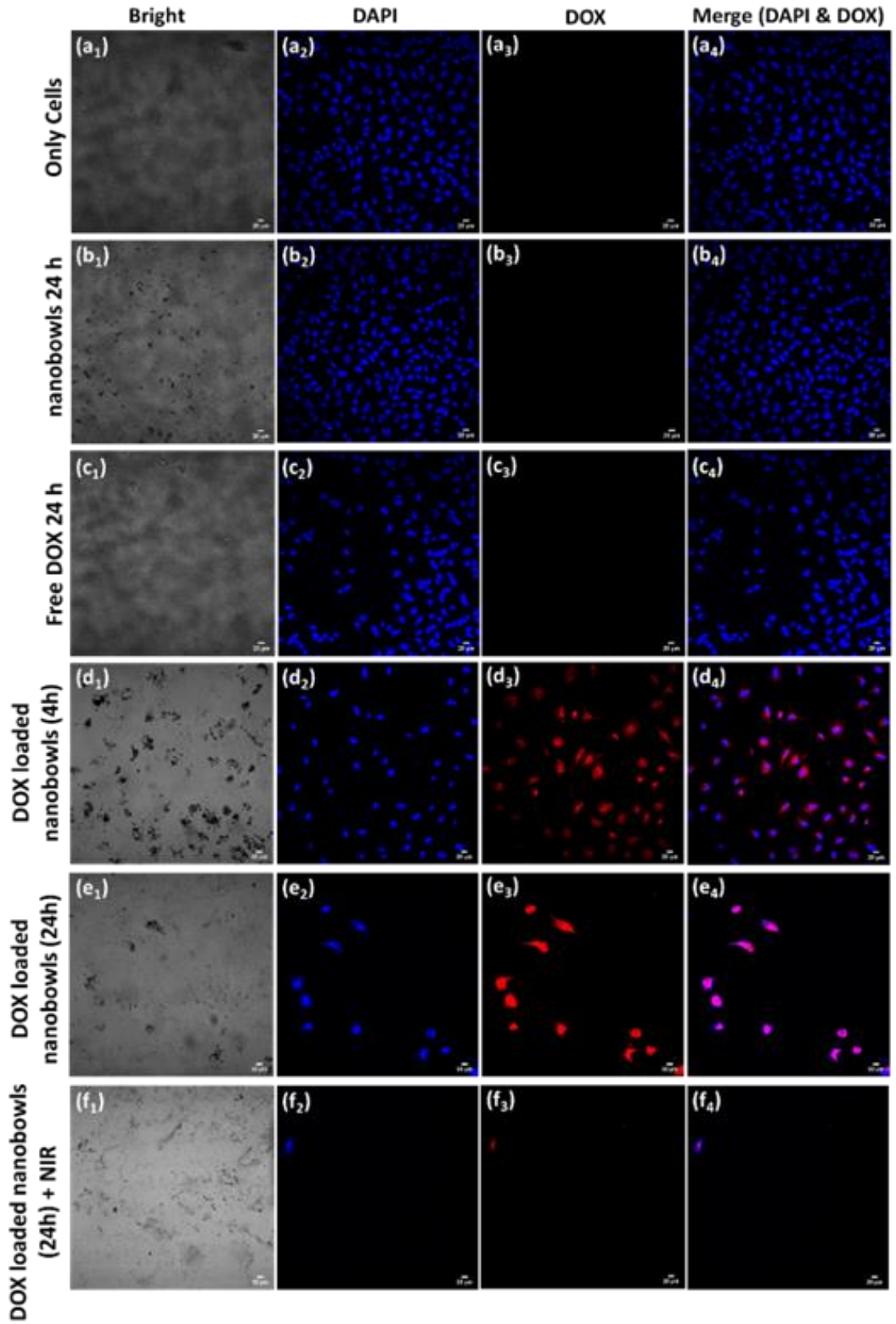

Figure 4.6. Confocal fluorescence images of HeLa cells after various treatments. NIR illumination for 5 min, 1 W/cm^2. Scale bars represent 20 µm.

4.4. Conclusions

In summary, we have introduced PDA mesoporous nanobowls as a new drug nanocarrier, which show capabilities for overcoming multiple drug resistance atond efficiently kill cancer cells with a combination of chemo- and photothermal therapy. In comparison to free DOX, PDA mesoporous nanobowls show significantly faster cellular uptake, highlighting them as an efficient drug nanocarrier. PDA nanobowls also showed excellent photothermal conversion efficiency under NIR illumination. These chemo- and photothermal agents were tested "*in vitro"* on HeLa cells, where cytotoxicity and viability of the cells were evaluated via PI and MTS assay testing respectively, along with confocal imaging analysis. Obtained results demonstrated a significant cytotoxic effect of combined treatments of DOX loaded PDA mesoporous nanobowls and NIR illumination on HeLa cells in comparison to free DOX, which suggests that PDA mesoporous nanobowls may offer a promising candidate for the development of synergistic chemo- and photothermal therapy to conquer multiple drug resistance.

4.5 References

(1) Yao, Y.; Zhou, Y.; Liu, L.; Xu, Y.; Chen, Q.; Wang, Y.; Wu, S.; Deng, Y.; Zhang, J.; Shao, A. Nanoparticle-Based Drug Delivery in Cancer Therapy and Its Role in Overcoming Drug Resistance. *Frontiers in Molecular Biosciences* **2020,** *7*, 193, DIO: 10.3389/fmolb.2020.00193.
(2) Bae, K. H.; Chung, H. J.; Park, T. G. Nanomaterials for Cancer Therapy and Imaging. *Molecules and Cells* **2011,** *31* (4), 295-302, DOI: 10.1007/s10059-011-0051-5.
(3) Dadwal, A.; Baldi, A.; Kumar Narang, R. Nanoparticles as Carriers for Drug Delivery in Cancer. *Artificial Cells, Nanomedicine, and Biotechnology* **2018,** *46* (sup2), 295-305, DOI: 10.1080/21691401.2018.1457039.
(4) Strojny, B.; Kurantowicz, N.; Sawosz, E.; Grodzik, M.; Jaworski, S.; Kutwin, M.; Wierzbicki, M.; Hotowy, A.; Lipińska, L.; Chwalibog, A. Long Term Influence of Carbon Nanoparticles on Health and Liver Status in Rats. *PloS One* **2015,** *10* (12), e0144821-e0144821, DOI: 10.1371/journal.pone.0144821.

(5) Mohammadpour, R.; Yazdimamaghani, M.; Cheney, D. L.; Jedrzkiewicz, J.; Ghandehari, H. Subchronic Toxicity of Silica Nanoparticles as A Function of Size and Porosity. *Journal of Controlled Release: Official Journal of the Controlled Release Society* **2019,** *304*, 216-232, DOI: 10.1016/j.jconrel.2019.04.041.
(6) Sani, A.; Cao, C.; Cui, D. Toxicity of Gold Nanoparticles (AuNPs): A Review. *Biochemistry and Biophysics Reports* **2021,** *26*, 100991, DOI: 10.1016/j.bbrep.2021.100991.
(7) Foroozandeh, P.; Aziz, A. A. Insight into Cellular Uptake and Intracellular Trafficking of Nanoparticles. *Nanoscale Research Letters* **2018,** *13* (1), 339, DOI: 10.1186/s11671-018-2728-6.
(8) Vácha, R.; Martinez-Veracoechea, F.; Frenkel, D. Challenges in Nanoparticle Delivery: Cellular Uptake and Intracellular Escape. *Biophysical Journal* **2013,** *104*, 622, DOI: 10.1016/j.bpj.2012.11.3443.
(9) Wang, X.; Zhang, H.; Chen, X. Drug Resistance and Combating Drug Resistance in Cancer. *Cancer Drug Resistance* **2019,** *2* (2), 141-160, DOI: 10.20517/cdr.2019.10.
(10) Chidambaram, M.; Manavalan, R.; Kandasamy, K. Nanotherapeutics to Overcome Conventional Cancer Chemotherapy Limitations. *Journal of pharmacy & pharmaceutical sciences: A Publication of the Canadian Society for Pharmaceutical Sciences, Société Canadienne Des Sciences Pharmaceutiques* **2011,** *14*, 67-77, DOI: 10.18433/J30C7D.
(11) Khafaji, M.; Zamani, M.; Golizadeh, M.; Bavi, O. Inorganic Nanomaterials for Chemo/Photothermal Therapy: A Promising Horizon on Effective Cancer Treatment. *Biophysical Reviews* **2019,** *11* (3), 335-352, DOI: 10.1007/s12551-019-00532-3.
(12) Chen, J.; Ning, C.; Zhou, Z.; Yu, P.; Zhu, Y.; Tan, G.; Mao, C. Nanomaterials as Photothermal Therapeutic Agents. *Progress in Materials Science* **2019,** *99*, 1-26, DOI: 10.1016/j.pmatsci.2018.07.005.
(13) Lv, Z.; He, S.; Wang, Y.; Zhu, X. Noble Metal Nanomaterials for NIR-Triggered Photothermal Therapy in Cancer. *Advanced Healthcare Materials* **2021,** *10* (6), e2001806, DOI: 10.1002/adhm.202001806.
(14) Li, Z.; Chen, Y.; Yang, Y.; Yu, Y.; Zhang, Y.; Zhu, D.; Yu, X.; Ouyang, X.; Xie, Z.; Zhao, Y.; Li, L. Recent Advances in Nanomaterials-Based Chemo-Photothermal Combination Therapy for Improving Cancer Treatment. *Frontiers in Bioengineering and Biotechnology* **2019,** *7*, 293, DOI: 10.3389/fbioe.2019.00293.
(15) Hu, K.; Xie, L.; Zhang, Y.; Hanyu, M.; Yang, Z.; Nagatsu, K.; Suzuki, H.; Ouyang, J.; Ji, X.; Wei, J.; Xu, H.; Farokhzad, O. C.; Liang, S. H.; Wang, L.; Tao, W.; Zhang, M.-R. Marriage of Black Phosphorus and Cu2+ as Effective Photothermal Agents for PET-Guided Combination Cancer Therapy. *Nature Communications* **2020,** *11* (1), 2778, DOI: 10.1038/s41467-020-16513-0.
(16) Maiti, D.; Tong, X.; Mou, X.; Yang, K. Carbon-Based Nanomaterials for Biomedical Applications: A Recent Study. *Frontiers in Pharmacology* **2019,** *9*, 1401, DOI: 10.3389/fphar.2018.01401.
(17) Zhang, F.; Peng, F.; Qin, L.; Yang, D.; Li, R.; Jiang, S.; He, H.; Zhang, P. pH/Near Infrared Dual-Triggered Drug Delivery System Based Black Phosphorus Nanosheets for Targeted Cancer Chemo-Photothermal Therapy. *Colloids and Surfaces. B, Biointerfaces* **2019,** *180*, 353-361, DOI: 10.1016/j.colsurfb.2019.04.021.
(18) Paris, J. L.; Baeza, A.; Vallet-Regí, M. Overcoming the Stability, Toxicity, and Biodegradation Challenges of Tumor Stimuli-Responsive Inorganic Nanoparticles for Delivery of Cancer Therapeutics. *Expert Opinion Drug on Delivery* **2019,** *16* (10), 1095-1112, DOI: 10.1080/17425247.2019.1662786.
(19) Nishizawa, N.; Kawamura, A.; Kohri, M.; Nakamura, Y.; Fujii, S. Polydopamine Particle as A Particulate Emulsifier. *Polymers* **2016,** *8*, 62, DOI: 10.3390/polym8030062.
(20) Poinard, B.; Neo, S. Z. Y.; Yeo, E. L. L.; Heng, H. P. S.; Neoh, K. G.; Kah, J. C. Y. Polydopamine Nanoparticles Enhance Drug Release for Combined Photodynamic and Photothermal Therapy. *ACS Applied Materials & Interfaces* **2018,** *10* (25), 21125-21136, DOI: 10.1021/acsami.8b04799.
(21) Sung, Y. K.; Kim, S. W. Recent Advances in Polymeric Drug Delivery Systems. *Biomaterials Research* **2020,** *24* (1), 12, DOI: 10.1186/s40824-020-00190-7.
(22) Ball, V. Polydopamine Nanomaterials: Recent Advances in Synthesis Methods and Applications. *Frontiers in Bioengineering and Biotechnology* **2018,** *6*, 109-109, DOI: 10.3389/fbioe.2018.00109.

(23) Vidallon, M. L. P.; Yu, F.; Teo, B. M. Controlling the Size and Polymorphism of Calcium Carbonate Hybrid Particles Using Natural Biopolymers. *Crystal Growth & Design* **2020,** *20* (2), 645-652, DOI: 10.1021/acs.cgd.9b01057.
(24) Liu, Y.; Ai, K.; Lu, L. Polydopamine and Its Derivative Materials: Synthesis and Promising Applications in Energy, Environmental, and Biomedical Fields. *Chemical Reviews* **2014,** *114* (9), 5057-5115, DOI: 10.1021/cr400407a.
(25) Liebscher, J.; Mrówczyński, R.; Scheidt, H. A.; Filip, C.; Hădade, N. D.; Turcu, R.; Bende, A.; Beck, S. Structure of Polydopamine: A Never-Ending Story? *Langmuir : the ACS Journal of Surfaces and Colloids* **2013,** *29* (33), 10539-48, DOI: 10.1021/la4020288.
(26) Zhu, Z.; Su, M. Polydopamine Nanoparticles for Combined Chemo- and Photothermal Cancer Therapy. *Nanomaterials (Basel)* **2017,** *7* (7), 160, DOI: 10.3390/nano7070160.
(27) Xing, Y.; Zhang, J.; Chen, F.; Liu, J.; Cai, K. Mesoporous Polydopamine Nanoparticles with Co-Delivery Function for Overcoming Multidrug Resistance *via* Synergistic Chemo-Photothermal Therapy. *Nanoscale* **2017,** *9* (25), 8781-8790, DOI: 10.1039/C7NR01857F.
(28) Tiwari, A. P.; Bhattarai, D. P.; Maharjan, B.; Ko, S. W.; Kim, H. Y.; Park, C. H.; Kim, C. S. Polydopamine-Based Implantable Multifunctional Nanocarpet for Highly Efficient Photothermal-Chemo Therapy. *Scientific Reports* **2019,** *9* (1), 2943, DOI: 10.1038/s41598-019-39457-y.
(29) Liu, Y.; Ai, K.; Liu, J.; Deng, M.; He, Y.; Lu, L. Dopamine-Melanin Colloidal Nanospheres: An Efficient Near-Infrared Photothermal Therapeutic Agent for In *Vivo* Cancer Therapy. *Advanced Materials* **2013,** *25* (9), 1353-1359, DOI: 10.1002/adma.201204683.
(30) Acter, S.; Vidallon, M. L. P.; King, J. P.; Teo, B. M.; Tabor, R. F. Photothermally Responsive Pickering Emulsions Stabilised by Polydopamine Nanobowls. *Journal of Materials Chemistry B* **2021**, *ISSN: 2050-750X*, 2050-7518, DOI: 10.1039/D1TB01796A.
(31) Guan, B. Y.; Zhang, S. L.; Lou, X. W. Realization of Walnut-Shaped Particles with Macro-/Mesoporous Open Channels Through Pore Architecture Manipulation and Their Use in Electrocatalytic Oxygen Reduction. *Angewandte Chemie International Edition* **2018,** *57* (21), 6176-6180, DOI: 10.1002/anie.201801876.
(32) Guan, B. Y.; Yu, L.; Lou, X. W. Formation of Asymmetric Bowl-Like Mesoporous Particles *via* Emulsion-Induced Interface Anisotropic Assembly. *Journal of the American Chemical Society* **2016,** *138* (35), 11306-11311, DOI: 10.1021/jacs.6b06558.
(33) Jiang, X.; Wang, Y.; Li, M. Selecting Water-Alcohol Mixed Solvent for Synthesis of Polydopamine Nano-Spheres Using Solubility Parameter. *Scientific Reports* **2014,** *4* (1), 6070, DOI: 10.1038/srep06070.
(34) Acter, S.; Vidallon, M. L. P.; Crawford, S.; Tabor, R. F.; Teo, B. M. Bowl-Shaped Mesoporous Polydopamine Nanoparticles for Size-Dependent Endocytosis into HeLa Cells. *ACS Applied Nano Materials* **2021**, *4* (9), 9536–9546, DOI: 10.1021/acsanm.1c01897.
(35) Acter, S.; Vidallon, M. L. P.; Crawford, S.; Tabor, R. F.; Teo, B. M. Efficient Cellular Internalization and Transport of Bowl-Shaped Polydopamine Particles. *Particle & Particle Systems Characterization* **2020,** *37*, 2000166, DOI: 10.1002/ppsc.202000166.
(36) Gratton, S. E. A.; Ropp, P. A.; Pohlhaus, P. D.; Luft, J. C.; Madden, V. J.; Napier, M. E.; DeSimone, J. M. The Efect of Particle Design on Cellular Internalization Pathways. *Proceedings of the National Academy of Sciences* **2008,** *105* (33), 11613, DOI: 10.1073/pnas.0801763105.
(37) Hoshyar, N.; Gray, S.; Han, H.; Bao, G. The Effect of Nanoparticle Size on In *Vivo* Pharmacokinetics and Cellular Interaction. *Nanomedicine (Lond)* **2016,** *11* (6), 673-692, DOI: 10.2217/nnm.16.5.
(38) Liu, X.; Wu, F.; Tian, Y.; Wu, M.; Zhou, Q.; Jiang, S.; Niu, Z. Size Dependent Cellular Uptake of Rod-Like Bionanoparticles with Different Aspect Ratios. *Scientific Reports* **2016,** *6* (1), 24567, DOI: 10.1038/srep24567.
(39) Li, H.; Zhang, W.; Tong, W.; Gao, C. Enhanced Cellular Uptake of Bowl-like Microcapsules. *ACS Applied Materials & Interfaces* **2016,** *8* (18), 11210-11214, DOI: 10.1021/acsami.6b02965.

(40) Mei, L.; Xu, K.; Zhai, Z.; He, S.; Zhu, T.; Zhong, W. Doxorubicin-Reinforced Supramolecular Hydrogels of RGD-Derived Peptide Conjugates for pH-Responsive Drug Delivery. *Organic & Biomolecular Chemistry* **2019,** *17* (15), 3853-3860, DOI: 10.1039/C9OB00046A.
(41) Lu, Z.; Douek, A. M.; Rozario, A. M.; Tabor, R. F.; Kaslin, J.; Follink, B.; Teo, B. M. Bioinspired Polynorepinephrine Nanoparticles as An Efficient Vehicle for Enhanced Drug Delivery. *Journal of Materials Chemistry B* **2020,** *8* (5), 961-968, DOI: 10.1039/C9TB02375E.
(42) Bi, D.; Zhao, L.; Yu, R.; Li, H.; Guo, Y.; Wang, X.; Han, M. Surface Modification of Doxorubicin-Loaded Nanoparticles Based on Polydopamine with pH-Sensitive Property for Tumor Targeting Therapy. *Drug Delivery* **2018,** *25* (1), 564-575, DOI: 10.1080/10717544.2018.1440447.
(43) Wang, X.; Xu, S.; Zhou, S.; Xu, W.; Leary, M.; Choong, P.; Qian, M.; Brandt, M.; Xie, Y. M. Topological Design and Additive Manufacturing of Porous Metals for Bone Scaffolds and Orthopaedic Implants: A Review. *Biomaterials* **2016,** *83*, 127-41, DOI: 10.1016/j.biomaterials.2016.01.012.
(44) Chen, F.; Xing, Y.; Wang, Z.; Zheng, X.; Zhang, J.; Cai, K. Nanoscale Polydopamine (PDA) Meets π–π Interactions: An Interface-Directed Coassembly Approach for Mesoporous Nanoparticles. *Langmuir : the ACS Journal of Surfaces and Colloids* **2016,** *32* (46), 12119-12128, DOI: 10.1021/acs.langmuir.6b03294.
(45) Kato, Y.; Ozawa, S.; Miyamoto, C.; Maehata, Y.; Suzuki, A.; Maeda, T.; Baba, Y. Acidic Extracellular Microenvironment and Cancer. *Cancer Cell International* **2013,** *13* (1), 89, DOI: 10.1186/1475-2867-13-89.
(46) Szatrowski, T. P.; Nathan, C. F. Production of Large Amounts of Hydrogen Peroxide by Human Tumor Cells. *Cancer Research* **1991,** *51* (3), 794-8.
(47) Wang, X.; Zhang, J.; Wang, Y.; Wang, C.; Xiao, J.; Zhang, Q.; Cheng, Y. Multi-Responsive Photothermal-Chemotherapy with Drug-Loaded Melanin-Like Nanoparticles for Synergetic Tumor Ablation. *Biomaterials* **2016,** *81*, 114-124, DOI: 10.1016/j.biomaterials.2015.11.037.
(48) Acter, S.; Vidallon, M. L. P.; Crawford, S.; Tabor, R. F.; Teo, B. M. Bowl-Shaped Mesoporous Polydopamine Nanoparticles for Size-Dependent Endocytosis into HeLa Cells. *ACS Applied Nano Materials* **2021,** *4* (9), 9536-9546, DOI: 10.1021/acsanm.1c01897.

Chapter 5

Photothermally Responsive Pickering Emulsions Stabilized by Polydopamine Nanobowls

This Chapter has been published: **Shahinur Acter,** Mark Louis P. Vidallon, Joshua P. King, Boon Mian Teo,* and Rico F. Tabor* (*J. Mater. Chem. B*, 2021, 9, 8962-8970).

Preface for Chapter 5

In this Chapter, polydopamine bowl-shaped mesoporous nanoparticles (PDA bowls) are presented as a new particulate stabilizer to produce photothermally responsive oil-in-water (o/w) Pickering emulsions without any addition of surfactant or surface modification. Formulated photothermally responsive Pickering emulsions are shown to be pH responsive, and due to the incorporation of PDA bowls, they show remarkable photothermal response under near infrared illumination. These photothermally responsive o/w Pickering emulsion systems show biocompatibility and long-term stability, offering potential in controlled drug release applications stimulated by NIR illumination.

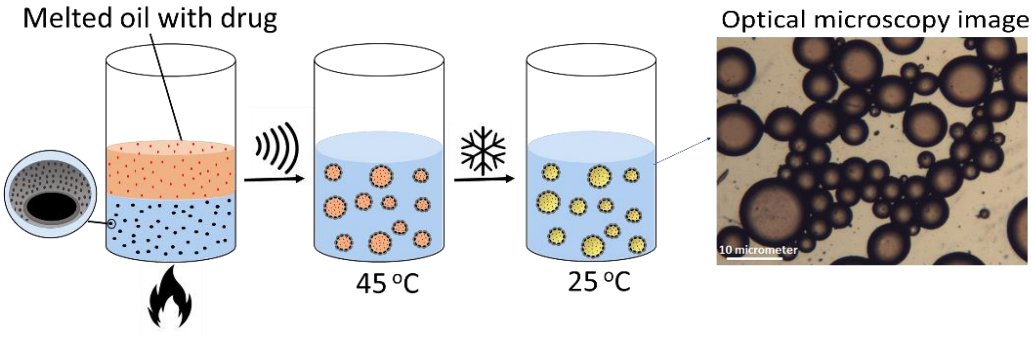

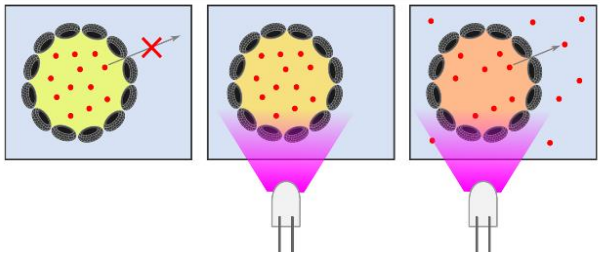

Abstract

Pickering emulsions with stimuli responsive properties have attracted mounting research attention owing to their potential for on-demand destabilization of emulsions. However, a combination of biocompatibility and long-term stability are essential to efficiently apply such systems in biomedical applications, and this remains a significant challenge. To address current limitations, here we report the formation of photothermally responsive oil-in-water (o/w) Pickering emulsions fabricated using biocompatible stabilisers and showing prolonged stability. For the first time, we explore polydopamine (PDA) bowl-shaped mesoporous nanoparticles (PDA nanobowls) as a Pickering stabilizer without any surface modification or other stabilizer present. As-prepared PDA nanobowl-stabilized Pickering emulsions are shown to be pH responsive, and more significantly show high photothermal efficiency under near-infrared illumination due the incorporation of PDA into the system, which has remarkable photothermal response. These biocompatible, photothermally responsive o/w Pickering emulsion systems show potential in controlled drug release applications stimulated by NIR illumination.

5.1 Introduction

Pickering emulsions are a type of emulsion composed of immiscible liquids (usually oil and water), and stabilized only by solid colloidal particles that adsorb at the oil/water interface.[1-2] In this unique configuration, solid particles surrounding the emulsion droplets (see Figure 5.1) provide steric hindrance, which prevent coalescence of the droplets, thus maintaining remarkable stability when compared to molecularly stabilized emulsion systems.[3-5] Pickering emulsions possess many advantages over conventional surfactant-stabilized emulsions, including decreased consumption of potentially hazardous surfactants, and increased long-term stability against coalescence.[4, 6] Due to these benefits and additional opportunities such as the use of biologically compatible and environmental friendly particles for stabilization, Pickering emulsions are now widely applied in a variety of industries, spanning petroleum, food, biomedicine, pharmaceuticals, and cosmetics.[7-10]

To enable further technological advances in such fields, Pickering emulsions with controllable stability are crucial for smart systems in food, cosmetics, and drug delivery applications.[11] Consequently, Pickering emulsions that can release their contents or otherwise modulate their properties in response to external stimuli have attracted significant research attention in recent years. A considerable effort has been made to develop Pickering emulsions that respond to changes in pH,[12-13] light,[14] temperature,[13] magnetic fields,[15] and CO_2/N_2.[16] Additionally, response to multiple stimuli is particularly valuable, offering improved controllable precision and a wider response range.[17] For instance, Brugger et al. reported dual-responsive Pickering emulsions with a combination of magnetic and temperature responsive properties,[18] whereas Zhang et al. demonstrated a CO_2 and redox dual-responsive

Pickering emulsion based on silica particles.[19] Most of the studies reporting stimuli responsive Pickering emulsions however use non-degradable or biologically incompatible particles such as SiO_2 or Fe_3O_4, which can lead to toxicity and accumulation risks.[20-22] Therefore, studies on biocompatible particle-based stimuli responsive Pickering emulsions with prolonged stability and degradability are urgently needed.

There are many factors regulating the stability of Pickering emulsions. The type of particulate emulsifier is one of them, and a wide range of particles have been reported to serve as Pickering emulsifiers such as silica (SiO_2), TiO_2, Fe_2O_3, graphene oxide, cellulose nanocrystals, and various polymer particles.[23-27] Recently, it has been reported that morphology of the particles can regulate the properties of Pickering emulsions, as shape plays a crucial role in controlling particle behavior at the interface and consequently their effectiveness as Pickering emulsifiers.[28-29] It has been demonstrated that anisotropic particles such as peanut-shaped, rod shaped, ellipsoidal, disc-like, dumbbell-shaped, etc. particles manifest as effective stabilisers, maintaining stability of the Pickering emulsion for prolonged periods due to their orientation at the oil-water interface.[30-32] For instance, de Folter et al. demonstrated that emulsions stabilized by cubic or peanut-shaped particles did not undergo coalescence for about a year post-preparation.[30]

Biomedical applications call for nontoxic, biocompatible, and stable materials, and from this point of view, polydopamine (PDA) nanoparticles can be considered as an ideal Pickering stabiliser.[2, 33-34] PDA is a melanin-like naturally inspired polymer, which is the result of self-polymerized of dopamine in alkaline conditions.[35] It is a mimetic mussel adhesive protein, due

to its unique chemical structure with catechol and amine groups, PDA has attracted significant focus as a coating material without the requirement for surface pre-treatment.[36] In addition to this list of attractive properties, recent studies have demonstrated that PDA experiences strong NIR absorption and high photothermal therapeutic energy conversion efficiency of 40%.[37] For example, Liu et al. found dopamine-melanin nanospheres have strong NIR absorption and high photothermal conversion efficiency, which could efficiently kill cancer cells and suppress tumour growth without damaging healthy tissues.[38] Moreover, PDA has flexibility in terms of the high degree of control in both shape and size of synthesized structures/coatings, in addition to favourable thermal stability, therefore, various shapes of PDA particles can be synthesized including spherical, nanobowls, and walnut-shaped, each with tunable size.[39-41] Among these various shapes of PDA particles, PDA bowl-shaped mesoporous nanoparticles (PDA nanobowls) possess unique morphology with an internal cavity and mesopores. In our previous study, we have demonstrated a size-controlled synthesis of PDA nanobowls, where the size of mesopores and internal cavity can be controlled by tuning reaction parameters. We also showed the nontoxic nature of such PDA nanobowls to biological cells, and the bowls showed a high degree of cellular internalization into HeLa cells.[42]

Herein, we demonstrate that PDA nanobowls can act as a Pickering stabiliser without any surface modification (see Figure 5.1), maintaining stability of prepared Pickering emulsions for a considerable period. The cavity of PDA nanobowls allow for unique wetting thermodynamics that make them particularly effective stabilisers at oil-water interface. Developed Pickering emulsions showed sensitivity to pH and demonstrated stimuli responsive

properties. By taking advantage of the photothermal properties of PDA, such Pickering emulsions indicate a strong photothermal response, which is beneficial for various biomedical applications including drug delivery (Figure 5.1).

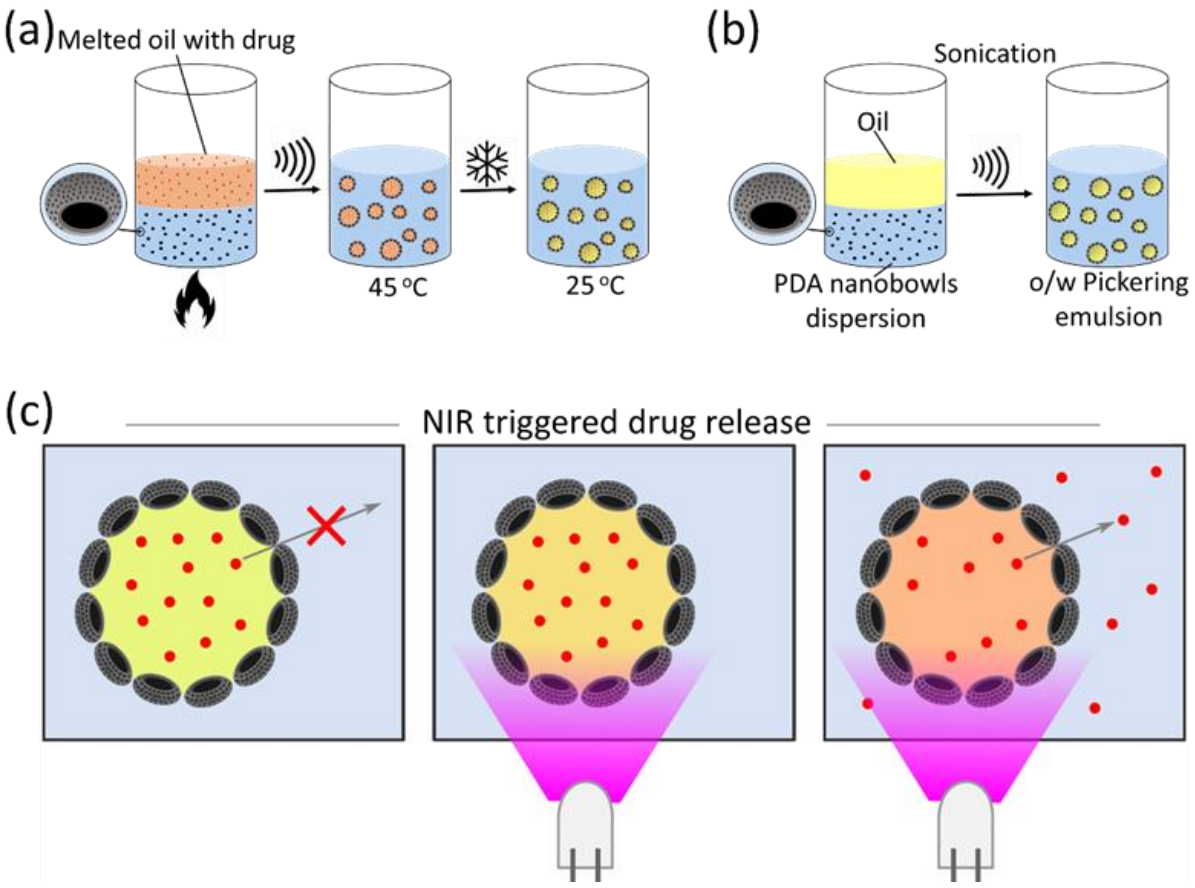

Figure 5.1. Schematic diagrams (a) and (b) show the formation of Pickering emulsion, and drug loaded Pickering emulsion respectively, stabilized by PDA nanobowls, and (c) shows NIR triggered drug release from drug loaded Pickering emulsion system under NIR illumination.

5.2 Experimental Section

5.2.1 Materials

Dopamine hydrochloride, trimethylbenzene (TMB, 98%), Pluronic® F-127, and acetylsalicylic acid (Aspirin), and para-toluenesulfonic acid were purchased from Sigma-Aldrich. Ammonia solution was from Ajax Finechem Pty., and ethanol (96%) was from Univa. Dimethyl sulfoxide (DMSO) was from Merck. Paraffin wax and stearic acid (98%) were obtained from TCI. All reagents were used as received, without further purification. Methyl stearate was prepared by esterification of stearic acid (10 g) in refluxing methanol (200 mL) with p-toluenesulfonic acid (0.2 g) as catalyst. After 6 h reaction time, residual methanol was removed by rotary evaporation, and the crude solid was purified by washing with deionised water to remove residual catalyst, following by drying in a vacuum oven overnight.

5.2.2 Synthesis and characterization of PDA nanobowls

PDA nanobowls were synthesized following a previously established method.[39] In our previous study, we demonstrated size controlled formation of PDA nanobowls, and following that protocol herein, we synthesized three different sizes of nanobowls by tuning reaction parameters.[43] Briefly, 1.5% (w/v) of dopamine hydrochloride (DA), 0.375 mL of 28% (wt.) ammonia, and 2 h polymerization time were used to prepare PDA nanobowls at around ~180 nm in size. A higher concentration of DA (2.5% (w/v)), longer polymerization time (24 h), and controlled pH with ammonia concentration 26.5% (wt.) and 25% (wt.) (0.375 mL) were ideal reaction parameters to prepare nanobowls at ~350 and ~520 nm respectively.[43] Other

components including 2.0% (v/v) trimethylbenzene (TMB, 98%), 1.0% (w/v) Pluronic® F127 (block copolymer), and 1:1 water and ethanol solvent with a total volume of 10 mL were kept constant for all three samples. After the desired reaction time, samples were washed with water-ethanol three to four times and re-dispersed in 10 mL of (1:1) water ethanol mixture for hydrothermal treatment. In a sealed Teflon-lined autoclave, samples were heated at 100 °C for 24 h in order to increase their stability. Consequently, PDA nanobowls expected to be stable at high temperature. Finally, samples were cooled to room temperature, washed with water by centrifugation (9000×g), and dried for characterization and future use. Hydrodynamic diameters and zeta potential of the samples were determined using dynamic light scattering (DLS) and phase analysis light scattering (PALS) respectively, using a Brookhaven NanoBrook Omni particle sizer and zeta potential analyser. Morphological and size analysis were done by transmission electron microscopy (TEM, FEI Tecnai G2 T20 electron microscope operating at 200 kV, using LaB6 emitter). Chemical characterization of PDA nanobowls was undertaken using a Cary 630 FTIR (Fourier Transform Infrared) spectrometer as in our previous study.[42]

5.2.3 Measurement of photothermal performance of PDA nanobowls

The photothermal conversion efficiency of various sizes of PDA nanobowls was investigated by monitoring the temperature elevation under NIR irradiation (from an OSLON® 9 PowerCluster IR, an array of nine OSRAM IR OSLON Black Series LEDs, wavelength = 850 nm, mounted on a heatsink and connected to a power source, providing 1 W cm^{-2} radiant power at the sample, which has a uniform luminance over any area up to 6.25 cm^{-2}) for 15 min. A volume of 300 µL of dispersions containing PDA nanobowls of various sizes at a concentration

of 100 μg/mL was deposited into wells of a 96 well plate. The temperature of these dispersions was recorded using a thermocouple probe every 30 s. All the measurements were done in triplicates.

5.2.4 Preparation and characterization of PDA nanobowl-stabilized Pickering emulsions

Washed and dried PDA nanobowls was used to prepare particle suspensions (1wt %) by adding pure water. In a glass vial, a 1:1 volume ratio of aqueous dispersions of the PDA nanobowls and oil (liquid paraffin wax or methyl stearate at 45°C) were placed with a total volume of 2 mL. These two heterogeneous phases were maintained at 45°C and then sonicated using a Branson Digital Sonifier® 450 at 20 kHz for 30 s to prepare PDA nanobowl-stabilized Pickering emulsion systems. Digital photographs were obtained to record emulsion stability, and the type of the emulsion (o/w versus w/o) system was evaluated by a drop test.[33] Further characterization of the Pickering emulsions was undertaken using a series of microscopic techniques including optical microscopy (OM), atomic force microscopy (AFM), and scanning electron microscopy (SEM). Prepared emulsion stability after settling overnight at room temperature was assessed by visual inspection. Drug loaded Pickering emulsions were prepared by dissolving the drug into the oil phase before emulsification. Herein, aspirin (acetylsalicylic acid) was used as a model drug, and this was dissolved in minimal DMSO to improve solubility in the oil phase.

5.2.5 Photothermal study of Pickering emulsions

Photothermal response of produced Pickering emulsions was explored using NIR (850 nm, 1 W cm^{-2}) illumination. This experiment was carried out by placing Pickering emulsion samples (solid emulsion at room temperature) in well plates, where the distance between the sample and the NIR was fixed at 1 cm for all the experiments. Upon NIR illumination, the temperature of the Pickering emulsion increased, thus melting the (previously solidified) oil droplets. This melting process was inspected by taking images in every 10 s using a Trinocular Inverted Fluorescence Microscope (IN300TC-FL, AmScope, USA) and a Point Grey CMOS camera controlled by FlyCapture image software. Subsequently, upon emulsion melting, drug molecules were able to partition into the aqueous phase, and samples were collected from the bottom of the well and analyzed using a Cary 60 UV–vis spectrophotometer (Agilent Technologies) to determine the released aspirin concentration.

5.3 Results and discussion

5.3.1 Formation of various sizes of PDA nanobowls

In this study, three different sizes of PDA nanobowls, at diameters of ~180, ~350, and ~520 nm were synthesized following the route developed in our previous study,[43] where an emulsion-induced interfacial anisotropic assembly method[39] was used and modified in order to obtain various sizes of PDA nanobowls. Size of the PDA nanobowls was controlled by tuning the concentration of the monomer (DA), polymerization time, and pH of the reaction environment.[43] The effective diameter and zeta potential of thus obtained PDA nanobowls

are shown in Table 5.1. As observed, all of these various sizes of nanobowls showed negative zeta potentials with moderate magnitudes (at around –40 mV), indicating colloidal stability of the nanobowls in dispersion due to their negative surface charge. The structure of PDA nanobowls contains catechol groups, most likely, deprotonation of the catechol alcohol groups render negative surface charge.[43-44] As observed in Table 5.11, the effective diameter of the PDA nanobowls increased with higher concentration of DA, prolonged polymerization time, and controlled pH of the reaction environment. These results are supported by TEM imaging analysis, confirming both the morphology and size of the products, with inner cavity and mesopores as observed in Figure 5.2 a–c. Chemical characterization of the PDA nanobowls was undertaken using Fourier transform infrared spectrometer (FTIR) in our previous study, indicating that two peaks at 1510 cm^{-1} and 1600 cm^{-1} are consistent with the indole or indoline structures. Peak at approximately 3370 cm^{-1} is in accordance with the presence of hydroxyl structures. The broad-band peaks from 3700−3300 cm^{-1} showed the formation of PDA, which are attributed to ν (N−H) and ν (O−H) stretching modes. The peaks at 2936−2881 cm^{-1} described the C−H stretching mode. Stretching of aromatic C−C bonds of indole are indicated by the peak at 1622 cm^{-1}. The peak at 1506 cm^{-1} is attributed to C−N bending in indolequinone and peak at 1040 cm^{-1} is attributed to C−H in-plane deformation.

Table 5.1. Dynamic light scattering and zeta potential analysis of various sizes of PDA nanobowls

Concentration of DA % (w/v)	Polymerization time (h)	Concentration of NH_4OH % (wt.)	Dynamic light scattering [45] ± SD	Polydispersity index (PDI) ± SD	Zeta potential (mV) ± SD
1.5	2	28.00	249.31 ± 16.40	0.27 ± 0.02	–38.56 ± 0.08
2.5	24	26.50	413.40 ± 16.21	0.24 ± 0.00	–40.37 ± 4.10
2.5	24	25.00	585.24 ± 11.42	0.24 ± 0.05	–44.27 ± 7.20

5.3.2 Pickering emulsion stabilized with PDA nanobowls

A suspension of PDA nanobowls in water (~0.1 wt.%) was used as an emulsifier to formulate a Pickering emulsion system at pH 4.2 using paraffin wax (liquid form) and methyl stearate (liquid form) as the oil phase. In order to investigate the impact of size of the PDA nanobowls, three different sizes of nanobowls were used to stabilize Pickering emulsions at the same pH value. As observed in digital photographs of the prepared Pickering emulsions in Figure 5.2d, the excess (lower) water phase is transparent after emulsification, indicating that all PDA nanobowls are participating in stabilizing Pickering emulsion droplets in the (upper) emulsion phase, where nanobowls are located specifically at the oil-water interfaces of these droplets. It can be anticipated that the nanobowls are adsorbed strongly and irreversibly at oil-water interfaces, as their detachment from interfaces is unflavoured due to the large detachment energy.[4, 46] In Figure 5.2, optical microscopy (OM) images (Figures 5.2 e, f, and g) clearly show the morphology of the Pickering emulsions stabilized with various sizes of PDA nanobowls (~180, ~350, and ~520 nm), where oil droplets are completely covered with black-coloured PDA nanobowls. It is notable that there are many non-spherical droplets, indicating jamming of the oil–water interface, as anticipated for true Pickering stabilization.[47] Given the average droplet radius of approximately 10 µm (Figure 5.S3), the total surface area of the emulsion sample (1 mL oil, 1 mL aqueous dispersion of bowls @ 1 wt%) is 0.30 m^2 from geometric considerations. For hexagonal close packing of particles at an interface (maximum surface fractional coverage = 0.91), the added quantity PDA nanobowls of 180 nm (diameter) bowls could occupy a total interfacial area of 0.22 m^2. This indicates that all nanobowls can indeed participate in stabilizing oil–water interface, and that either the interface is not entirely covered, the particles do not pack ideally (i.e. do not hexagonally close pack) or that inter-

particle repulsion at the interface increases the effective area occupied by each particle. It seems that the latter two of these possibilities are most likely and most supported by obtained microscopy data. This calculation however is in any case congruent with the observation that all particles appeared to be participating in stabilizing emulsion droplets, and no residual particles were observed in the aqueous sub-natant phase. Additionally, no noticeable difference was observed in the size or morphology of the oil droplets in all these Pickering emulsions stabilized with differently sized PDA nanobowls, which is most likely an effect of the fact that the same quantity of PDA nanobowls were used in each case, along with the same sonication parameters, applied to all three formulations.

To further confirm the location and orientation of the PDA nanobowls, atomic force microscopy (AFM) characterization was undertaken, facilitated by the solid nature of the oil cores of these droplets at room temperature. As observed, nanobowls are located specifically at the surface of the oil droplets (Figure 5.3a) and these bowls are almost exclusively facing their cavity to attach to the surface of the oil droplet, presenting their mesoporous rear face to the aqueous solution (Figure 5.3b). These images are presented as phase mode images, which highlight the energy dissipation between the AFM cantilever tip and surface, and here best highlight the mesopores of the PDA nanobowls. Corresponding height images are provided in supporting information (Figure 5.S1).

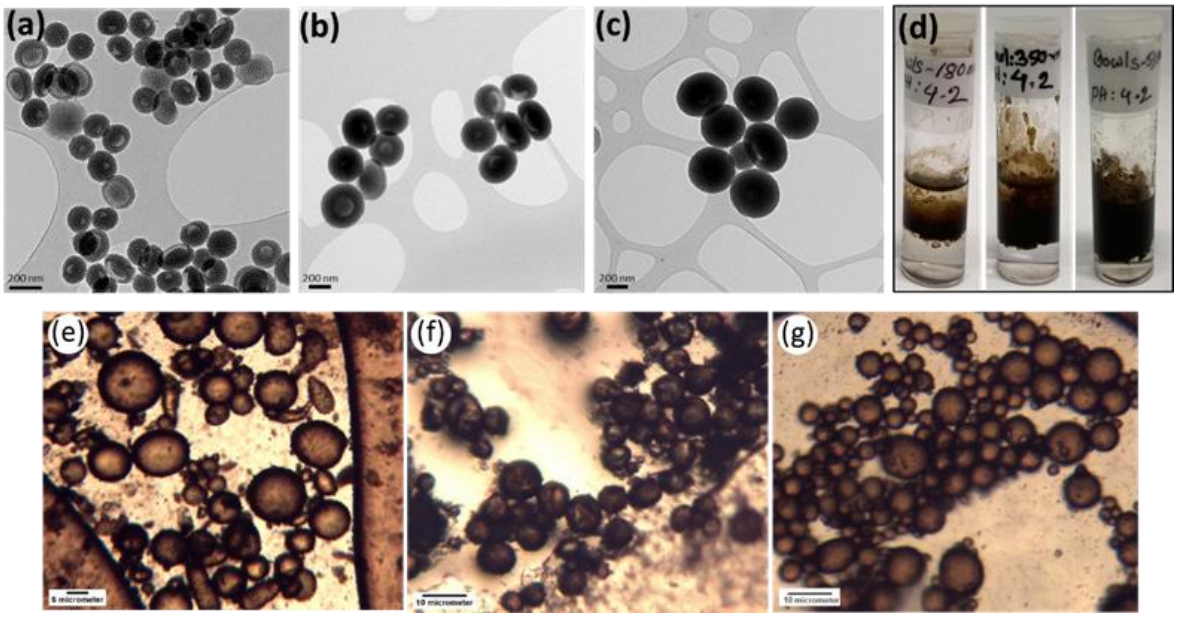

Figure 5.2. Transmission electron microscopy (TEM) images (a to c) of polydopamine nanobowls (a) ~180 nm, (b) ~350 nm, and (c) ~520 nm. Figure (d) represents digital photograph (Dimensions: 5528 x 5681 pixels) of Pickering emulsion stabilized with various sizes of PDA nanobowls, (e to g) optical microscopy (OM) images of Pickering emulsion stabilized with (e) ~180 nm, (f) ~350 nm, and (g) ~520 nm PDA nanobowls. The scale bars in (a–c) 200 nm, (d) 5 µm, and (e–f) 10 µm.

The morphology of these Pickering emulsions was further examined by scanning electron microscopy (SEM) imaging, where a distinct view of two oil droplets found covered with PDA nanobowls was obtained (Figure 5.3d). Upon close inspection of the SEM image, the location the PDA nanobowls was further confirmed, revealing that they are using their curvature to attach to the oil droplet using the cavity side (Figure 5.3e). This is logical based on surface area and surface energy considerations, as the cavity side represents a greater surface area for wetting by the oil phase.

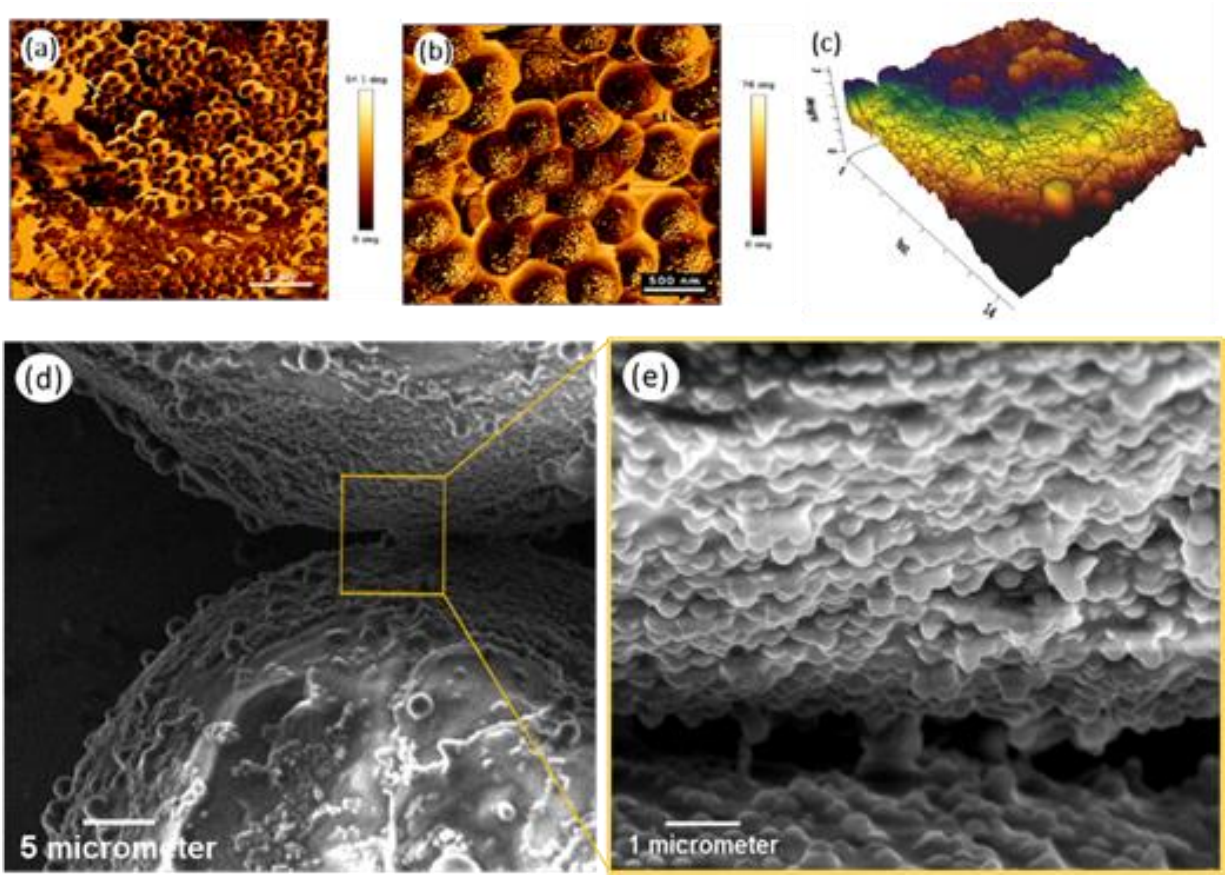

Figure 5.3. Atomic force microscopy (AFM) phase images of the surface of a solidified Pickering emulsion droplet stabilized by ~350 nm nanobowls (a), with highly-magnified view (b), and 3D height image (c). Scanning electron microscopy (SEM) images, (d) shows two oil droplets covered with PDA nanobowls, and (e) highly-magnified view shows the orientation of PDA bowls on the surface of the droplets.

The particle's spontaneous adsorption at the oil-water interface indicates that this must be a free energy lowering process, and therefore, a greater wetted area of particle will represent a lower energy state at the interface. Like other anisotropic shaped particles (peanut-shaped), these PDA nanobowls exhibit an immovable orientation upon adsorption due to their curvature.[30] Indeed, these PDA nanobowls stabilized Pickering emulsion were stable for over

a year due to limitation of droplet coalescence (Figure 5.S2). This phenomenon can be described as the result of their unique interfacial packing and orientation, which was favourable for the promoting stability of the Pickering emulsion against further coalescence or ripening.[30, 48-49]

A drop test was undertaken to confirm the emulsion type (i.e. water-in-oil or oil-in-water). One drop of the emulsion was added separately to a drop of water or oil and its ease of dispersion was assessed by visual inspection, which confirmed that the developed Pickering emulsion is an oil-in-water type, as shown in Figure 5.S4.This is anticipated from Bancroft's rule, as the PDA nanobowls are easily dispersed in the aqueous phase but are essentially non-dispersible in the oil phase.[50]

To investigate the impact of pH on the morphology of the Pickering emulsion, this emulsion was prepared at various aqueous phase pH values with a fixed concentration of PDA nanobowls. Optical microscopy was then used to investigate the pH sensitivity of the PDA nanobowl stabilized Pickering emulsions; obtained results demonstrated strong evidence of pH dependent behaviour. As shown in Figure 5.4 a–e, fine PDA nanobowl stabilized droplets were obtained in acidic pH, whereas at higher pH values, apparent detachment of PDA nanobowls occurred due to increasing negative surface charge of the PDA nanobowls in higher pH (Figure 5.S5) as well as the oil–water interface, making them mutually repelled from oil/water interface.[34, 47, 51] It has been suggested that in higher pH, emulsion droplets become stabilized by adsorbed OH- ions on their surfaces,[52] whereas, the amount of OH present in

the system in lower pH is not sufficient to solely stabilize the emulsion droplets, therefore, PDA nanobowls serve as stabilizer.[34]

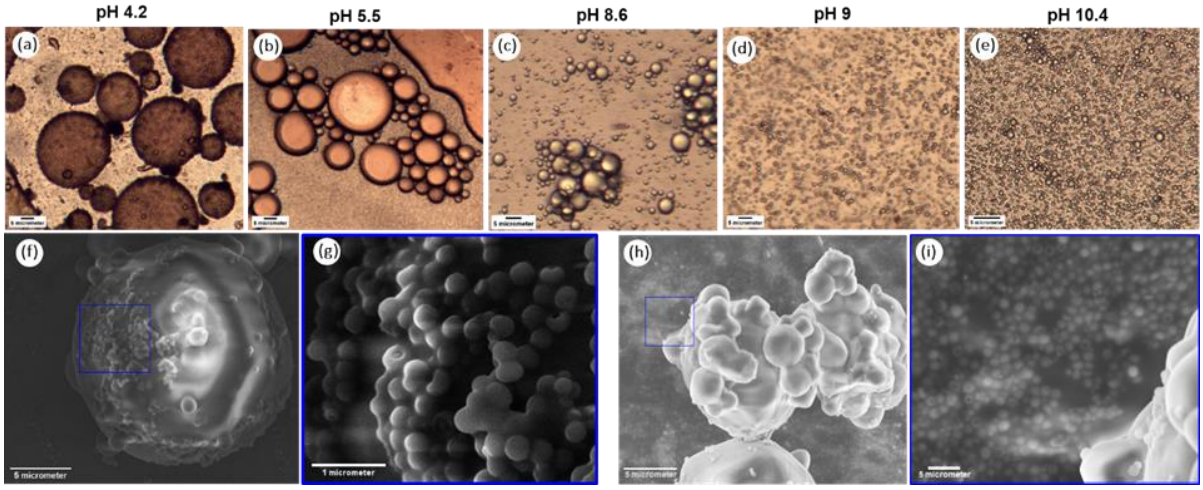

Figure 5.4. Morphological analysis of the Pickering emulsion droplets in various pH, OM images at top (a to e) show the changes of Pickering emulsion with increasing pH value. SEM images (f to i) at the bottom, show the oil droplet of the Pickering emulsion prepared at pH 4.2 (f), where the oil droplet is covered with PDA nanobowls at low magnified view and (g) high-magnified view shows the orientation of PDA nanobowls on the oil droplet. SEM images (h) and (i) are showing the oil droplet of the Pickering emulsion prepared at pH 10.4, (h) shows the droplets are not covered with PDA nanobowls and high-magnified view (i) shows the location of PDA nanobowls.

These findings were further investigated by obtaining SEM micrographs, and as shown in Figure 5.4 f and g, Pickering emulsion prepared in acidic medium (pH 4.2), the droplets are covered with PDA nanobowls. In contrast, for Pickering emulsions prepared at a higher pH value (pH 10.4), nanobowls are not observed on the surface of the droplet (Figure 5.4 h) and

the majority of the nanobowls are located in the background (Figure 5.4i), suggesting poor adsorption of PDA nanobowls due to charge repulsions from the oil–water interface.[47]

5.3.3 Photothermal responsive property of prepared Pickering emulsion

With an aim to explore photothermally responsive behavior of these Pickering emulsions, first we investigated the photothermal response characteristics of PDA nanobowls, inspired by previous studies of photothermal response behavior of PDA nanoparticles.[2] PDA has a similar structure to melanin, which has the ability to absorb light in the near-infrared region.[53] Consequently, PDA nanobowls suspended in water absorb light under NIR illumination and convert it into thermal energy. Subsequently, the generated heat is transferred to the surrounding medium (water), thus the temperature of PDA nanobowl suspensions rises with increasing duration of NIR exposure (Figure 5.5a).[54] Herein, various sizes of PDA bowls were illuminated with NIR at 850 nm, with 1 W cm–2 power for 15 min. As observed in Figure 5.5a, the temperature increases initially linearly with different diameters of PDA nanobowls before saturating, and both the initial rate of temperature increase and final temperature reached are dependent on PDA bowl size. The recorded temperatures after 15 min of NIR exposure of PDA nanobowl dispersions were 73.33 ºC (~180 nm), 78 ºC (~350 nm), and 86.33 ºC (~520 nm). In contrast, the temperature of water (without the PDA nanobowls) reached a maximum of only 32.6 ºC after 15 min of NIR illumination (Figure 5.5a). Note that, there was no sign of degradation of PDA nanobowls observed under NIR irradiation.

To investigate the photothermal response of PDA nanobowl (~350 nm) stabilized Pickering emulsions, an emulsion was exposed to NIR (at 850 nm, with 1 W cm–2). Here, methyl stearate was used as the oil phase, which is solid in room temperature (melting point 39 ºC).[55] After encapsulation in the emulsion system, methyl stearate started to melt at around 42 ºC. After 260 s of NIR illumination, a complete transformation (from solid state to liquid) was observed in the Pickering emulsion system, and the recorded temperature was 57 ºC for the sample with highest density of nanobowls as shown in the digital photographs in Figure 5.5b.

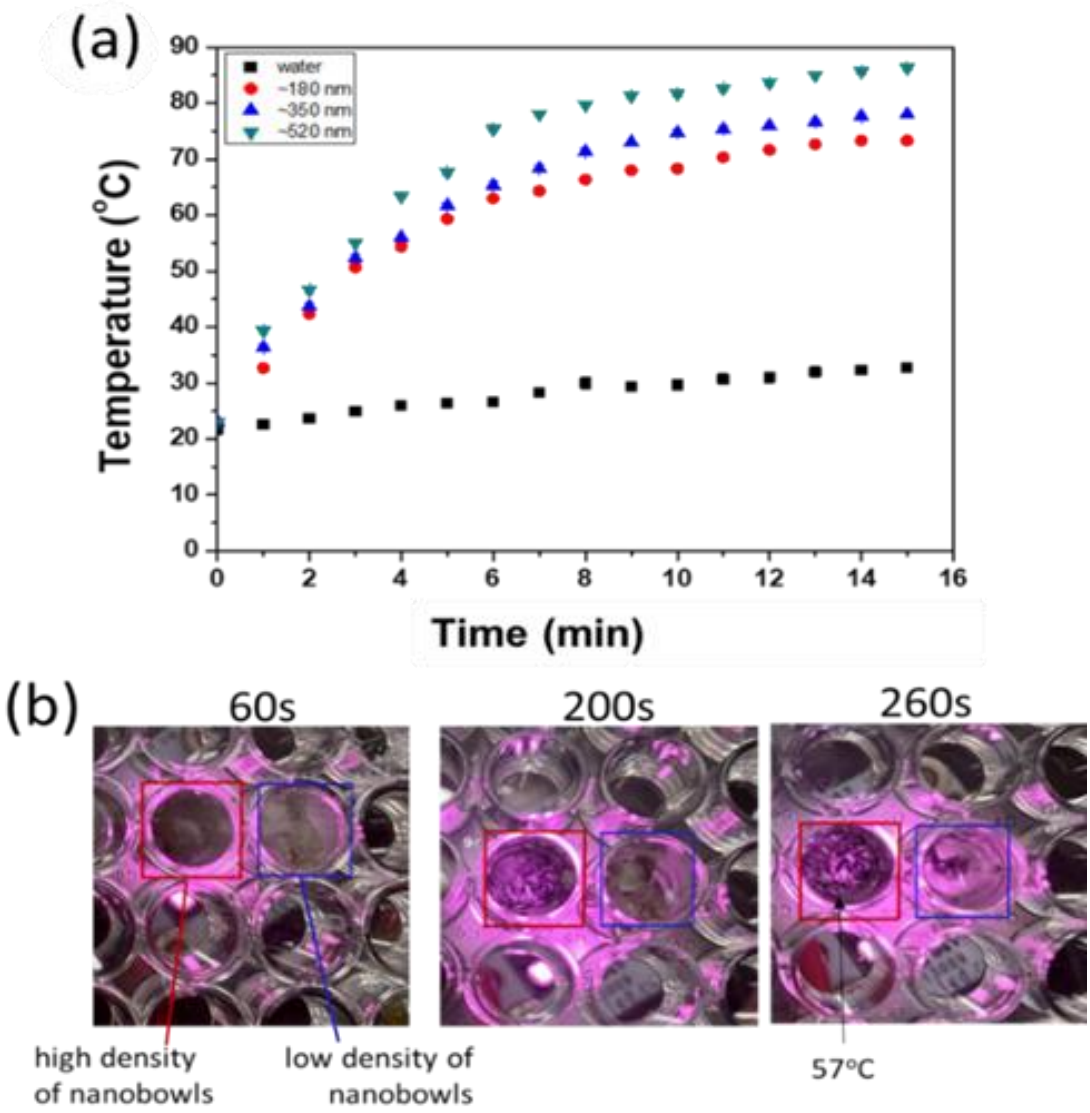

Figure 5.5. (a) Photothermal effect of various sizes of PDA nanobowls under NIR illumination (100 μg/mL PDA nanobowls, 1 Wcm^{-2} NIR illumination power) for 15 min, (b) Digital images showing melting process of Pickering emulsion (methyl stearate oil phase, stabilized by ~350 nm PDA nanobowls at pH 4.2) upon NIR irradiation at 60, 200, and 260 s.

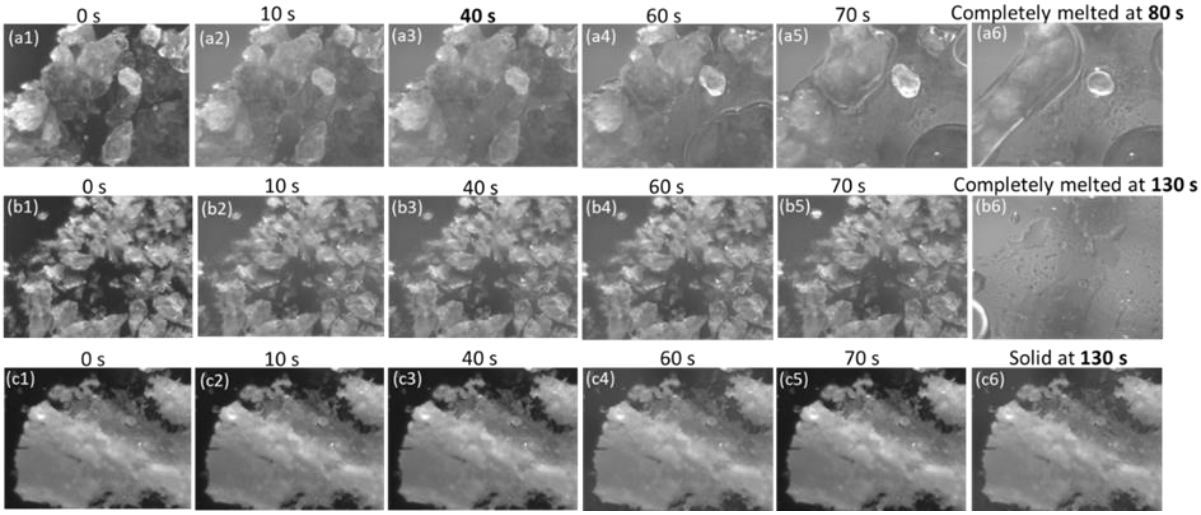

Figure 5.6. Digital images show the breaking/melting process of Pickering emulsion system/ Pickering emulsion droplets (prepared with methyl stearate and stabilized with ~350 nm PDA bowls at pH 4.2) over time under NIR irradiation, (a1 to a6) sample with high density of PDA nanobowls, (b1 to b6) sample with low density of PDA nanobowls, and (c1 to c6) only methyl stearate.

Note that as anticipated, the concentration of PDA nanobowls had a significant impact on this melting process, as the Pickering emulsion sample (Pickering emulsion droplets) with a higher concentration of PDA nanobowls melted more quickly, indicating faster temperature increase in the emulsion system due greater absorption of NIR light.

To further confirm the above findings, this melting process was recorded in every 10 s. As shown in Figure 5.6, the sample (Pickering emulsion) with high density of PDA nanobowls (a1 to a6) started to melt at 40 s (Figure 5.6a3), completely melting at 80 s (Figure 5.6a6). In contrast, a significantly longer time (130 s) (Figure 5.6b6) was taken to melt the sample with

lower density of PDA nanobowls (b1 to b6), while methyl stearate without PDA nanobowls (control) (c1 to c6) remained completely solid after 130 s (Figure 5.6c6). These results further confirm the key role of PDA nanobowls, which act not only as Pickering stabilizer but also as a potent photothermal transducer (introducing stimuli responsive properties) for these Pickering emulsions.

5.3.4 NIR controlled drug release

By taking the advantage of the prepared Pickering emulsion with its unique combination of biologically compatible and photothermal response properties, we propose that this system could be effectively applied in various biomedical applications including drug delivery. Here we show a proof of concept by releasing drug molecules from the Pickering emulsion system upon NIR illumination by melting waxy ester (methyl stearate) droplets containing a model drug compound. This investigation was conducted by adding drugs into the (liquid) oil phase before emulsification and cooling as shown in the schematic diagram in Figure 5.7a. Upon NIR illumination, the drug loaded Pickering emulsion droplets melted, consequently releasing drug molecules as shown in the schematic diagram in Figure 5.7b. The concentration of released drugs was monitored over time and analyzed by UV-vis spectrometry.

As observed in Figure 5.S6, no drug release was observed without NIR illumination as emulsion melting did not occur (Figure 5.S6a), and consequently the drug remained trapped within the solid oil droplets and was not released.

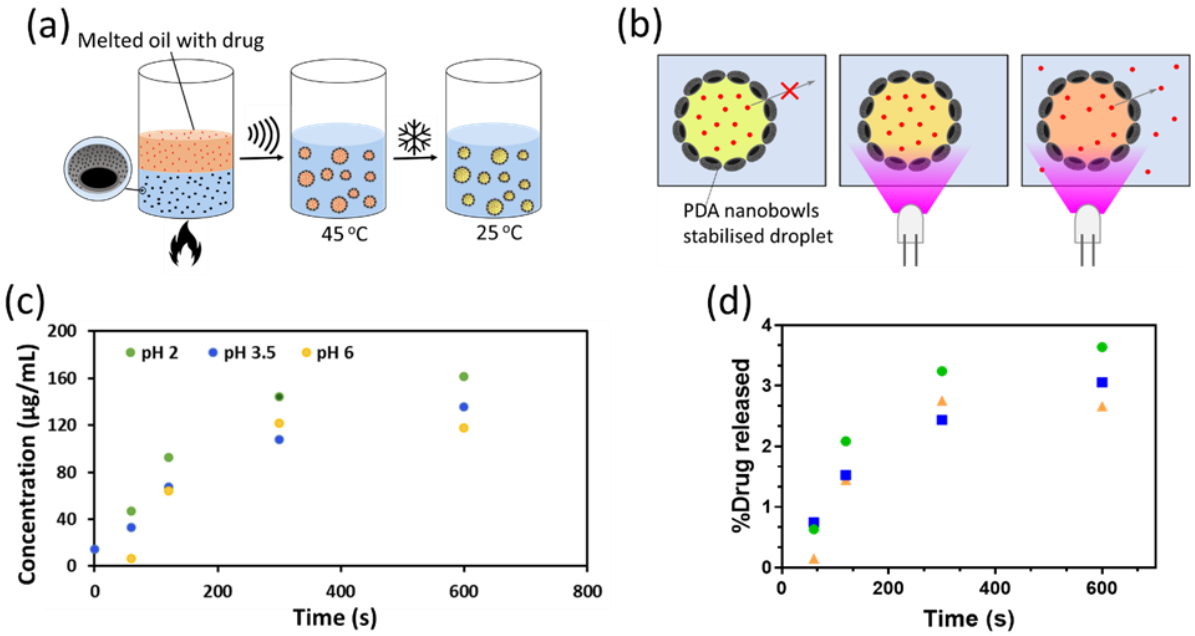

Figure 5.7. Schematic diagrams (a) and (b) show the preparation of drug loaded Pickering emulsion and NIR triggered drug release from drug loaded oil droplet respectively. Figure (c) shows time-dependent aspirin release at various pH conditions, and (d) shows the concentration of drug released under NIR illumination at various pH values.

In contrast, under NIR illumination, the emulsion droplets melted, allowing the drug molecules to partition between the liquid oil and aqueous phases, and thus releasing a proportion of the encapsulated drug (Figure 5.S6 b to d). The concentration of released drug increased with NIR exposure time (Figure 5.7c and Figure 5.S6 b to d). In order to investigate the drug release trend as a function of pH, this experiment was conducted in various pH aqueous media, and only minor differences were observed in drug release profiles in different pH environments (Figure 5.S6 and Figure 5.7c). The concentration of released drug was quantified by comparing UV-vis data with a standard curve (Figure 5.S7). As melting of the methyl stearate encapsulating phase progressed, it was noted that the concentration of

released drug increased with longer periods of NIR illumination (Figure 5.7d), although the overall release was quite low compared to the total drug loading within the oil phase. This is likely due to favourable partitioning of aspirin into the oil phase, as indicated by its log *P* value of 1.14; that is, aspirin is around 13× more soluble in an oily (octanol) phase than water,[56] and we anticipate that this partitioning would be approximately the same between water and methyl stearate used as the oil phase here.

Nonetheless, this proof of concept experiment demonstrates the possibility to trigger the release of a drug on demand by application of NIR irradiation to a smart emulsion. Collectively, PDA nanobowls can act as the sole stabilizer to form Pickering emulsions that possess an excellent combination of biocompatibility and biodegradability with photothermal response and prolonged emulsion stability and these emulsions can be stimulated to release active compounds on demand.

5. 4. Conclusion

In this study, we explored the application of polydopamine (PDA) nanobowl as a Pickering stabilizer without any surface modification. Stability of produced emulsions was maintained for over one year due to limitation of coalescence and ripening of the PDA nanobowls stabilized droplets. By using an oil core with melting point moderately above room temperature, solidifiable emulsion droplets were produced that could be addressed with light in order to melt and release their contents. This provides a valuable mechanism for controlling partitioning of actives, with potential uses in on-demand drug delivery.

Owing to the photothermal properties of PDA, this Pickering emulsion displayed remarkable photothermal response, which offers significant benefits for various biomedical applications including NIR controlled/triggered drug delivery applications. Taken together, prepared PDA nanobowls stabilized Pickering emulsions offer a unique combination of excellent biocompatibility and long-term stability with potential for NIR controlled drug release application, which may meet current challenges to be addressed by responsive Pickering emulsions for biomedical applications.

5.5 Conclusion

(1) Saigal, T.; Dong, H.; Matyjaszewski, K.; Tilton, R. D. Pickering Emulsions Stabilized by Nanoparticles with Thermally Responsive Grafted Polymer Brushes. *Langmuir: the ACS Journal of Surfaces and Colloids* **2010,** *26* (19), 15200-15209, DOI: 10.1021/la1027898.
(2) Xing, Y.; Zhang, J.; Chen, F.; Liu, J.; Cai, K. Mesoporous Polydopamine Nanoparticles with Co-Delivery Function for Overcoming Multidrug Resistance *via* Synergistic Chemo-Photothermal Therapy. *Nanoscale* **2017,** *9* (25), 8781-8790, DOI: 10.1039/C7NR01857F.
(3) Liu, K.; Jiang, J.; Cui, Z.; Binks, B. P. pH-Responsive Pickering Emulsions Stabilized by Silica Nanoparticles in Combination with A Conventional Zwitterionic Surfactant. *Langmuir : the ACS Journal of Surfaces and Colloids* **2017,** *33* (9), 2296-2305, DOI: 10.1021/acs.langmuir.6b04459.
(4) Binks, B. P. Particles as Surfactants—Similarities and Differences. *Current Opinion in Colloid & Interface Science* **2002,** *7* (1), 21-41, DOI: 10.1016/S1359-0294(02)00008-0.
(5) Xu, J.; Ma, A.; Liu, T.; Lu, C.; Wang, D.; Xu, H. Janus-Like Pickering Emulsions and Their Controllable Coalescence. *Chemical Communications* **2013,** *49* (92), 10871-10873, DOI: 10.1039/C3CC46738D.
(6) Li, X.; Li, J.; Gong, J.; Kuang, Y.; Mo, L.; Song, T. Cellulose Nanocrystals (CNCs) with Different Crystalline Allomorph for Oil in Water Pickering Emulsions. *Carbohydrate Polymers* **2018,** *183*, 303-310, DOI: 10.1016/j.carbpol.2017.12.085.
(7) Liu, B.; Zhu, Y.; Tian, J.; Guan, T.; Li, D.; Bao, C.; Norde, W.; Wen, P.; Li, Y. Inhibition of Oil Digestion in Pickering Emulsions Stabilized by Oxidized Cellulose Nanofibrils for Low-Calorie Food Design. *RSC Advances* **2019,** *9* (26), 14966-14973, DOI: 10.1039/C9RA02417D.
(8) Mwangi, W. W.; Lim, H. P.; Low, L. E.; Tey, B. T.; Chan, E. S. Food-Grade Pickering Emulsions for Encapsulation and Delivery of Bioactives. *Trends in Food Science & Technology* **2020,** *100*, 320-332, DOI: 10.1016/j.tifs.2020.04.020.

(9) Albert, C.; Beladjine, M.; Tsapis, N.; Fattal, E.; Agnely, F.; Huang, N. Pickering Emulsions: Preparation Processes, Key Parameters Governing Their Properties and Potential for Pharmaceutical Applications. *Journal of Controlled Release* **2019,** *309*, 302-332, DOI: 10.1016/j.jconrel.2019.07.003.
(10) Wei, Y.-s.; Niu, Z.-c.; Wang, F.-q.; Feng, K.; Zong, M.-h.; Wu, H. A Novel Pickering Emulsion System as the Carrier of Tocopheryl Acetate for its Application in Cosmetics. *Materials Science and Engineering: C* **2020,** *109*, 110503, DOI: 10.1016/j.msec.2019.110503.
(11) Tang, J.; Quinlan, P. J.; Tam, K. C. Stimuli-Responsive Pickering Emulsions: Recent Advances and Potential Applications. *Soft Matter* **2015,** *11* (18), 3512-3529, DOI: 10.1039/C5SM00247H.
(12) Fujii, S.; Read, E. S.; Binks, B. P.; Armes, S. P. Stimulus-Responsive Emulsifiers Based on Nanocomposite Microgel Particles. *Advanced Materials* **2005,** *17* (8), 1014-1018, DOI: 10.1002/adma.200401641.
(13) Ngai, T.; Behrens, S. H.; Auweter, H. Novel Emulsions Stabilized by pH and Temperature Sensitive Microgels. *Chemical Communications* **2005,** (3), 331-333, DOI: 10.1039/B412330A.
(14) Li, Z.; Shi, Y.; Zhu, A.; Zhao, Y.; Wang, H.; Binks, B. P.; Wang, J. Light-Responsive, Reversible Emulsification and Demulsification of Oil-in-Water Pickering Emulsions for Catalysis. *Angewandte Chemie International Edition* **2021,** *60* (8), 3928-3933, DOI: 10.1002/anie.202010750.
(15) Bielas, R.; Surdeko, D.; Kaczmarek, K.; Józefczak, A. The Potential of Magnetic Heating for Fabricating Pickering-Emulsion-Based Capsules. *Colloids and Surfaces B: Biointerfaces* **2020,** *192*, 111070, DOI: 10.1016/j.colsurfb.2020.111070.
(16) Jiang, J.; Ma, Y.; Cui, Z.; Binks, B. Pickering Emulsions Responsive to CO_2/N_2 and Light Dual Stimuli at Ambient Temperature. *Langmuir : the ACS Journal of Surfaces and Colloids* **2016,** *32* (34), 8668-8675, DOI: 10.1021/acs.langmuir.6b01475.
(17) Jiang, J.; Zhang, D.; Yin, J.; Cui, Z. Responsive, Switchable Wormlike Micelles for CO_2/N_2 and Redox Dual Stimuli Based on Selenium-Containing Surfactants. *Soft Matter* **2017,** *13* (37), 6458-6464, DOI: 10.1039/C7SM01308F.
(18) Brugger, B.; Richtering, W. Magnetic, Thermosensitive Microgels as Stimuli-Responsive Emulsifiers Allowing for Remote Control of Separability and Stability of Oil in Water-Emulsions. *Advanced Materials* **2007,** *19* (19), 2973-2978, DOI: 10.1002/adma.200700487.
(19) Zhang, Y.; Guo, S.; Ren, X.; Liu, X.; Fang, Y. CO(2) and Redox Dual Responsive Pickering Emulsion. *Langmuir: the ACS Journal of Surfaces and Colloids* **2017,** *33* (45), 12973-12981, DOI: 10.1021/acs.langmuir.7b02976.
(20) Kim, I.-Y.; Joachim, E.; Choi, H.; Kim, K. Toxicity of Silica Nanoparticles Depends on Size, Dose, and Cell Type. *Nanomedicine: Nanotechnology, Biology and Medicine* **2015,** *11* (6), 1407-1416, DOI: 10.1016/j.nano.2015.03.004.
(21) Malhotra, N.; Lee, J.-S.; Liman, R. A. D.; Ruallo, J. M. S.; Villaflores, O. B.; Ger, T.-R.; Hsiao, C.-D. Potential Toxicity of Iron Oxide Magnetic Nanoparticles: A Review. *Molecules* **2020,** *25* (14), 3159, DOI: 10.3390/molecules25143159.
(22) Zhu, Y.; Fu, T.; Liu, K.; Lin, Q.; Pei, X.; Jiang, J.; Cui, Z.; Binks, B. P. Thermoresponsive Pickering Emulsions Stabilized by Silica Nanoparticles in Combination with Alkyl Polyoxyethylene Ether Nonionic Surfactant. *Langmuir: the ACS Journal of Surfaces and Colloids* **2017,** *33* (23), 5724-5733, DOI: 10.1021/acs.langmuir.7b00273.
(23) Yu, S.; Zhang, D.; Jiang, J.; Xia, W. Redox-Responsive Pickering Emulsions Stabilized by Silica Nanoparticles and Ferrocene Surfactants at A Very Low Concentration. *ACS Sustainable Chemistry & Engineering* **2019,** *7* (19), 15904-15912, DOI: 10.1021/acssuschemeng.9b01881.
(24) Demina, P. A.; Bukreeva, T. V. Pickering Emulsion Stabilized by Commercial Titanium Dioxide Nanoparticles in the Form of Rutile and Anatase. *Nanotechnologies in Russia* **2018,** *13* (7), 425-429, DOI: 10.1134/S1995078018040043.
(25) Kim, Y. J.; Liu, Y. D.; Seo, Y.; Choi, H. J. Pickering-Emulsion-Polymerized Polystyrene/Fe_2O_3 Composite Particles and Their Magnetoresponsive Characteristics. *Langmuir: the ACS Journal of Surfaces and Colloids* **2013,** *29* (16), 4959-4965, DOI: 10.1021/la400523w.

(26) Mi, X.; Wang, X.; Gao, C.; Su, W.; Zhang, Y.; Tan, X.; Gao, J.; Liu, Y. Modified Reduced Graphene Oxide as Stabilizer for Pickering w/o Emulsions. *Journal of Materials Science* **2020,** *55* (5), 1946-1958, DOI: 10.1007/s10853-019-04066-7.
(27) Lee, J.; Chang, J. Y. Pickering Emulsion Stabilized by Microporous Organic Polymer Particles for the Fabrication of a Hierarchically Porous Monolith. *Langmuir: the ACS Journal of Surfaces and Colloids* **2018,** *34* (39), 11843-11849, DOI: 10.1021/acs.langmuir.8b02576.
(28) Yang, Y.; Fang, Z.; Chen, X.; Zhang, W.; Xie, Y.; Chen, Y.; Liu, Z.; Yuan, W. An Overview of Pickering Emulsions: Solid-Particle Materials, Classification, Morphology, and Applications. *Frontiers in Pharmacology* **2017,** *8*, 287-287, DOI: 10.3389/fphar.2017.00287.
(29) Iwashita, Y. Pickering–Ramsden Emulsions Stabilized with Chemically and Morphologically Anisotropic Particles. *Current Opinion in Colloid & Interface Science* **2020,** *49*, 94-106, DOI: 10.1016/j.cocis.2020.05.004.
(30) de Folter, J. W. J.; Hutter, E. M.; Castillo, S. I. R.; Klop, K. E.; Philipse, A. P.; Kegel, W. K. Particle Shape Anisotropy in Pickering Emulsions: Cubes and Peanuts. *Langmuir : the ACS Journal of Surfaces and Colloids* **2014,** *30* (4), 955-964, DOI: 10.1021/la402427q.
(31) Jiang, H.; Sheng, Y.; Ngai, T. Pickering Emulsions: Versatility of Colloidal Particles and Recent Applications. *Current Opinion in Colloid & Interface Science* **2020,** *49*, 1-15, DOI: 10.1016/j.cocis.2020.04.010.
(32) Yang, T.; Wei, L.; Jing, L.; Liang, J.; Zhang, X.; Tang, M.; Monteiro, M. J.; Chen, Y.; Wang, Y.; Gu, S.; Zhao, D.; Yang, H.; Liu, J.; Lu, G. Q. M. Dumbbell-Shaped Bi-Component Mesoporous Janus Solid Nanoparticles for Biphasic Interface Catalysis. *Angewandte Chemie International Edition* **2017,** *56* (29), 8459-8463, DOI: 10.1002/anie.201701640.
(33) Nishizawa, N.; Kawamura, A.; Kohri, M.; Nakamura, Y.; Fujii, S. Polydopamine Particle as a Particulate Emulsifier. *Polymers* **2016,** *8*, 62, DOI: 10.3390/polym8030062.
(34) Xu, J.; Ma, A.; Liu, T.; Lu, C.; Wang, D.; Xu, H. Janus-Like Pickering Emulsions and Their Controllable Coalescence. *Chemical Communications (Cambridge, England)* **2013,** *49*, 10871, DOI: 10.1039/c3cc46738d.
(35) Liu, Y.; Ai, K.; Lu, L. Polydopamine and Its Derivative Materials: Synthesis and Promising Applications in Energy, Environmental, and Biomedical Fields. *Chemical Reviews* **2014,** *114* (9), 5057-5115, DOI: 10.1021/cr400407a.
(36) You, Y.-H.; Lin, Y.-F.; Nirosha, B.; Chang, H.-T.; Huang, Y.-F. Polydopamine-Coated Gold Nanostar for Combined Antitumor and Antiangiogenic Therapy in Multidrug-Resistant Breast Cancer. *Nanotheranostics* **2019,** *3* (3), 266-283, DOI: 10.7150/ntno.36842.
(37) Zhu, Z.; Su, M. Polydopamine Nanoparticles for Combined Chemo- and Photothermal Cancer Therapy. *Nanomaterials (Basel)* **2017,** *7* (7), 160, DOI: 10.3390/nano7070160.
(38) Liu, Y.; Ai, K.; Jianhua, L.; Deng, M.; He, Y.; Lu, L. Dopamine-Melanin Colloidal Nanospheres: An Efficient Near-Infrared Photothermal Therapeutic Agent for In *Vivo* Cancer Therapy. *Advanced materials (Deerfield Beach, Fla.)* **2013,** *25*, 1353-1359, DOI: 10.1002/adma.201204683.
(39) Guan, B. Y.; Yu, L.; Lou, X. W. Formation of Asymmetric Bowl-Like Mesoporous Particles *via* Emulsion-Induced Interface Anisotropic Assembly. *Journal of the American Chemical Society* **2016,** *138* (35), 11306-11311, DOI: 10.1021/jacs.6b06558.
(40) Yang, L.; Wang, C.; Ye, Z.; Zhang, P.; Wu, S.; Jia, S.; Li, Z.; Zhang, Z. Anisotropic Polydopamine Capsules with an Ellipsoidal Shape that Can Tolerate Harsh Conditions: Efficient Adsorbents for Organic Dyes and Precursors for Ellipsoidal Hollow Carbon Particles. *RSC Advances* **2017,** *7* (35), 21686-21696, DOI: 10.1039/C7RA02235B.
(41) Guan, B. Y.; Zhang, S. L.; Lou, X. W. Realization of Walnut-Shaped Particles with Macro-/Mesoporous Open Channels Through Pore Architecture Manipulation and Their Use in Electrocatalytic Oxygen Reduction. *Angewandte Chemie International Edition* **2018,** *57* (21), 6176-6180, DOI: 10.1002/anie.201801876.

(42) Acter, S.; Vidallon, M. L. P.; Crawford, S.; Tabor, R. F.; Teo, B. M. Efficient Cellular Internalization and Transport of Bowl-Shaped Polydopamine Particles. *Particle & Particle Systems Characterization* **2020,** *37*, 2000166, DOI: 10.1002/ppsc.202000166.
(43) Acter, S.; Vidallon, M. L. P.; Crawford, S.; Tabor, R. F.; Teo, B. M. Bowl-Shaped Mesoporous Polydopamine Nanoparticles for Size-Dependent Endocytosis into HeLa Cells. *ACS Applied Nano Materials* **2021,** *4* (9), 9536-9546, DOI: 10.1021/acsanm.1c01897.
(44) Liebscher, J.; Mrówczyński, R.; Scheidt, H. A.; Filip, C.; Hădade, N. D.; Turcu, R.; Bende, A.; Beck, S. Structure of Polydopamine: A Never-Ending Story? *Langmuir : the ACS Journal of Surfaces and Colloids* **2013,** *29* (33), 10539-10548, DOI: 10.1021/la4020288.
(45) Burrows, N. D.; Vartanian, A. M.; Abadeer, N. S.; Grzincic, E. M.; Jacob, L. M.; Lin, W.; Li, J.; Dennison, J. M.; Hinman, J. G.; Murphy, C. J. Anisotropic Nanoparticles and Anisotropic Surface Chemistry. *The Journal of Physical Chemistry Letters* **2016,** *7* (4), 632-641, DOI: 10.1021/acs.jpclett.5b02205.
(46) Aveyard, R.; Binks, B. P.; Clint, J. H. Emulsions Stabilised Solely by Colloidal Particles. *Advances in Colloid and Interface Science* **2003,** *100-102*, 503-546, DOI: 10.1016/S0001-8686(02)00069-6.
(47) McCoy, T. M.; Pottage, M. J.; Tabor, R. F. Graphene Oxide-Stabilized Oil-in-Water Emulsions: pH-Controlled Dispersion and Flocculation. *The Journal of Physical Chemistry C* **2014,** *118* (8), 4529-4535, DOI: 10.1021/jp500072a.
(48) Loudet, J. C.; Alsayed, A. M.; Zhang, J.; Yodh, A. G. Capillary Interactions Between Anisotropic Colloidal Particles. *Physical Review Letters* **2005,** *94* (1), 018301, DOI: 10.1103/PhysRevLett.94.018301.
(49) Loudet, J. C.; Yodh, A. G.; Pouligny, B. Wetting and Contact Lines of Micrometer-Sized Ellipsoids. *Physical Review Letters* **2006,** *97* (1), 018304, DOI: 10.1103/PhysRevLett.97.018304.
(50) Ruckenstein, E. Microemulsions, Macroemulsions, and the Bancroft Rule. *Langmuir: the ACS Journal of Surfaces and Colloids* **1996,** *12* (26), 6351-6353, DOI: 10.1021/la960849m.
(51) Anjali, T. G.; Basavaraj, M. G. General Destabilization Mechanism of pH-Responsive Pickering Emulsions. *Physical Chemistry Chemical Physics* **2017,** *19* (45), 30790-30797, DOI: 10.1039/C7CP04665K.
(52) Beattie, J. K.; Djerdjev, A. M. The Pristine Oil/Water Interface: Surfactant-Free Hydroxide-Charged Emulsions. *Angewandte Chemie International Edition* **2004,** *43* (27), 3568-3571, DOI: 10.1002/anie.200453916.
(53) Hauser, D.; Septiadi, D.; Turner, J.; Petri-Fink, A.; Rothen-Rutishauser, B. From Bioinspired Glue to Medicine: Polydopamine as A Biomedical Material. *Materials (Basel)* **2020,** *13* (7), 1730, DOI: 10.3390/ma13071730.
(54) Moustaoui, H.; Saber, J.; Djeddi, I.; Liu, Q.; Diallo, A. T.; Spadavecchia, J.; Lamy de la Chapelle, M.; Djaker, N. Shape and Size Effect on Photothermal Heat Elevation of Gold Nanoparticles: Absorption Coefficient Experimental Measurement of Spherical and Urchin-Shaped Gold Nanoparticles. *The Journal of Physical Chemistry C* **2019,** *123* (28), 17548-17554, DOI: 10.1021/acs.jpcc.9b03122.
(55) Kurtz, F. E. Chromatography of Methyl Stearate, Methyl Oleate, Methyl Linoleate and Methyl Linolenate: A Concept of Amplified Chromatographic Separations. *Journal of the American Chemical Society* **1952,** *74* (8), 1902-1909, DOI: 10.1021/ja01128a008.
(56) Dołowy, M.; Pyka, A. Lipophilicity Study of Salicylic and Acetylsalicylic Acids Using Both Experimental and Calculations Methods. *Journal of Liquid Chromatography & Related Technologies* **2015,** *38* (4), 485-491, DOI: 10.1080/10826076.2014.913527.

Chapter 6

Conclusions and Future Direction

6.1 Project conclusions

In this thesis, we have fabricated various shapes (spherical and bowl-shaped) and sizes of polydopamine (PDA) nanoparticles to explore their potential in drug delivery systems. PDA nanoparticles have a range of excellent properties that make them suitable for application in various biomedical settings, some of which have been demonstrated here. To be more specific, the shape- and size-dependent cellular internalization efficiency of PDA nanoparticles has been investigated, wherein human cervical cancer (HeLa) cells are used as a model cell line. Due to the composition of PDA, its surface is functionalized with catechol/quinone moieties; therefore, it offers the potential to either anchor drug molecules onto produced nanoparticles by physical bonding such as π–π stacking or hydrogen bonding as well as via covalent tethering. Drug loading and release efficiency of PDA nanoparticles in an acidic environment have been studied here, indicating the role of these interactions. Moreover, PDA has an excellent photothermal conversion efficiency as it has the ability to absorb visible and infrared light and convert this into heat. In this thesis, PDA bowls have been demonstrated as photothermal agents for cancer treatment. Additionally, we have shown that PDA bowls can act as a particulate stabilizer for photothermally responsive Pickering emulsions, with further applications in controlled release of drug molecules. PDA bowls offer advantages directly arising from their structure in this instance: simply, their cavity allows for unique wetting thermodynamics that makes them particularly effective stabilizers at the oil-water interface.

These studies began with making PDA nanoparticles of various shapes and sizes to understand the impact of these features on particle properties. Monodispersed, spherical PDA nanoparticles were fabricated through a facile process carried out at room temperature with mild stirring in a high pH environment, and similar sized PDA bowl-shaped mesoporous nanoparticles were synthesized by an emulsion-induced interfacial anisotropic assembly method. The formation process of PDA bowl-shaped mesoporous nanoparticles initiates with interface formation between trimethylbenzene and water in an emulsion system stabilized by non-ionic surfactant Pluronic® F-127 (F127), followed by growth of island-shaped mesostructured PDA seeds at the immiscible liquid (TMB/water) interface. These island-shaped mesostructured PDA seeds assemble to form composite micelles (F127/trimethylbenzene/PDA) and this is a key step in the formation of the cavity and mesopores of the nanoparticle.

Considering their morphological advantages in drug delivery applications, size-dependent formation of PDA bowl-shaped mesoporous nanoparticles was conducted. In a series of experiments, each reaction component was tuned in order to investigate their impact on the size and morphology of obtained PDA bowl-shaped mesoporous nanoparticles. Finally, obtained results demonstrated that a suitable concentration of monomer (dopamine), an appropriate pH of the reaction environment, and an adequate polymerization time are all crucial factors in size-controlled formation of PDA bowl-shaped mesoporous nanoparticles.

In Chapter 2, shape-dependent cellular internalization behavior of similarly sized PDA nanoparticles was investigated in HeLa cells, where we demonstrated a significant difference

in the cellular internalization behavior of PDA bowls compared to equivalent spherical particles. We observed both a faster rate of cellular uptake of PDA bowls in comparison to their spherical counterparts as well as a greater overall internalization. Intracellular distribution of the nanoparticles was also determined, where PDA bowls after entering the cells were evenly distributed without any signs of aggregation, unlike spherical particles, which aggregated upon cellular internalization. We thereby observed a significant impact of the shape of PDA nanoparticles on their cellular internalization behavior, which can be described as arising from a preferential attachment onto the cell membrane from the high curvature edge of PDA bowls that offers easier enwrapping by cell membranes, allowing for greater internalization of PDA bowls over their spherical counterparts.

This study was extended by synthesizing various sizes of PDA bowls and investigating their size-dependent cellular internalization behavior. In Chapter 3, we revealed the impact of each component of the emulsion-induced anisotropic assembly method on the formation and growth of PDA bowls. After conducting a series of experiments, we established precise experimental conditions for the size-controlled formation of PDA bowls with well-defined and reproducible physicochemical properties. We also demonstrated that the size of PDA bowls plays an exceptionally important role in cellular internalization processes. Not only was uptake efficiency of PDA bowls significantly controlled by their size, but also it played a dominant role in their intracellular trafficking. Herein, endocytosis pathways of HeLa cells have been studied, where we observed a governing role of the size of the PDA bowl in determining their preferred endocytosis pathways by which they are internalized into HeLa cells.

Considering the efficient cellular internalization behavior of selected PDA bowls, in Chapter 4, we loaded anti-cancer drugs into these PDA bowls, which were thereby transported into HeLa cells and released into the intracellular environment. A range of experimental results suggesting that PDA bowls can act as an efficient drug nanocarrier were obtained, showing the bowls' capability in carrying anti-cancer drug molecules into cells and broadly distributing them in the intracellular environment, causing a significantly larger number of cell death events in comparison with free anti-cancer drug. On top of that, in this Chapter, we explored the excellent photothermal conversion efficiency of PDA bowls under NIR illumination. Herein, PDA bowls are clearly identified as promising chemo- and photothermal agents. After a series of *in vitro* experiments on HeLa cells, these cells were evaluated via biochemical assay testing and confocal imaging analysis, where we observed a significant cytotoxic effect of combined treatments of anti-cancer drug-loaded PDA bowls and NIR illumination on HeLa cells in comparison to free anti-cancer drug. Obtained results suggest that PDA bowls are not only an efficient drug nanocarrier, but may also offer a promising candidate for the development of synergistic chemo- and photothermal therapy to conquer multiple drug resistance.

We explored an interesting property of PDA bowls in Chapter 5: due to their cavity, bowls show unique wetting thermodynamics that makes these anisotropic nanoparticles an effective particulate stabilizer at the oil–water interface. Taking advantage of the photothermal conversion efficiency of PDA bowls, herein we prepared photothermally responsive Pickering emulsions without any surface modification. The stability of Pickering emulsion systems was tested in various pH conditions, and we observed that acidic

environments are most suitable for the formation of such Pickering emulsions, where oil droplets were fully covered with PDA bowls, limiting coalescence and ripening of the droplets. Solidifiable emulsion droplets were fabricated by using an oil core with a melting point moderately above room temperature. The produced solidifiable emulsion had long-term stability, biocompatibility, and showed remarkable photothermal response under NIR illumination, indicating potential for various biomedical applications including NIR-triggered drug delivery.

Taken together, this thesis presents a facile method for the formation of various sizes of biocompatible anisotropic nanoparticles in the form of PDA bowls. By investigating the impact of various reaction parameters of the synthesis method, a decisive experimental condition was achieved to reliably obtain three different sizes of PDA bowls. These anisotropic nanoparticles have shown the ability to cross biological barriers more quickly and become internalized into cells more efficiently relative to their spherical counterparts. In addition to their biological interactions, the physical properties of PDA bowls make them appealing: they have excellent colloidal stability due to their small size, mesoporous structure, and diverse surface chemistry. Moreover, the chemical structure of PDA is beneficial to enable loading of a sufficient amount of drug molecules into these particles, allowing them to transport drugs inside cells faster. Once inside cells, PDA bowls distribute well throughout the intracellular environment, causing faster cellular death in comparison to cells incubated with free drug molecules.

From a formulation standpoint, the surface wettability of PDA bowls is beneficial in enabling them to act as a particulate stabilizer to prepare a novel type of Pickering emulsion. Furthermore, their excellent photothermal response has been significantly advantageous for their ultimate success, not only in combined chemo- and photothermal therapeutic agents for cancer treatment but also their efficiency as an NIR-controlled drug delivery system. In each case, the chemistry of PDA and specific morphological features of the particles' mesoporous bowl-shaped structure is seen to be essential in delivering the properties needed to achieve these outcomes.

6.2 Outlook and future directions

There are many potential areas in which this work could be continued and extended. In the formation and design of drug nanocarriers, size and surface functionalization are important factors for their ultimate success. The size of drug nanocarriers has an active role in their cellular uptake efficiency, intracellular trafficking, and cytotoxicity. Following the size-controlled formation strategy of PDA bowl-shaped mesoporous nanoparticles in Chapter 3, smaller-sized bowls with a larger cavity can be synthesized with intact mesopores in the future. PDA offers easy functionalization due to the presence of amino or mercapto-nucleophiles, which may improve its efficiency as a drug nanocarrier. Further, PDA's surface chemistry contains groups suited as reducing and capping agents that could be useful for growing gold nanoparticles on the surface of PDA, which may offer the combined physicochemical advantages of PDA and gold in drug nanocarrier design. Moreover, the surface properties of PDA are beneficial for binding with various drug molecules through π–π

stacking or hydrogen bonding as well as via covalent tethering. Additionally, the parent emulsion-induced anisotropic assembly method used to produce the PDA bowls used in this work could be applied to form bowl-shaped particles of other neurotransmitters such as norepinephrine, epinephrine, serotonin, etc. which have similar structures to dopamine.

Due to their unique morphology and surface properties, PDA bowl-shaped mesoporous nanoparticles have shown great potential in drug delivery systems to overcome some of the key challenges that plague development of nanoparticulate based drug carriers. The cavity of PDA bowl-shaped mesoporous nanoparticles may offer an exciting opportunity to use these materials for ultrasound-enhanced site-specific drug delivery systems. Considering the surface functionalization of PDA, PDA bowl-shaped mesoporous nanoparticles could be used as receptor-mediated targeting drug carriers, which involves antibodies, peptides or sugar moieties that can be physically or chemically conjugated onto the surface of the PDA bowls to be beneficial in specific uptake by the target cells.

Our current study has shown the efficiency of PDA bowl-shaped mesoporous nanoparticles in stimulus-triggered drug release, as well as demonstrating its potential in combined treatment towards conquering multidrug resistances via chemo- and photothermal therapy for cancer treatment. This study could be extended to the next step by *in vivo* studies in animal models and clinical investigation. However, a few scientific gaps needed to be addressed before applying these systems in animal models. An extensive understanding and range of assessment protocols are needed in order to monitor various aspects of PDA bowl-shaped mesoporous nanoparticles as a drug carrier *in vivo*, including pharmacokinetics,

biodistribution, target site accumulation, local distribution at the target site, localization in healthy tissues, and kinetics of drug release. Moreover, mucopenetrative properties, immunogenic response, and biodegradation behavior of PDA bowl-shaped mesoporous nanoparticles need to be addressed before applying such systems in an animal model. Additionally, it is important to investigate these parameters as a function of dose, dosage form, and route of administration, in order to establish safe limits for human use before clinical trials of PDA bowl-shaped mesoporous nanoparticles as a drug carrier system can be considered.

Appendix

Appendix A

Supporting Information for Chapter 2

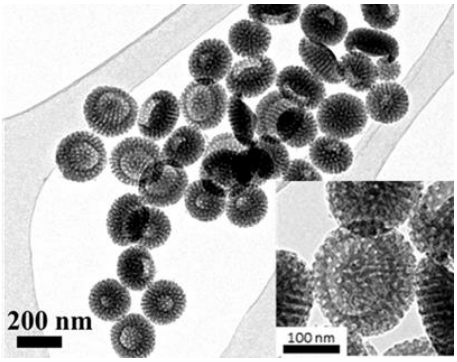

Figure 2.S1. TEM image of bowl-shaped PDA nanoparticles (~200 nm); mesochannels are clearly seen in high-magnified view.

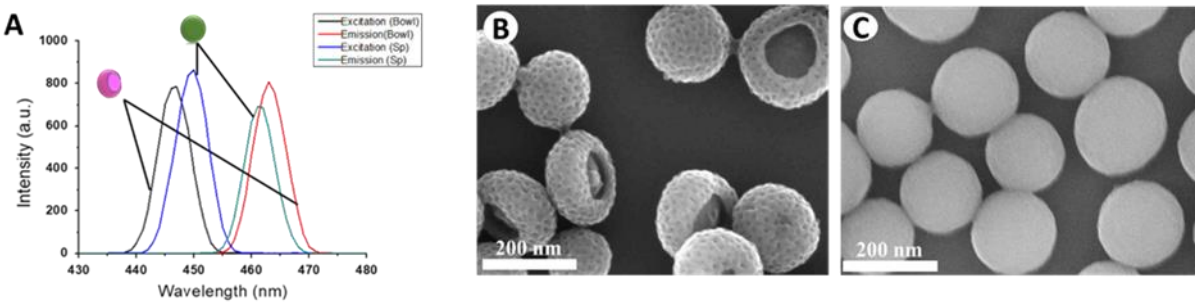

Figure 2.S2. A) Comparison of fluorophore intensity of PDA bowl-shaped and spherical nanoparticles measured by fluorescence spectrophotometer, B) and C) SEM images of PDA bowl-shaped and spherical nanoparticles, respectively, after Rh 6 G labelling.

No. of particles/ mL and fluorophore molecules on each particles:

To calculate the number of particles per 1 mL, volume and surface area of particle have been measured followed by the calculation of $Mass = Vol\ x\ Density$ and number of particles/mg.

Number of fluorophore molecules on each particles has been estimated by comparing the sample to a standard curve. The concentration of the dye was adjusted to obtained similar fluorescence intensity by fluorescence spectrophotometer.

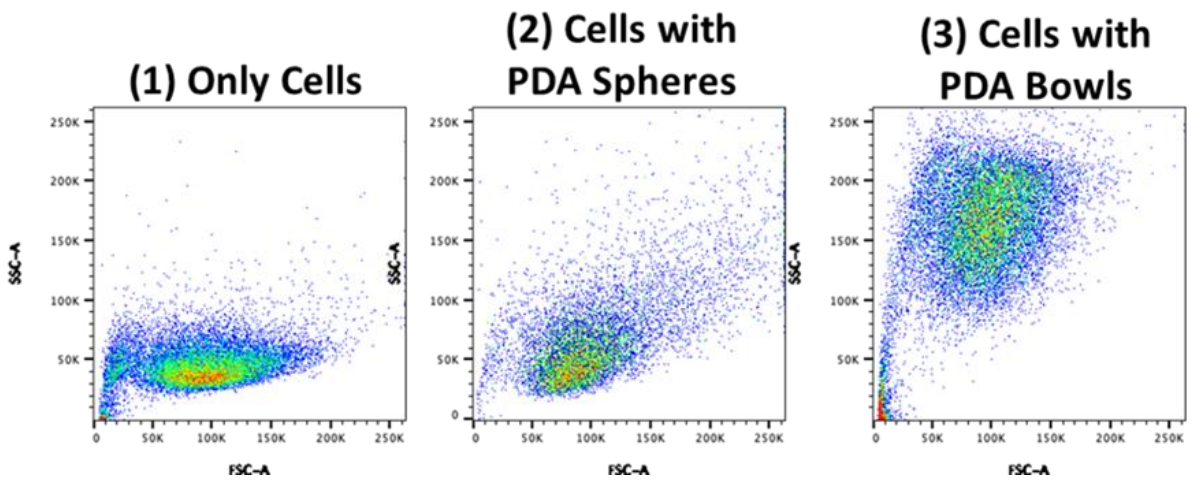

Figure 2.S3. Flow cytometer light scattering plots: side scattering (SSC-A) versus forward scattering (FSC-A) of HeLa cells showing the changes of size and granularity of the cells, (1) control, (2) cells with PDA spheres, (3) cells with PDA bowls. Live cells were used for flow cytometer analysis.

Table 2.S1. Particles size analysis, polydispersity and zeta potential of PDA bowl-shaped and spherical nanoparticles.

Sample Type	Temperature	Solvent	Hydrodynamic diam. (nm)	Std Dev. Of DLS	Polydispersity Index (PDI)	Zeta Potential (mV)	Std Dev. Of Zeta
PDA Bowls	RT	DI water	369.81	24.85	0.102	-38.14	0.31
PDA Spheres	RT	DI water	389.09	25.54	0.215	-46.10	0.17
PDA Bowls	37 °C	70% Complete Medium+ 30% PBS	431.47	18.63	0.319	-38.75	0.28
PDA Spheres	37 °C	70% Complete Medium+ 30% PBS	452.43	132.16	0.421	-38.34	0.22

Appendix B

Supporting Information for Chapter 3

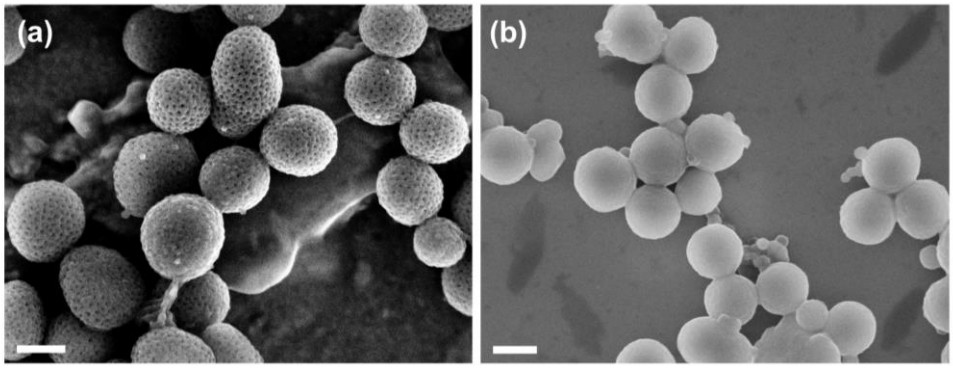

Figure 3.S1. Scanning electron microscopy (SEM) images of polydopamine nanoparticles prepared at various temperatures: (a) 60°C and (b) 80°C (M5). Scale bars: 100 nm.

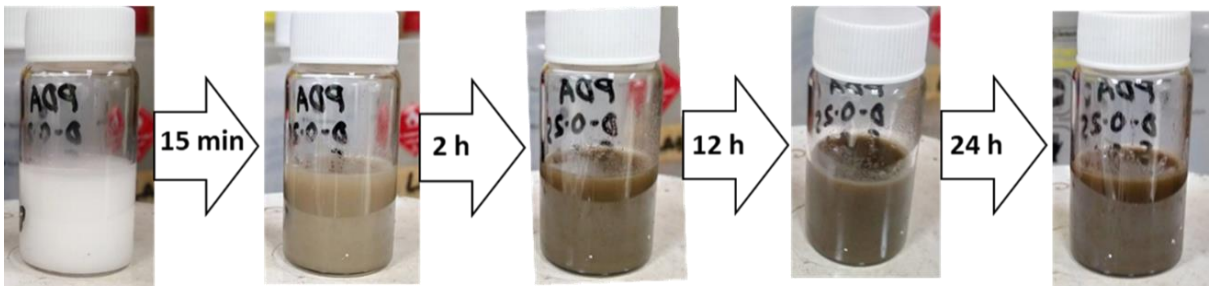

Figure 3.S2. Digital images showing the color change of the reaction mixture with time during the polymerization of dopamine to synthesize of PDA bowl-shaped mesoporous nanoparticles at room temperature.

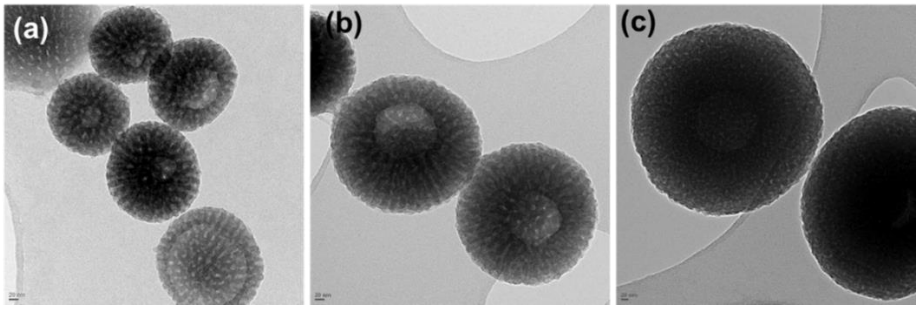

Figure 3.S3. High-magnification TEM images of PDA bowls. Samples were prepared with (a) 1.5% (w/v) of dopamine and 28% of ammonia (M1), (b) 2.5% (w/v) of dopamine and 26.5% of ammonia (M8), and (c) 2.5% (w/v) of dopamine and 25% of ammonia (M8). The concentration of TMB and F127 were fixed at 2% (v/v) and 1% (w/v) respectively, with 1:1 water: ethanol ratio in 24 h of reaction time at room temperature. Scale bar: 20 nm.

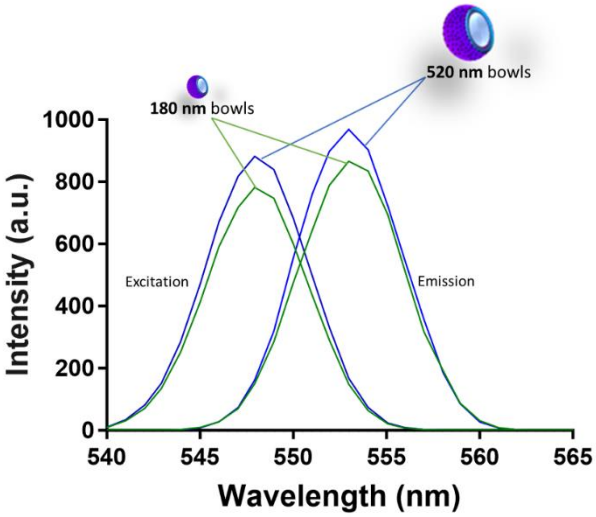

Figure 3.S4. Comparison of fluorophore intensity of PDA bowls at ~180 and ~520 nm measured by fluorescence spectrophotometer.

No. of particles/ mL and fluorophore molecules on each particles:
To calculate the number of particles per 1 mL, volume and surface area of particle have been measured followed by the calculation of $Mass = Vol\ x\ Density$ and number of particles/mg. Number of fluorophore molecules on each particles has been estimated by comparing the sample to a standard curve. The concentration of the dye was adjusted to obtained similar fluorescence intensity by fluorescence spectrophotometer.

Appendix C

Supporting Information for Chapter 4

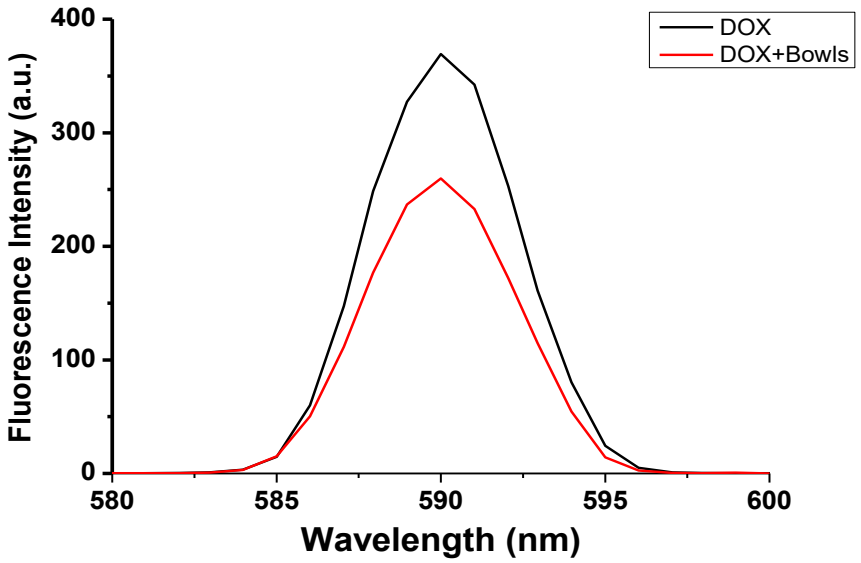

Figure 4.S1. Fluorescence intensity of DOX and PDA mesoporous nanobowls/DOX.

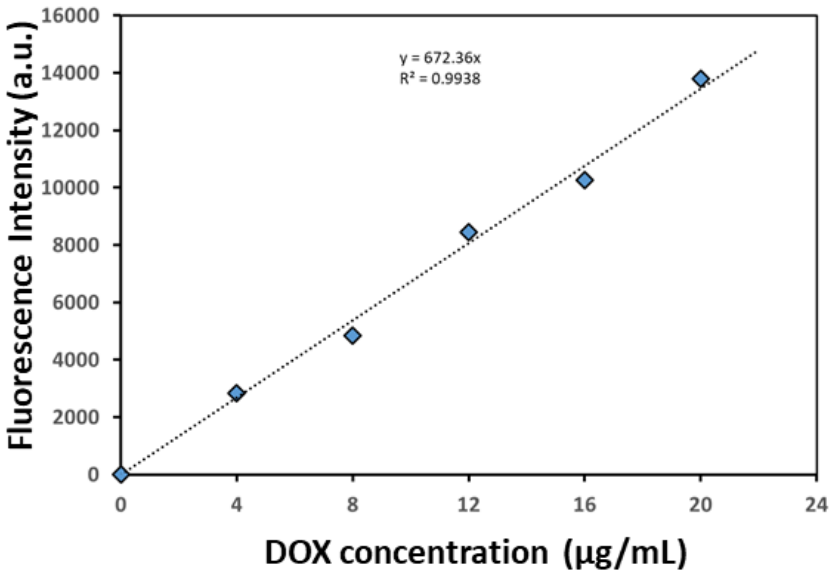

Figure 4.S2. Standard curve of DOX.

Appendix D

Supporting Information for Chapter 5

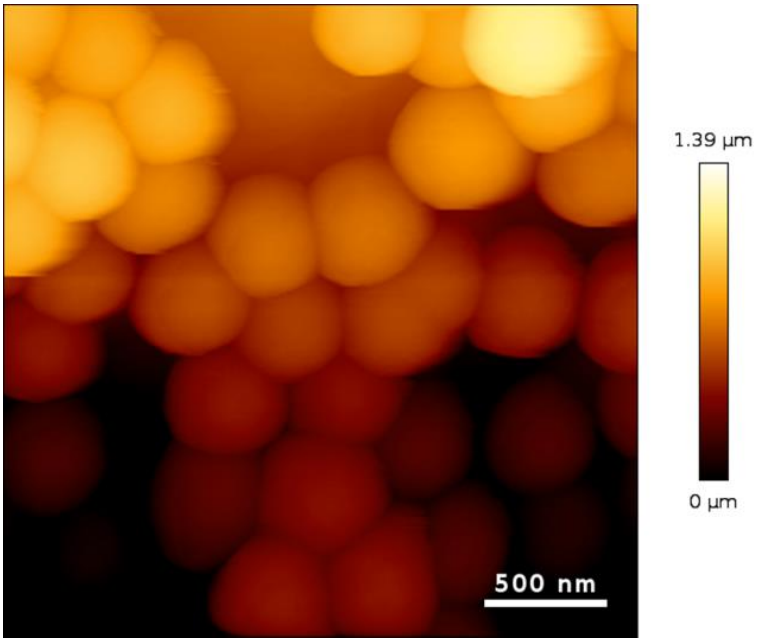

Figure 5.S1. AFM height image of Pickering emulsion (solid) stabilised by PDA nanobowls (~350 nm, pH 4.2).

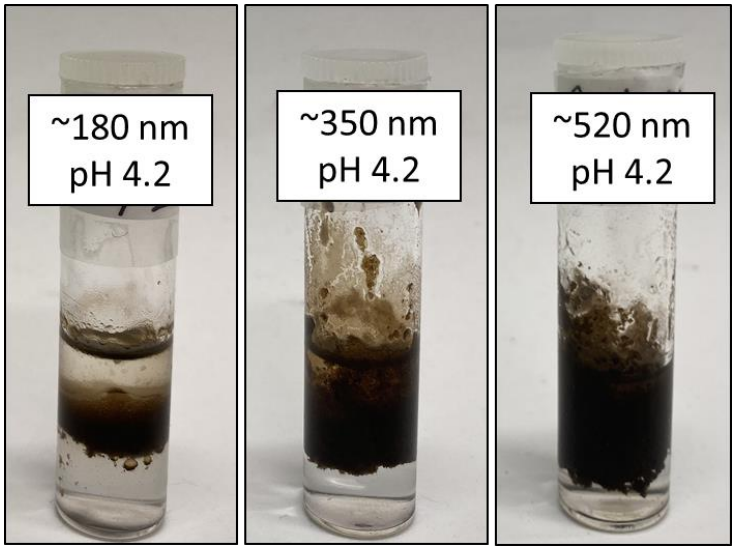

Figure 5.S2. Digital images of the Pickering emulsion stabilized with PDA nanobowls after one year of post preparation.

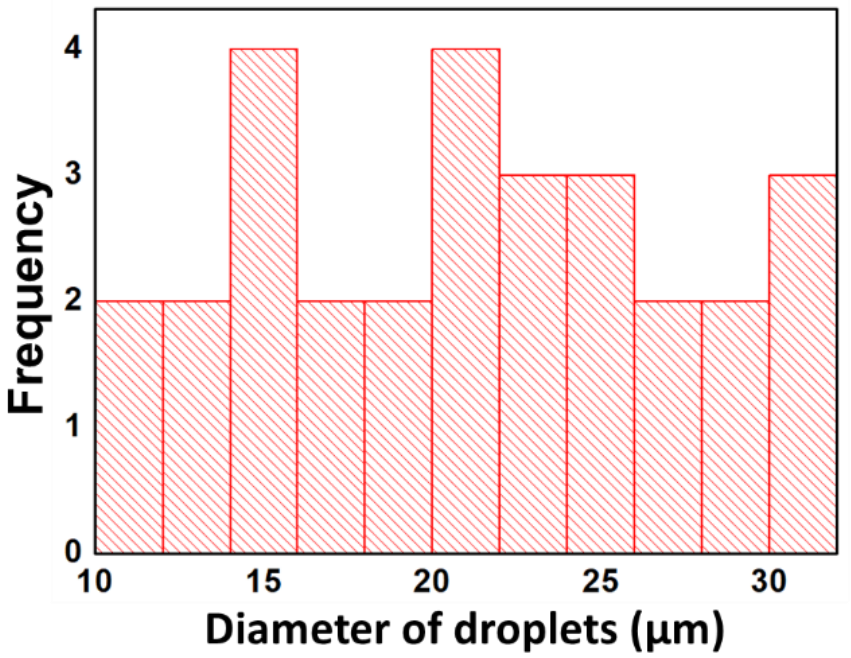

Figure 5.S3. Histograms of the droplet size distribution prepared at pH 4.2 stabilized with ~180 nm size PDA nanobowls.

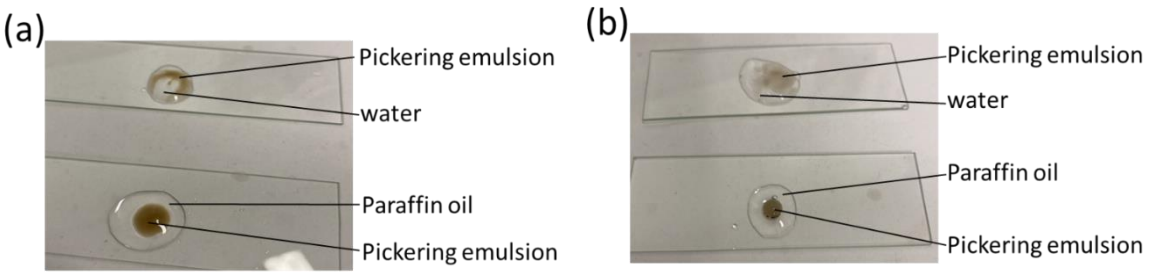

Figure S4. Digital images showing drop test of the Pickering emulsion prepared at (a) pH 4.2 and (b) pH 10.4, stabilized with PDA nanobowls.

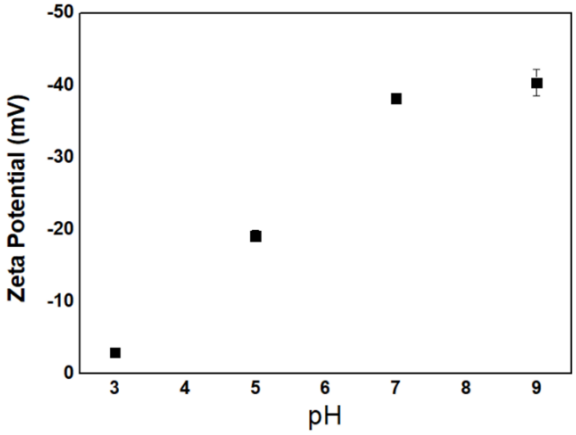

Figure 5.S5. Surface charge of PDA nanobowls in various pH.

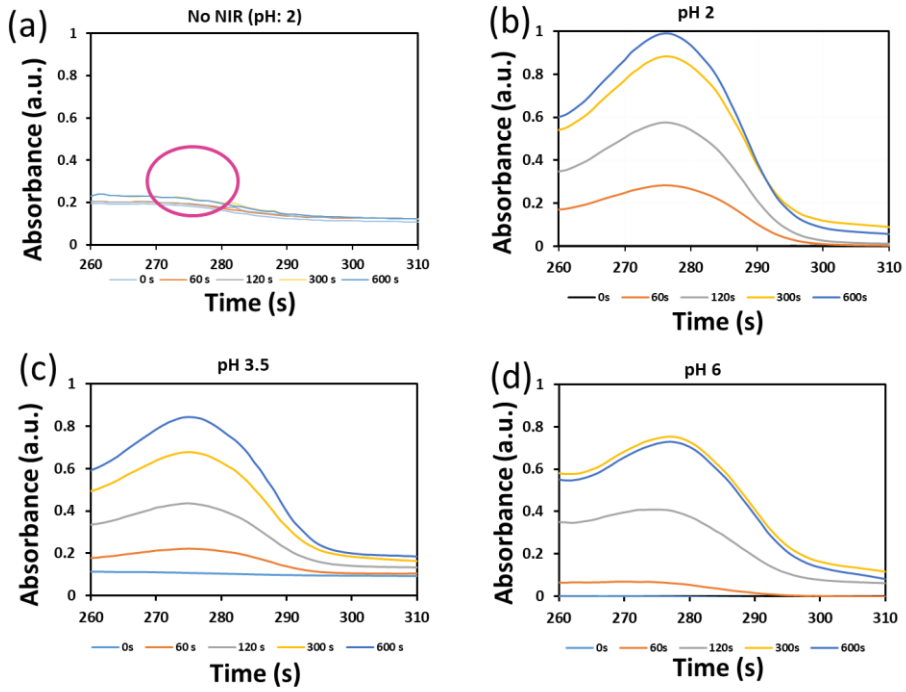

Figure 5.S6. UV-Vis spectra show characteristics trend of aspirin release from Pickering emulsion (stabilized with ~350 nm PDA nanobowls) without and under near-infrared illumination, (a) Without NIR illumination, (b), (c), and (d) Under NIR illumination (time dependent aspirin release in various pH).

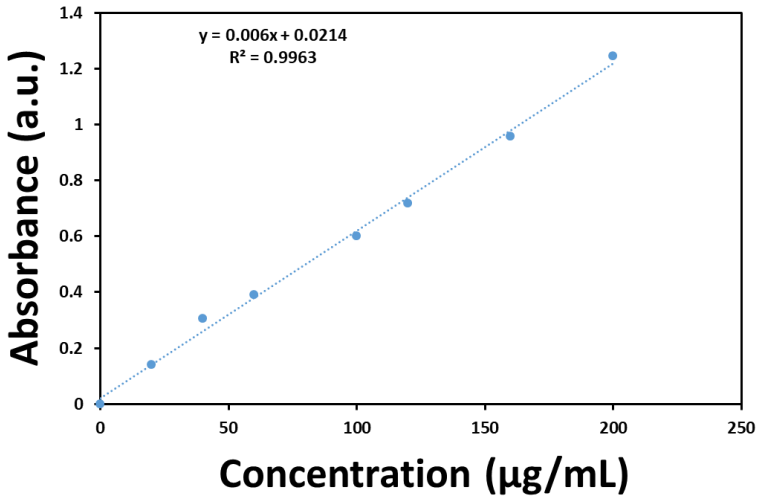

Figure 5.S7. Standard curve of aspirin.